A Study on Low-temperature Ignition of DME-Air Mixture at Atmospheric Pressure

（DME 混合気の常圧下における低温着火に関する研究）

Jian GAO

A Study on Low-temperature Ignition of DME-Air Mixture at Atmospheric Pressure

（DME 混合気の常圧下における低温着火に関する研究）

By

Jian GAO

A DISSERTATION SUBMITTED TO THE DEPARTMENT OF MECHANICAL AND SPACE ENGINEERING, HOKKAIDO UNIVERSITY

IN PARTIAL FULFILMENT OF THE REQUIREMENTS FOR THE DEGREE OF

DOCTOR OF PHILOSOPHY

IN MECHANICAL AND SPACE ENGINEERING

Advisor: Yuji NAKAMURA

March 2014

Abstract

Dimethyl ether (DME: CH_3OCH_3) has been considered as a promising alternative fuel due to its merits of favorable compression ignition property and little soot formation in combustion field. A deep understanding of low-temperature ignition of DME is important in two engineering aspects: the design of engine and the safety for preventing accidental explosions. The ignition of DME exhibits a two-stage mode, which shows complexity due to the existence of the negative temperature coefficient (NTC) effect. Research gap still exists related to the ignition kinetics of DME at atmospheric pressure. The objective of this study is to develop an experimental system that could clarify the ignition characteristics of DME. Special attention is given to the transition from a cool flame to a hot flame. Furthermore, the existing ignition kinetic model of DME is expected to be validated using the developed system. Suggestions are expected to be proposed to improve the detailed low-temperature ignition kinetics of DME.

In Chapter 1, significance of the present research, as well as the two-stage ignition regime is introduced. Then, previous studies on DME ignition kinetics are briefly summarized. Finally, objective and scope of this dissertation are shown.

Chapter 2 shows the first trial to capture low-temperature ignition of DME, which is conducted in a 1400 mm long, straight shaped, Pyrex flow reactor. The observed periodic behaviors with ignition, flame propagation, and extinction are interpreted. Two distinct flames, weak flame and hot flame, are identified. The weak flame is found to transit to the hot flame with decreasing of equivalence ratio. Time sequential analyses are conducted, indicating that the intermediates, such as formaldehyde, methyl formate and formic acid, which formed due to the mild oxidation, are completely consumed by the subsequent hot flame.

In Chapter 3, in order to achieve clear observation of flame motions, the flow reactor is updated. Thanks to the updated reactor, the mechanism of the periodic weak flame behavior

is clarified for the first time. It is indicated that the weak flame occurrence is accompanied by the formation of the intermediate product species, such as formaldehyde and methyl formate. Therefore, the weak flame might be cool flame, or flame formed due to the significant suppression of the transition from a cool flame to a hot flame. Moreover, it is found that the ignition disappears at above 590 K, indicating the negative temperature coefficient (NTC) zone is encountered. Gas analyses are conducted toward the periodic ignition behaviors in the ignition regime, as well as the stable oxidation conditions in the NTC zone. The results are further discussed based on the detailed chemical kinetics. It is proposed that a new chain-propagation pathway might exist via the decomposition of the species HPMF (hydroperoxy-methyl formate, $HOOCH_2OCHO$) and become pronounced at above 540 K, which suppresses the transition from a cool flame to a hot flame.

In Chapter 4, to investigate the ignition kinetics, numerical computations are performed using the plug-flow reactor model accounting for heat transfer between gas mixture and reactor. This model predicts well the ignition limit in experiments, however, fails to predict the transition from a cool flame to a hot flame. Reaction pathway analyses suggest that the competition between the β-scission reaction and the molecular oxygen addition reaction of the methoxy-methyl radical (CH_3OCH_2) could strongly influence the transition. This influence is further investigated via applying a slight modification of the activation energy of the β-scission reaction of the CH_3OCH_2 radical. Depending on this modification, both ignition limit and ignition regime against equivalence ratio are well predicted: a two-stage ignition regime corresponds to a hot flame occurrence in the experiments, and a transition suppressed ignition regime corresponds to a weak flame occurrence in the experiments, respectively. In addition, the kinetic model with the modification shows reasonable agreement with shock tube ignition delay time results. It is shown that the modification strongly influences the reactivity in the NTC region, therefore influences the transition from a cool flame to a hot flame. Further

investigations determining the rate constants of the reactions of the CH_3OCH_2 radical may be needed to improve the DME ignition kinetics.

In Chapter 5, conclusions are briefly summarized and recommendations for future work are proposed.

Acknowledgements

First and foremost, I would like to express my sincere gratitude to my advisor, Prof. Yuji Nakamura, for his contributions of time, ideas, and encouragement through my study at Hokkaido University. Prof. Nakamura is the greatest mentor and it has been a great fortune to be his student. He has taught me, not only on combustion science, but also the right attitude in which to conduct research and toward life.

I would like to thank Prof. Osamu Fujita, Prof. Hideyuki Ogawa, and Prof. Nobuyuki Oshima for their service on my doctoral committee and also for their help on my study and research in the past years. I appreciate Prof. Kazuaki Sasaki, Prof. Masao Watanabe, Prof. Takashi Nakamura, Prof. Harunori Nagata, Prof. Takemi Chikahisa, Prof. Gen Shibata, and Prof. Mitsutomo Hirota (Muroran Inst. Tech.) for reviewing my thesis.

I want to acknowledge my master-course advisor, Prof. Daiqing Zhao (GIEC, CAS), for her continuous encouragement and valuable instruction. She is the first tutor who led me into the field of combustion fundamental research. I especially appreciate her for the efforts to introduce me to the Ph.D. program at Hokkaido University under Prof. Nakamura's supervision.

I wish to thank Prof. Osamu Fujita, and Prof. Hiroyuki Ito for their generous help on my study and research. I very much appreciate Prof. Fujita for his kind help to accept me as a research student in my first half year at HU. I thank Ms. Miho Taga for her kind help for dealing a lot of paper works related to my research and business trips.

I would like to thank Dr. Liqiao Jiang (GIEC,CAS), Prof. Fei Qi and Mr. Zhandong Wang (USTC), for the collaborations and stimulating discussions with them in conducting the JSPS-CAS joint project.

I also wish to thank Dr. Akter Hossain, Dr. Yangkyun Kim, Mr. Nepal Chandra Roy, Mr.

Hui Yan, and Mr. Sunghwan Youn in our laboratory, for the inspiring discussions with them. I appreciate Mr. Taichi Usuki, Mr. Shinya Goitsuka for their help for manufacturing my experimental set-ups. Thanks also go to other members in our laboratory as well as the former graduate students, for their generous help that makes my life smooth here at HU.

I have met many good friends at HU. It is hard to acknowledge all of them here. Some of them are Yanhua Lei, Xiaojing Sui, Tan Cheng, Yingjie Liu, Qian Xiong, Huiying Cai, Xinyan Huang (IC, London), Longhua Hu (USTC) and Andres Osorio (UC Berkeley). I am grateful to them for their friendship and the parties enjoyed with them in the past years gave me warmness and happiness.

I wish to acknowledge China Scholarship Council (CSC) for providing me a scholarship for 42 months under the State Scholarship Fund to pursue my study in Japan as a Ph.D. student.

Finally, it is with profound gratitude that I thank my parents, Shun Gao and Xiuyan Li, for their endless love. With their support, I am able to fully devote myself to my study.

Table of Contents

List of figures

List of tables

Nomenclature

A	Cross-section area
c_p	Specific heat at constant pressure
d	Inner diameter of reactor
h	Specific enthalpy
M	Mass flow rate
Nu	Nusselt number
T	Temperature
u	Flow velocity
W	Molecular weight
x	Spatial coordinate
Y	Mass fraction
λ	Thermal conductivity
$\dot{\omega}$	Molar production rate
ρ	Density
Da	Damköhler number
ϕ	Equivalence ratio
V	Flame front velocity

S	Flame propagation speed
t	Time
Δx	Grid size in numerical calculation
E	Activation energy

subscripts

k	Species index
R	Reactor
g	Gas
ex	Experimental

Chapter 1: Introduction

1.1 Overview and significance

Dimethyl ether (DME: CH_3OCH_3), as the simplest linear ether, has been considered as a promising alternative fuel due to many merits [1, 2]. It is a low toxic and multi-source fuel that can be synthesized from at a competitive price from coal, natural gas derived methanol, and biomass. It has been proposed for uses as a fuel or additive in diesel engines because of the high cetane number of 55-60, which makes it suitable for compression ignition [3]. Since there is no carbon-carbon bond in the DME molecule to act as a seed for polymerization leading to polyaromatic hydrocarbons, it has been proved to be able to reduce the soot emission [4, 5]. Additionally, DME is a multi-use fuel could be used for electric power generation, and in domestic application (e.g. heating and cooking) [6]. It has similar physical properties to liquid petroleum gas (LPG) thus the existing LPG technology could be used for DME without modification to these energy systems.

Table 1-1 Physical properties of DME as fuel in comparison to other relating fuels. [7]

Property	DME	Methane	Propane	Methanol	Gas oil
Chemical Formula	CH_3OCH_3	CH_4	C_3H_8	CH_3OH	-
Boiling point (℃)	-25.1	-161.5	-42.0	64.6	180-360
Liquid density (g/cm^3,20℃)	0.67	-	0.49	0.79	0.84
Gas density (vs. air)	1.59	0.55	1.52	-	-
Saturated vapor pressure (MPa,25℃)	0.6	-	0.9	-	-
Cetane number	55-60	0	5	5	40-55
Lower Heating value (MJ/kg)	28.8	50.2	46.4	20.1	42.7
Lower Heating value (MJ/m^3)	59.2	35.8	90.9	-	-

Low-temperature ignition of DME is of practical interest in the following two folds. First, from the standpoint of engine application, the low-temperature ignition property is important for the ignition timing control to prevent knocking, etc. Second, the leakage of DME may cause fire accidents and produce harmful species due to the relatively higher reactivity at low-temperature compared with conventional hydrocarbons [8]. Therefore, a better understanding of low-temperature ignition mechanism is of significance to improve the performance of engine combustion as well as the safety during the transportation, storage and other related industrial process.

1.2 Two-stage ignition

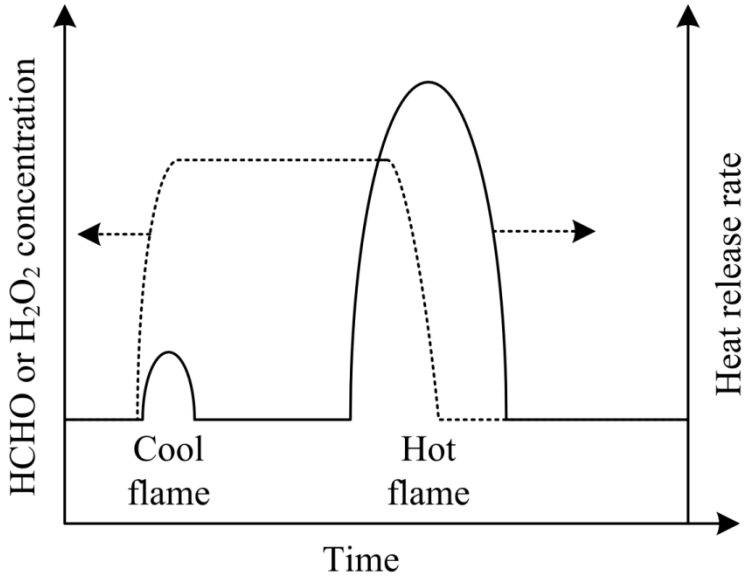

Figure 1.1 Schematic of two-stage ignition mode

DME is one of the simplest fuels that exhibit two-stage ignition mode [9]. The two-stage ignition (or oxidation) mode is not limited to DME, but also has been found in many other practical fuels, such as oxygenated fuels (diethyl ether (DEE) [10], acetaldehyde [11] etc.) and straight chain alkanes (n-butane [12-14], n-hexane [15, 16], n-heptane [17-21], n-decane [22], etc.). As shown in Fig. 1.1, the two-stage mode includes the first-stage ignition resulting in a cool flame and the second-stage ignition resulting in a hot flame. Two essential features are dominant in this mode: "cool flame" and NTC (Negative Temperature Coefficient) behavior. So-called "cool flame", which results from chain-branching reactions [23, 24], is usually accompanied by single or multiple small temperature increments in time and very weak blue luminescence due to excited formaldehyde (HCHO) [25]. Closely linked with cool flame zone (usually around 550 K), there is a range where the oxidation reactivity decreases with increase in temperature, is called "NTC" (negative temperature coefficient) zone (usually around 650 K). Once cool flame occurs, the system temperature will increase, thus the NTC

zone is encountered and suppressed the chain-branching that makes it back to "steady" state (mild stable oxidation). On the other hand, when the heat release of the cool flame reaches a sufficient level, the cool flame may induce the subsequent hot flame, which commonly occurs in the compression ignition process of HCCI engine [26-29], is usually known as the transition from a cool flame to a hot flame.

The transition from a cool flame to a hot flame would be the results from the complex interactions of intermediate species [30]. The decomposition of the H_2O_2 that accumulated in the cool flame stage is suggested to be the most important reaction to induce the subsequent hot flame by producing two active OH radicals by following reactions:

$$H_2O_2 + M \rightarrow 2OH + M \qquad \text{(R1.1)}$$

On the other hand, HCHO, as a major intermediate species in low-temperature oxidation, acts as a principal pre-cursor to induce the subsequent second-stage ignition. The main oxidation process of HCHO is:

$$HCHO + OH \rightarrow HCO + H_2O \qquad \text{(R1.2)}$$

$$HCO + O_2 \rightarrow HO_2 + CO \qquad \text{(R1.3)}$$

The produced OH radicals by R1.1 promote the reaction R1.2 and R1.3, which lead to the formation of HO_2. On the other hand, the formation of H_2O_2 obviously relies on HO_2:

$$HO_2 + HO_2 \rightarrow H_2O_2 + O_2 \qquad \text{(R1.4)}$$

Then the formation of H_2O_2 through R1.4 promotes R1.1. In this way, R1.1, R1.2, R1.3 and R1.4 consist of a repeating cycle with OH production. With this cycle, HCHO is consumed continuously and mainly converted to CO. Potential perturbations, such as the heat release of cool flame, could initiate this cycle. Moreover, since the first-stage ignition results in rapid formation of HCHO and H_2O_2 while the second-stage results in rapid consumption, HCHO and H_2O_2 are usually used as indicators to distinguish cool flame and hot flame.

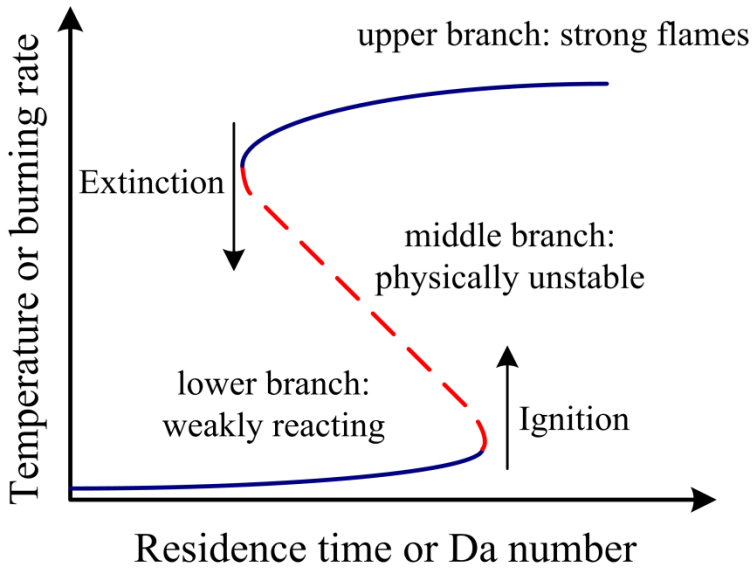

Figure 1.2 Representative S-curve for ignition [31]

It is well known that, for steady systems such as the jet-stirred reactor (JSR), ignition is conventionally defined as the turning point on the well-known "S-curve" as shown by the schematics in Fig. 1.2 [31]. The upper and lower branches are known to be stable. The upper branch indicates strongly burning flames, the lower branch indicates weak reactions without identifiable flames, and the middle branch is known to be unstable and cannot be obtained experimentally. The upper turning point is regarded as the extinction state of strong flames due to the reduced Damkohler number (*Da*) or residence time. Similarly, the lower

turning point is considered as the ignition state, because the steady state solution jumps from the lower branch to the upper branch due to increased *Da* or residence time.

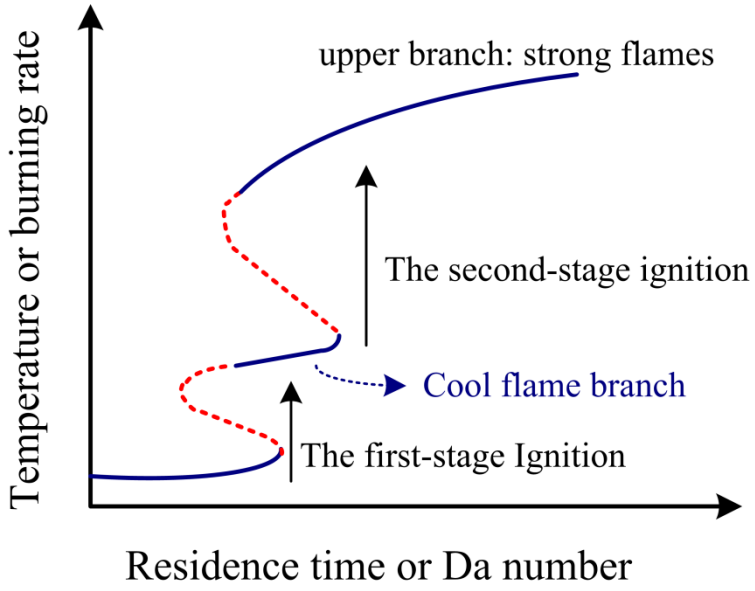

Figure 1.3 Complicated S-curve for ignition of DME-air mixture in a jet-stirred reactor [32]

However, the typical S-curve could show complexity for the fuels involved with the existing NTC effect. Numerically, Shan et al. [32] captured multiple ignition and extinction turning points exist on the "S" curve of DME/air mixture. Besides the conventional lower weakly reaction branch and the upper strong flame branch, additional cool flame branch was predicted, as shown in Fig. 1.3.

It should be further noted that, conventionally, the two-stage ignition mode is considered to occur in premixed systems (above mentioned [10-13, 15, 17]). However, recent studies have also found cool flames in non-premixed systems such as counter-flow diffusion flames [33, 34] and droplet combustion [35-37].

1.3 Summary of previous kinetics studies related to DME oxidation

In 1990s, the atmospheric chemistry of DME was studied with attention to the reactions of methoxymethyl radical (CH_3OCH_2) with itself, chlorine (Cl_2), and oxygen (O_2) [38-42]. Sehested et al. [39] and Maricq et al. [40] suggested that the reaction between CH_3OCH_2 radicals and O_2 proceeded along two distinct pathways between 230 and 350 K. For instance, At 296 K, the formation of methoxymethyl-peroxy radicals (CH_3OCH_2OO) dominated at pressures above 10 Torr, while the formation of formaldehyde (HCHO) and hydroxyl radicals (OH) dominated at pressures less than 10 Torr. Jenkin et al. [41] found that the self-reaction of CH_3OCH_2OO radicals could lead to the formation of methyl formate (CH_3OCHO) and hydroperoxy radicals (HO_2) at 298 K. Japar et al. [42] indicated that the consumption of DME was accompanied by the formation of CH_3OCHO at 700 Torr and 295 K.

The earliest detailed kinetic models for DME oxidation were developed by Dagaut et al. [43, 44] and Curran et al. [45] by using jet-stirred reactors (JSR). Then, Liu et al. [46] investigated the oxidation of DME at atmospheric pressure using a plug-flow reactor (PFR). Considered range of the temperature was from 513 K to 973 K and the residence time was set at 2-4 s. The products of reaction were determined by Fourier transform infrared spectrometer (FTIR). The results showed that the reaction rate of DME oxidation was enhanced with increasing of temperature from 533 K and reached a maximum at approximately 633 K, after which the negative temperature coefficient (NTC) zone was encountered. More importantly, based on their observation, it was indicated that the formic acid (HCOOH) should be a major intermediate of the low-temperature oxidation, which had been excluded in the previous models.

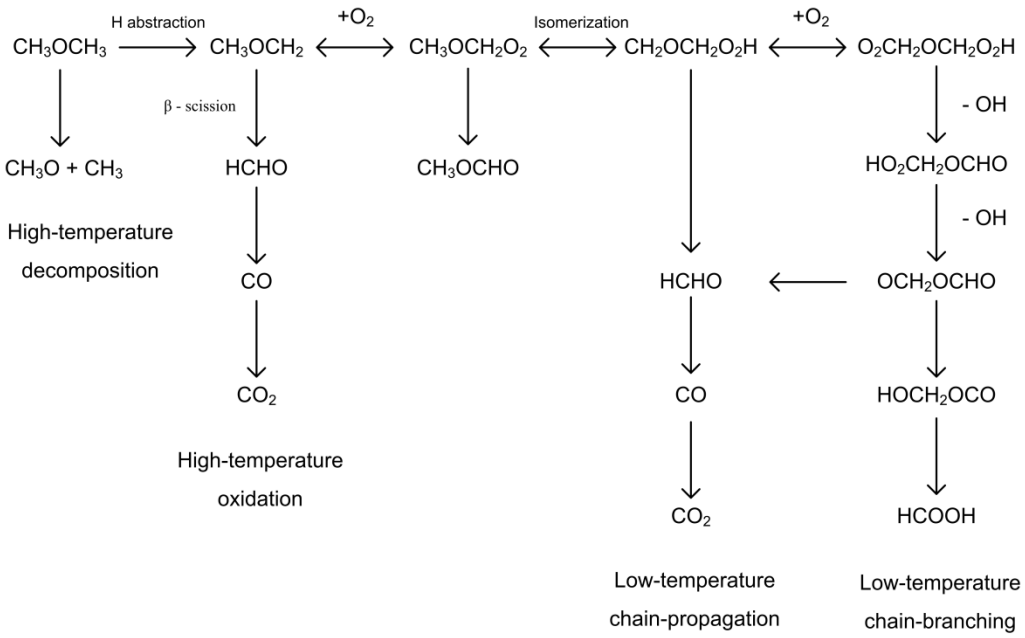

Figure 1.4 Overall reaction scheme of the kinetic model DME-2000 [47, 48] and DME-2007 [49]

In 2000, Curran et al. proposed an updated model [47, 48] (termed as "DME-2000") with including the chemistry leading to formation and oxidation of formic acid (HCOOH). Figure 1.4 shows the overall reaction scheme of this model. The model starts with the abstraction of a hydrogen atom (H) from a DME molecule by a highly reactive radical, like OH radical, to form a CH_3OCH_2 radical, followed by the formation of a CH_3OCH_2OO radical after a barrier-less reaction with O_2, and then the CH_3OCH_2OO radical isomerize to form a CH_2OCH_2OOH radical. In the temperature range of 530-600 K, CH_2OCH_2OOH radicals combine with O_2 to lead chain-branching pathways, which often results in a "cool flame". The term "cool" implies that this so-called flame does not reach its adiabatic flame temperature and the reacting mixture is not completely consumed. As temperature increases, the reaction rate decreases in the temperature range of 600-725 K due to the β-scission of CH_2OCH_2OOH radicals, where there is a negative temperature coefficient (NTC) zone; the DME consumption is suppressed by the chain-propagation pathway of decomposition of CH_2OCH_2OOH into two

HCHOs and one OH radical. Lastly, when the temperature becomes higher than 730 K, the reactivity of the system increases again to induce rapid consumption of the remained fuel due to the breaking of the HO-OH bond in hydrogen peroxides. This is the second stage ignition with the non-chain-branching ignition mechanism.

Finally, Zhao et al. proposed a updated model [49] (termed as "DME-2007") based on optimizing the model DME-2000. DME-2007 has almost same reaction pathways with DME-2000, but improved the DME unimolecular decomposition reaction. This model well predicts the experimental results of jet-stirred reactors (JSR) [43-45], plug-flow reactors (PFR) [47, 48], shock tubes reactors (STR) [50], and others [51-55].

The two-stage oxidation behavior of DME has also been captured by Oshibe et al. [56] at atmospheric pressure using a micro flow reactor with a controlled temperature profile. Stable double weak flames were observed when the supplied rate was low (i.e., small velocity was imposed). The existence of low-temperature oxidation was conjectured by the production of HCHO occurring upstream the experimental first weak flame. Recently, the oxidation of DME in the cool flame and NTC zones were further investigated by using laminar flow reactors at atmospheric pressure [57, 58], and special attentions were paid to the production of the key intermediate product species, such as formic acid (HCOOH), methyl formate (CH_3CHO), and hydrogen peroxide (H_2O_2).

1.4 Motivations and objectives

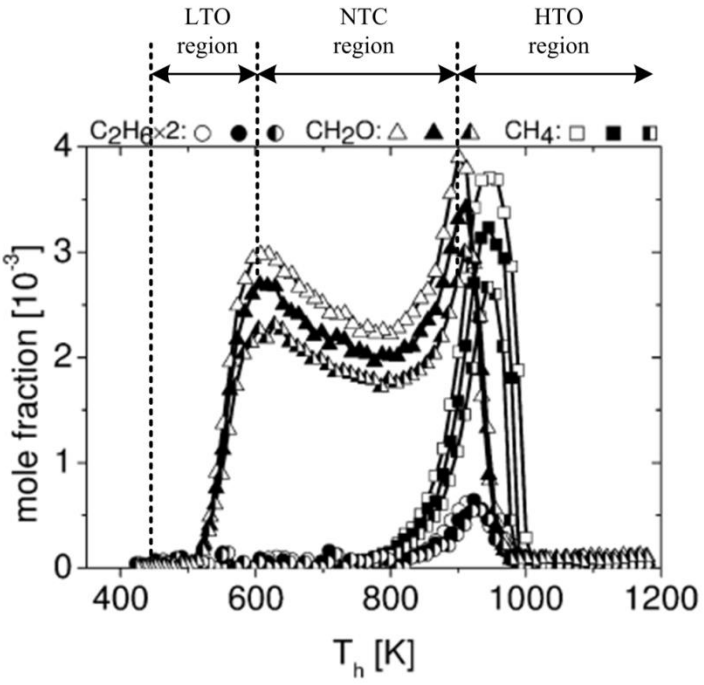

Figure 1.5 Identification of LTO, NTC, and HTO regions of DME in a plug-flow reactor [57]

As stated above, the kinetic models for DME oxidation are developed mainly based on typical reactors, such as jet-stirred reactor (JSR), plug-flow reactor (PFR). Conventionally, in JSR and PSR, high dilution (e.g., with 70-90% N2) and short residence time (e.g., 2 s) are applied and approximately zero-dimensional isothermal or adiabatic conditions are achieved. Concentration measurements of fuel, oxygen, and product species are conducted in wide temperature ranges. For example, as shown in Fig. 1.5 [57], the intermediate product HCHO is significantly formed due to low-temperature oxidation (LTO) and consumed due to high-temperature oxidation (HTO). In a mediate temperature range, the HCHO concentration decreases as temperature increases, where the NTC effect is pronounced. In this way, the LTO, NTC and HTO regions could be identified.

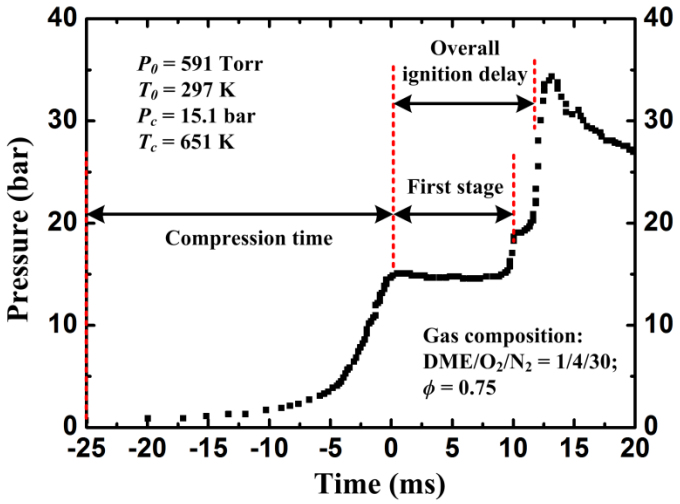

Figure 1.6 Example pressure history during an ignition experiments in a rapid compression machines (RCM) [59]

On the other hand, studies on compression ignition in rapid compression machines (RCM) (e.g., [59-61]) and shock tube reactors (STR) (e.g., [50, 62]) are considered as two powerful methods to validate and refine the existing kinetic models. The agreement between the measured and computational ignition delay results is used as the criterion to evaluate the existing kinetic models. Figure 1.6 shows a typical pressure trace for the ignition of DME/O_2/N_2 mixture (ϕ = 0.75) in a RCM [59] at initial condition of 297 K and 591 Torr, along with the definitions of the first-stage and ignition delay and overall ignition delay . Specifically, ignition delays are defined as the time elapsed from the end of compression stroke to the instant of maximum pressure gradient deduced from the pressure history.

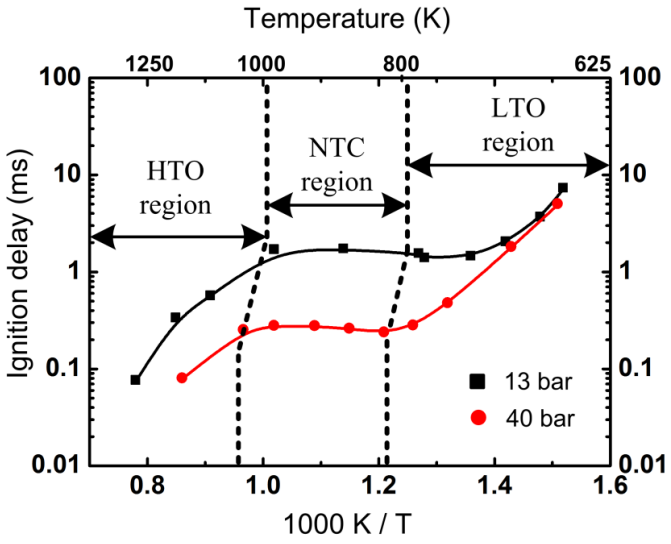

Figure 1.7 Identification of LTO, NTC, and HTO regions of DME in a shock tube reactor [50]

Compressed ignition process of homogeneous fuel-air mixtures under thermodynamic conditions similar to engine have also been investigated in STRs (e.g., [50, 62]). What's different from RCM, the compression in STR is realized not by pistons, but by incident and reflected shock waves. The compression time is considered to be sufficiently short (in the order of μs) compared to the ignition delay times (in the order of *m*s), permitting the investigation of typical diesel engine fuel components at high pressures. The LTO, NTC, and HTO regions could be identified via measurements of ignition delay times. For example [50], as shown in Fig. 1.7, the ignition delay time linearly decreases as temperature increses in the HTO region as well as in the LTO region. While the HTO and LTO region are seperated by a NTC region, where the ignition delay time does not change too much, or slightly increases as temperture increases.

Therefore, as discussed above, the igntion kinetic model is actually established mainly based on the idealistic isothermal or adiabatic conditions in the conventional reactors, such as JSR and PFR. While considering ignition is a process that includes complicated transient processes with an abrupt "switch" from low temperature to high temperature, validations of the kinetic models against well-controlled ignition processes are necessary. Validation of ignition

delay times in RCM or STR is a powerful way to evaluate the kinetic models; however, most of those studies are limited to high pressure compression ignition processes. A simple question maybe posed that, will a cool flame transit to a hot flame at atmospheric pressure? To our best knowledge, no related research could be found to answer this question. This is always important as a safety issue as mentioned in the earlier sections. Additionally, the transition from a cool flame to a hot flame is considered to be strongly influenced by NTC effect. Although it has been indicated that the transition depends on the system reaching the critical temperature at which H_2O_2 decompose into OH radicals, the dominant kinetics in the transition process prior to reach this critical temperature needs further investigation to make it clear.

The objective of this study is to develop an experimental system that could capture low-temperature ignition of DME at atmospheric pressure, especially the transition from a cool flame to a hot flame. Characteristics related to the two-stage ignition mode of DME are expected to be elucidated. Furthermore, the existing oxidation kinetic model of DME is expected to be validated using the developed system. Suggestions based on the validations are expected to be proposed to improve the ignition kinetics.

1.5 Organization of the dissertation

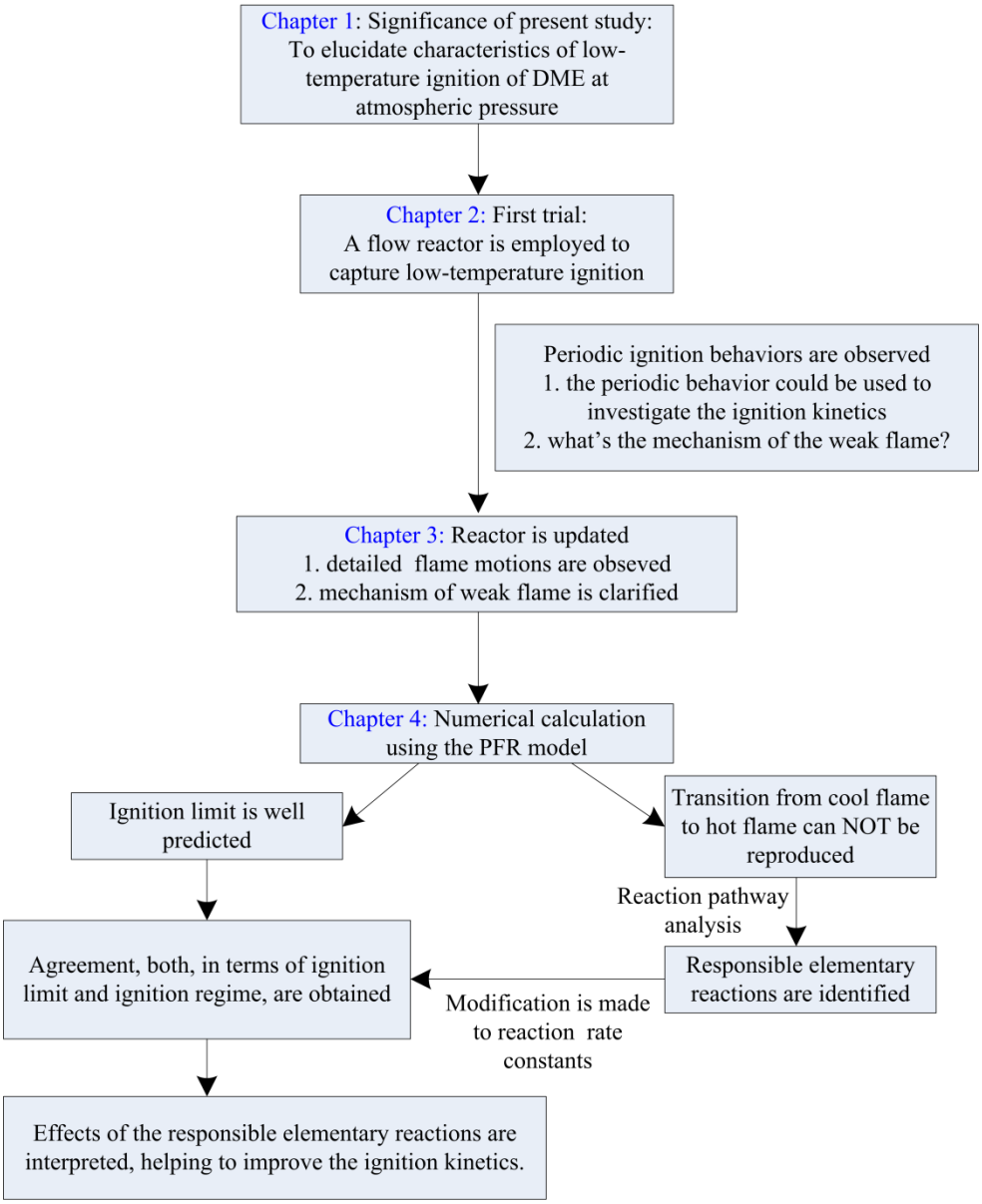

Figure 1.8 Flow chart of the present study

The flow of the present study is shown in Fig. 1.8. Specifically, in Chapter 2, the first attempt to capture the low-temperature ignition of DME in a 1.4 meters long flow reactor is reported. Special attention is given to the observed periodic ignition-propagation-extinction behaviors. Time-sequential gas analyses are conducted to understand the chemical kinetics related to the observed weak flames and hot flames.

Chapter 3 shows the experimental results obtained in an updated flow reactor. The updated transparent flow reactor enables us, not only to clearly observe the hot flame and weak flame motions, but also to confirm the NTC behavior at between 590 K and 730 K. The mechanism of the weak flame is elucidated via multi-position and time-sequential gas analyses.

In Chapter 4, in order to better understand the experimental phenomenon as well as investigate the detailed kinetics, numerical computation is performed using a plug-flow reactor model. Good agreement is found in terms of ignition limit; however, discrepancy exists in terms of transition from a cool flame to a hot flame. Reaction pathway analyses are conducted to find the reactions responsible for the transition. The influence of the key reactions is further discussed based on a modification of the reaction rate constants.

In Chapter 5, conclusions of the present study are summarized, and the recommendations to pursue the future work are proposed.

Chapter 2: Periodic Low-temperature Ignition Behaviors in a Preheated Flow Reactor

In this chapter, low-temperature ignition characteristics of dimethyl ether (DME)/air mixture are studied in an external heated, straight-shaped, plug-flow reactor under atmospheric pressure. Low-temperature ignition of the mixture is attained under a specific narrow range of temperature and equivalence ratio with relatively longer exposure time. Besides the normal hot flame captured in the previous work [63, 64], weak flames are observed for the first time. In order to investigate the low-temperature ignition kinetics, time-sequential gas sampling and analyses are conducted against a typical periodic ignition behavior involved with both weak flames and hot flames.

2.1 Experimental method

Fig. 2.1 shows the schematic of the experimental setup used in this study. Premixed DME/air mixture is supplied into a straight 1400 mm long Pyrex tube (referred as reactor, hereafter) with the inner and outer diameter of 12 mm and 15 mm. Oshibe et al. [56] has claimed that the wall chemical effects are not significant in a 2 mm diameter flow reactor for DME oxidation at 1 atm, therefore, the wall chemical effects in the present system could be safely considered as negligible. Ribbon heater is surrounded in order to control the temperature of the whole reactor. Several small slits are intentionally made for visual access to the luminous emission by the inner reacting flow. A digital video camera (Sony HDR-XR500, 30 frames per second) is used to record the auto-ignition events. *K*-type thermocouples (junction diameter of 1.0 mm) are inserted at 400 and 900 mm from the inlet (later, we may call these points are simply “400 mm” or “900 mm”). The thermocouple junction (sensor part) is placed on the axis of the reactor in order to monitor the temperature of

the flowing gas. Preliminary, we measure multi-points temperature and confirmed that the temperature along the reactor is uniform within an error of 2.0 K at the objective temperature of 500 K. Flow rate of DME is controlled by a mass flow controller (Kofloc model-5100), while flow rate of air is controlled by an orifice flow rate controlling system, which has been calibrated by a bubble flow meter (the accuracy is over 99%).

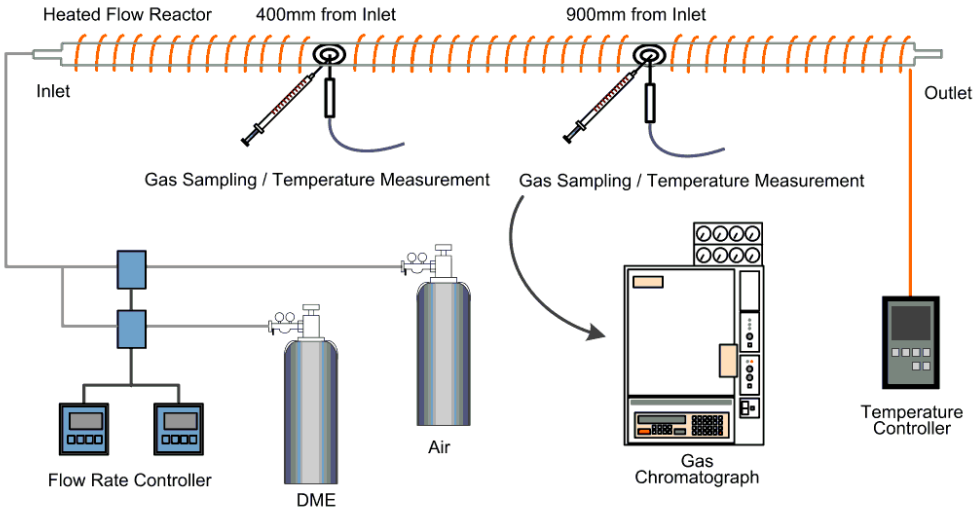

Figure 2.1 Schematic of experimental setup.

Gas sampling points are fixed at 400 mm and 900 mm as well. Gas in the reactor is sampled by a 2.0-ml-volume Pyrex syringe (TOP type-0310) and analyzed by direct injection of 1.0 ml sample into a gas chromatograph (Shimadzu GC-14B) with a thermal conductivity detector (TCD). The Syringe is preheated to 383 K to prevent possible condensations of the sample prior to injection. Hydrogen (H_2), oxygen (O_2), nitrogen (N_2), methane (CH_4) and carbon monoxide (CO) are separated by a molecule sieve 5A 80/100 column, and carbon dioxide (CO_2), acetylene (C_2H_2), formaldehyde (HCHO), dimethyl ether (DME), water (H_2O), methyl formate (CH_3OCHO), and formic acid (HCOOH) are separated by a Proapak T 50/80 column with temperature programming, which starts at 383 K, holding for 23 minutes, and then increases to 443 K at a rate of 20 K/min, keeps at 443 K for 19 minutes. Calibrations for

HCHO, H_2O, CH_3OCHO, and HCOOH are conducted by using the vaporization gases of corresponding solutions.

Here let us give the typical sequence to induce the first ignition in this study. First, the gas temperature is controlled at 483 K, mixture flow rate at 44.2 ml/min, and mixture equivalence ratio at 1.5-2.0. In that case, the oxidation process slowly proceeds without any subsequent auto-ignition to possibly reach equilibrium states; this is called "stable oxidation" hereafter. The stable oxidation is remained for about two or three hours in order to ensure to stay the equilibrium states, then the temperature is increased or decreased with the heating rate of about 11 K/min within the range from 463 K to 513 K. The ignition occurs at certain temperature, which was considered as the "optimal auto-ignition temperature". After tens of minutes of mild oxidation at the optimal auto-ignition temperature, the first ignition is finally achieved.

Once ignition is experienced, the flame is generated and propagates passing through the thermocouples. Then the flame is quenched at the inlet and temperature of gas in the reactor starts to decrease gradually until the controlled temperature as the fresh DME/air mixture flows into the reactor. Following some delays, re-ignition occurred periodically or chaotically. The temperature increment as well as the periodic duration (in the case of periodic behavior) depends on the flow velocity, temperature, and equivalence ratio of the mixture.

The supplied mixture flow rate is fixed to 78 ml/min. At 488 K, the corresponding flow velocity is 18.8 mm/s, and the corresponding exposure time is about 21 s and 48 s at 400 mm and 900 mm, respectively. Adopting this flow rate, the ignition is found at around 900 mm so that we could capture the temperature history at the ignition position.

2.2 Low-temperature ignition regime

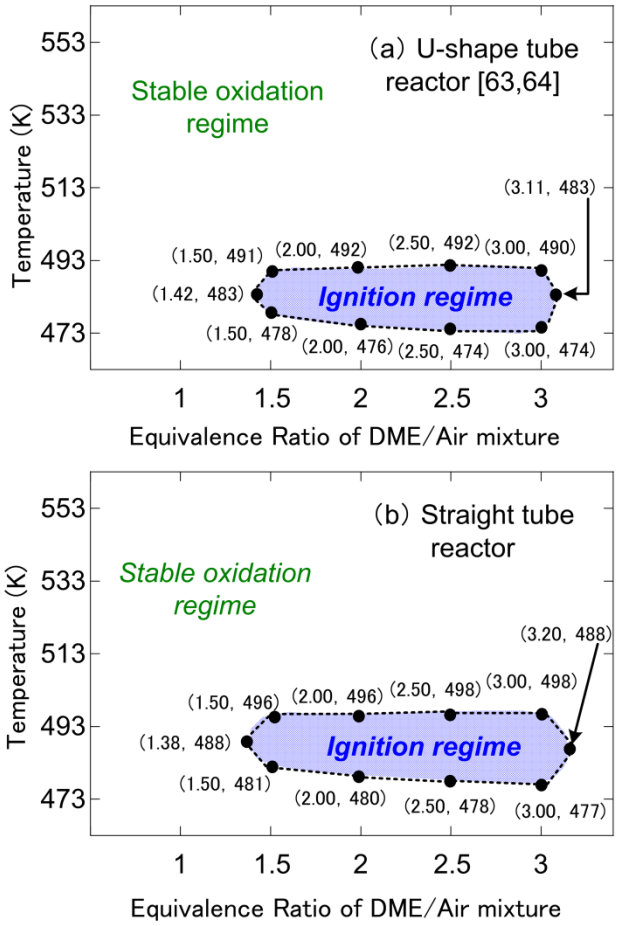

Figure 2.2 Low-temperature ignition regime of DME-air mixture.

Fig. 2.2 shows the obtained ignition regime in temperature-equivalence ratio plane. Note that the definition of ignition herein is the sudden temperature rise associated with observable luminous light emission. The ignition could be only found in the limited range of temperature and equivalence ratio shown as blue shadow in the Figure, otherwise no apparent light emission or temperature rise was detected, mild oxidation slowly occurred instead. The ignition regime obtained in the present study is consistent with our previous results by using a U-shape reactor [63, 64] except for about 5 K differences in upper and lower boundary. These differences could result from the uncertainties of the K type thermocouples (±2.5 K),

temperature disunities along the reactor (2.0 K), and the irregular shape of the previous U-shape reactor.

After ignition is experienced, two kinds of flames are identified: one is a dim blue flame, which might partially consume the mixture gas, is defined as “weak flame”; the other one is a relatively bright flame, which might completely consume the mixture gas, is defined as “hot flame”. Appearances of these two modes of flame depend on the condition applied here. In the following, let us discuss this issue in detail.

2.3 Periodic ignition-propagation-extinction behavior

2.3.1 Equivalence ratio dependence

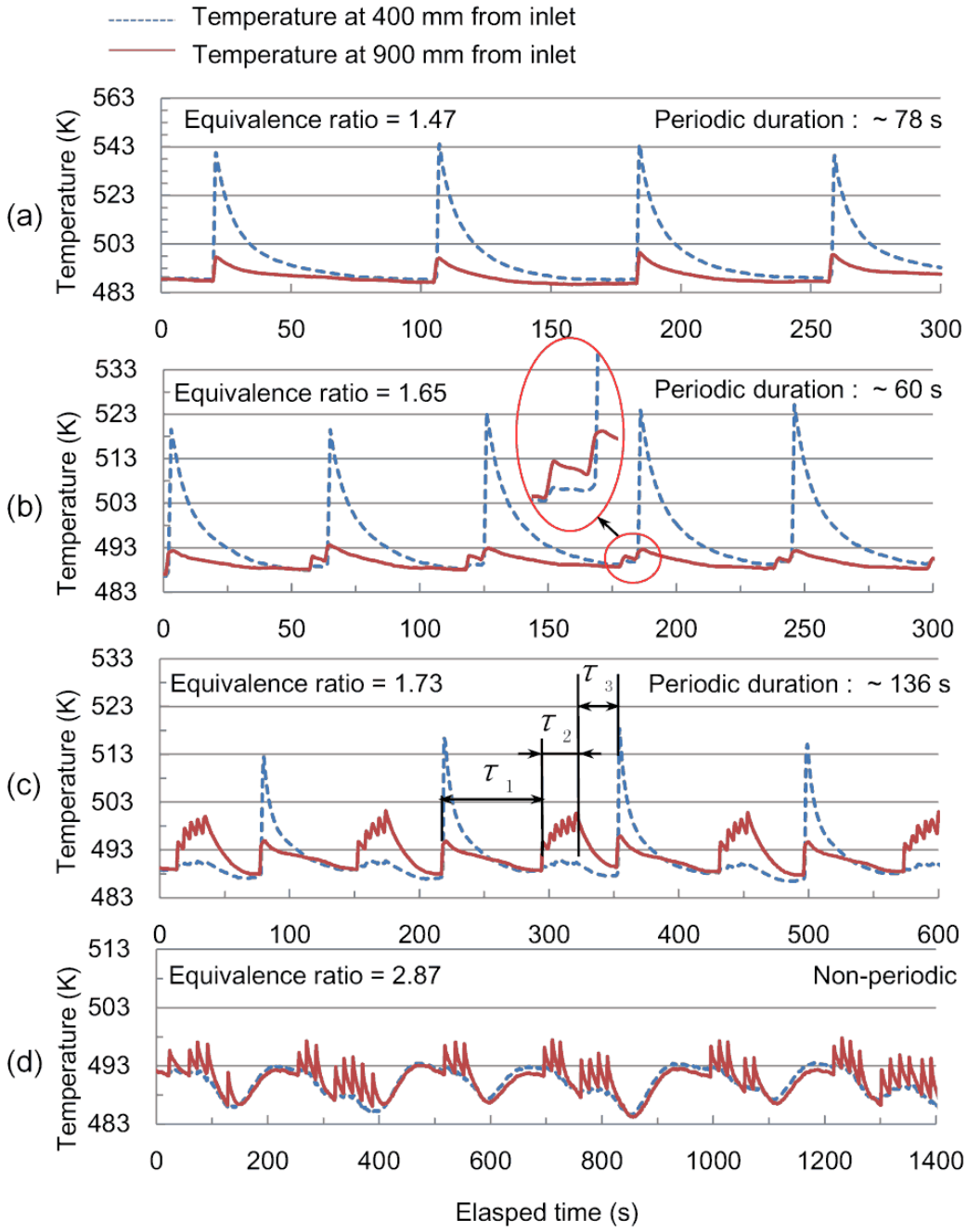

Figure 2.3 Temperature histories of various periodic ignition behaviors.

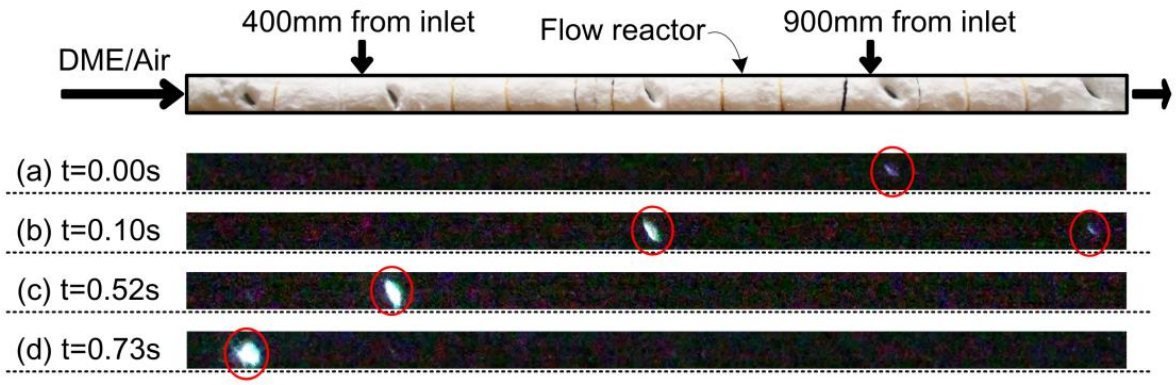

Figure 2.4 Direct photographs of the hot flame propagation. Red cycles indicate the locations where the flames were observed.

Fig. 2.3 shows a series of temperature histories at different equivalence ratios of the mixture. The temperature is controlled at 488 K. Equivalence ratios are: (a) 1.47; (b) 1.65; (c) 1.73; (d) 2.87. The blue dashed line represents the temperature history at 400 mm from inlet, while the red solid line represents that at 900 mm from inlet. Note that the measured temperature at the ignition becomes much lower than the actual field temperature due to insufficient residence time to reach thermal equilibrium, thus the thermocouple signal in this study is only used to detect the time when the generated flame passes through that location. Periodic hot flames are obtained at the equivalence ratio of 1.47, as shown in Fig. 2.3-a. Under this condition, a luminous hot flame appears after the ignition at around 900 mm and then propagates both upstream and downstream, eventually is quenched at the inlet and outlet. The flame propagation is recorded by the video camera as shown in Fig. 2.4. The circles indicate the locations where the flames are captured. The hot flame propagates throughout the tube thus refreshes the whole reactor. Then the fresh mixture gas flows into the reactor, and re-ignition is experienced when and where the ignition condition meets. In this way, we have periodic ignition behaviors. The periodic duration is about 78 s, which is quite robust.

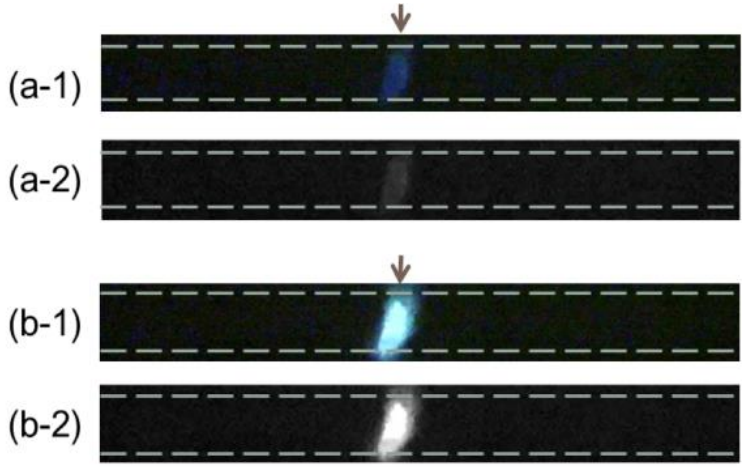

Figure 2.5 Flame images taken by a digital video camera at 900 mm from inlet. (a-1) direct image of weak flame; (a-2) gray scale image of weak flame; (b-1) direct image of hot flame; (b-2) gray scale image of hot flame

As the equivalence ratio increases from 1.47 to 1.65, the hot flame at 900 mm is "separated" into two flames, namely a weak flame and a subsequent hot flame. Fig. 2.3-b shows the temperature history under this condition. As indicated by the cycle in the figure, the former peak corresponds to a dim blue flame (weak flame), while the latter one corresponds to a relatively bright flame (hot flame). Flame images taken by the video camera at 900 mm are shown in Fig. 2.5. Fig. 2.5-a-2 and b-2 are the gray scale images, and the gray value of the hot flame (62.38 a.u.) is more than three times higher than that of the weak flame (17.22 a.u.), suggesting that the hot flame is much brighter than the weak flame. Fig. 2.6 depicts the potential flame motions against this behavior with the cycle duration of 60 s, schematically.

When the equivalence ratio is set to 1.73, another periodic ignition behavior is obtained, the temperature history of which is shown in Fig. 2.3-c. The frequency of the periodic behavior is also robust at about 136 s per cycle. Each cycle includes three featured periods: (1) The first mild oxidation period τ_1, the duration of which is about 74-78 s; (2) The multiple "weak flames" period τ_2, which involves about 5-7 weak flames, and (3) The second mild oxidation

period τ_3. The time interval between the neighboring two weak flames in τ_2 is about 5-7 s. The weak flames here also initially appear at around 900 mm. Multiple small oscillations

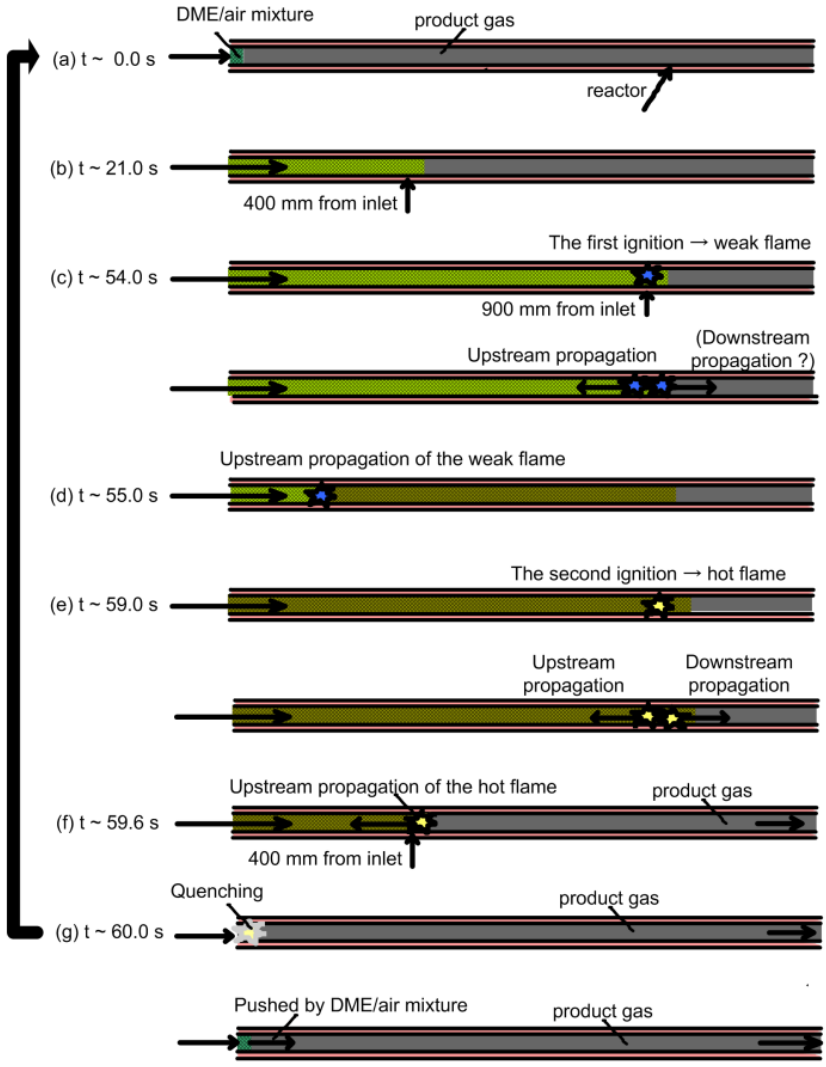

Figure 2.6 Schematic illustration of a periodic two-stage ignition behavior.

in temperature can be observed at 400 mm simultaneously, which should be due to the upstream propagation of the weak flame. After the multiple weak flames appear, no flaming is detected during the period of τ_3, which takes about 40-50 s until a hot flame appears at

around 900 mm. The hot flame consumes all fuel components by propagation throughout the reactor, and then proceeds to next cycle.

As the equivalence ratio increases higher than 1.80, the reaction system shows a behavior with chaotic weak flames, as shown in Fig. 2.3-d. Weak flames are observed, however the hot flame is never attained at such higher equivalence ratio. Additionally, any apparent periodic behavior is captured under this condition, but random appearances of weak flames are always experienced.

Table 2-1 Flame responses against various DME/air mixture equivalence ratios. Temperature is controlled at 488K. (○: existence, ×: nonexistence)

equivalence ratio		<1.38	1.38~1.58	1.58~1.80	1.80~3.20	>3.20
flame response	hot flame	×	○	○	×	×
	weak flame	×	×	○	○	×

Table 2-1 summarizes the different flame responses against the equivalence ratio. It is indicated that the sequence of flame responses observed in the auto-ignition regime as the equivalence ratio decreases is:

[weak flames] → [weak flame(s) + hot flame] → [hot flame].

2.3.2 Similarities to FREI [17, 56, 65, 66]

Similar periodic ignition and extinction behaviors, termed flames with repetitive extinction and ignition (FREI), have been observed in a heated microchannel for variety of hydrocarbons mixture such as methane-air [65, 66], DME-air [56] , and n-heptane-air [17]. The ignition of FREI occurs downstream due to the high wall temperature (>1000K) and the ignition front propagates upstream. The flame is finally quenched in the upstream due to the

large heat loss to the low temperature wall. Following some time delays after quenching, re-ignition is experienced as the fresh mixture flows in. In the present study, the reactor temperature was always controlled at relatively low temperatures (<500 K), not like that in the series of previous FREI studies. This is the reason why we have extremely longer ignition delays (tens of seconds) compared with that in the study [56] (20-100Hz, i.e. 0.01-0.05 s delay, for DME/air mixture).

A recent paper by Nakamura et al. [67] investigated the detailed process of FREI for a methane/air mixture. It numerically reproduced the flame bifurcation due to the separation of the unburned mixture in high-temperature ignition phase. What's more important, this paper newly found that the intermediates such as CO, CH_3, OH, and H could cause bifurcations of heat release peak in the weak reaction phase (at the low-temperature side). It is interesting to see that, as stated above, the bifurcated flames have been observed in the present study (i.e. the hot flame occurs at around 900 mm and propagates upstream and downstream). However, due to the fact that different kinds of intermediate products should be produced during the ignition events in the present system, there is no guarantee that the scenario leading to the ignition here is consistent with the FREI study (e.g., [67]). Moreover, the main objective in this study is to investigate the trigger of the two-stage ignition in the low-temperature, which occurs somewhere in the "long" mixing zone between the fuel and the products; it could generate key important intermediates there. In this way, the species analysis during the ignition event is very important. In the next, we will discuss the issues about the intermediates based on the gas analysis results obtained by GC.

2.4 Time-sequential gas analyses

Time-sequential gas analyses are conducted in the case of the typical periodic ignition behavior shown in Fig. 2.3-c, each cycle of which includes multiple weak flames and one hot flame. The reason to pick this condition is that, mild oxidation, weak flames and hot flames are all included in each cycle, which enable us to investigate the roles of the intermediates in the transition from mild oxidation to weak flame, and then hot flame.

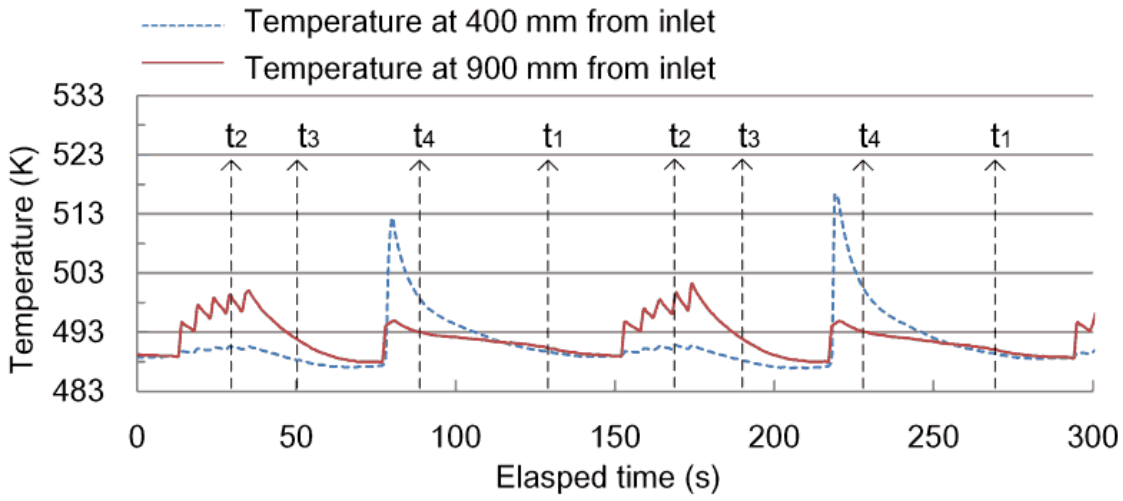

Figure 2.7 Gas sampling moments in each cycle.

The blue dashed line represents the temperature history at 400 mm, while the red solid line represents that at 900 mm. t_1: 50 s after the hot flame; t_2: 15 s after the first weak flame; t_3: 15 s after the last weak flame; t_4: 10 s after the hot flame.

Four sampling moments (t_1 to t_4) in each cycle, as shown in Fig. 2.7, are set as follows:

t_1: 50 s after the hot flame;

t_2: 15 s after the first weak flame;

t_3: 15 s after the last weak flame;

t_4: 10 s after the hot flame.

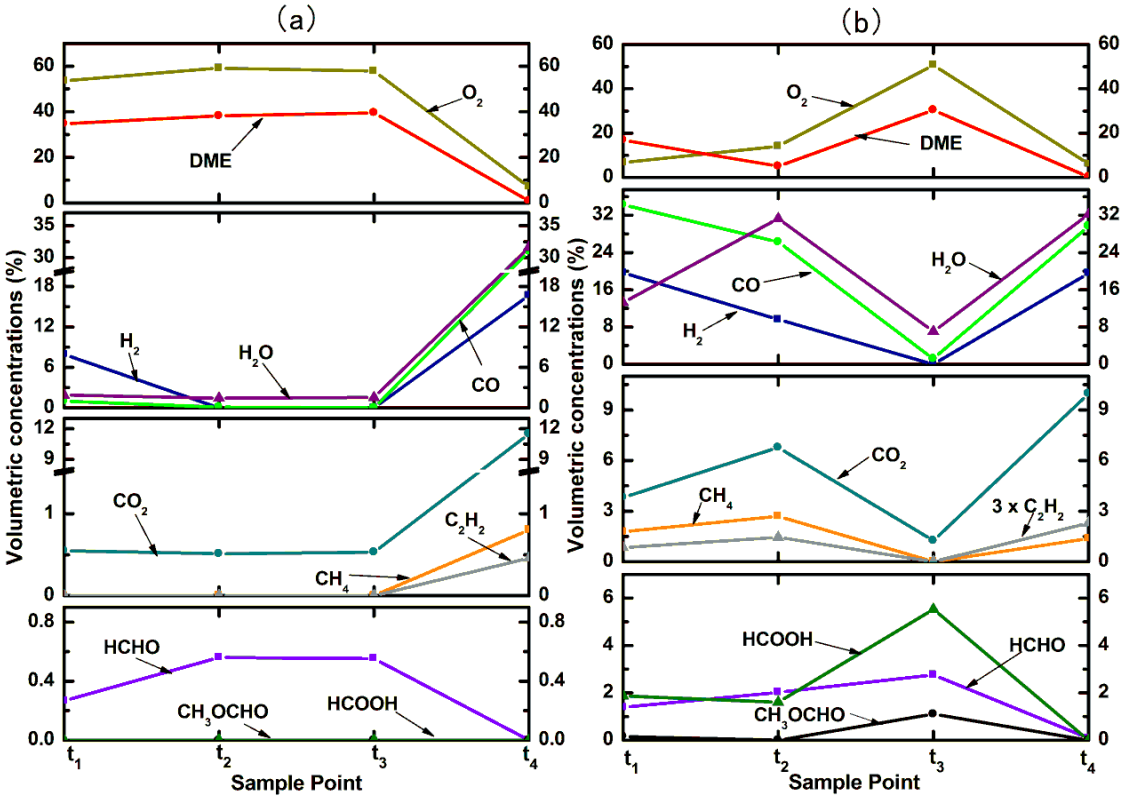

Figure 2.8 Species volumetric concentrations normalized without N_2 towards the typical periodic ignition behavior shown in Fig. 2.3-c.

(a) gas compositions at 400 mm; (b)gas compositions at 900 mm.

For gas sampling, rapid extraction is accomplished within one second (< 1.0 s) to ensure that the sampling was made at the objective sampling moment. As long as the extraction time is controlled as less than one second, no apparent difference in gas analysis results is found with different extraction speeds. Considering the sampling volume (1.0 ml) is much smaller than the volume of the reactor tube (about 158 ml), the disturbance to the flow field is considered as negligible. The gas sampling is made at 400 mm and 900 mm. Thanks to the concrete periodic behavior, we are able to conduct several times of analyses at each sampling moment to ensure the reproducibility of the results. Fig. 2.8 shows the gas analysis results. The volumetric concentrations of all species are normalized without nitrogen.

As stated previously, it takes about 21 s and 48 s for the fresh mixture gas to reach at 400 mm and 900 mm, respectively. Therefore, gas composition at t_1 for the location of 400 mm should be mostly replaced by the fresh DME/air mixture except certain quantity of H_2 (it might be due to the relatively higher diffusion coefficient of H_2). Interestingly, at the 900 mm point, the relatively large amount of CO, CO_2 and H_2O exist; they might be the products of upstream propagated hot flame in the previous cycle. More importantly, it should be noted that HCHO and HCOOH also exist there; probably these would be originally formed by the mild oxidation of DME/air mixture, not the low-temperature ignition.

Point t_2 is during the multiple weak flames period τ_2, as indicated in Fig. 2.3-c. It is understood that, the weak flame can only partially consume the DME/air mixture, thus DME and O_2 always exist at this time. Compared with t_1, the volumetric concentration of CH_4 and C_2H_2 at 900 mm is higher, which indicates that CH_4 and C_2H_2 might be the products due to the weak flames.

Point t_3 is after the last weak flame of period τ_2, i.e. during the second mild oxidation period τ_3. Thanks to the previous oxidation periods τ_1 and τ_2, a plenty of intermediates accumulate in the system. Therefore, the intermediates including HCHO, HCOOH and CH_3OCHO reach their maximum concentrations at 900 mm. No HCOOH and CH_3OCHO are detected at 400 mm, which might be due to the insufficient time to produce and accumulate there. The disappearances of CH_4 and C_2H_2 at this time imply that both of them result from flames (weak or hot) but not the mild oxidation.

As mentioned previously, the second mild oxidation period τ_3 is ended by a hot flame, which occurs at around 900 mm and then refreshes the reactor by flame propagation. As shown at t_4, DME and other intermediate species (HCHO, HCOOH and CH_3OCHO) are completely consumed and converted into CO, CO_2, H_2O, H_2, CH_4, and C_2H_2. The

propagation of the hot flame makes it almost uniform throughout the reactor, showing that the composition at 400 mm is almost same as that at 900 mm.

2.5 Potential low-temperature ignition kinetics

According to the existing model proposed by Fischer et al. [48], the mechanism of DME oxidation at low-temperature is dominated by the competition between the chain-propagation and chain-branching reaction steps. The chain-branching steps should be responsible for the low-temperature auto-ignition (explosion). As stated above, chain-branching in the DME oxidation system depends on the availability of the CH_2OCH_2OOH radical. This chain-branching precursor is expected to be relatively stable and has a long lifetime below 600 K [43, 48, 68]. During the experimental work by Liu et al. [46], the reactions responsible for the low-temperature ignition were first detected at about 533 K with residence time of 3.9 s. It is suggested that the longer exposure time in our study may give a fairly long enough time for the CH_2OCH_2OOH radical accumulating and reacting with O_2, and then undergo the decomposition reactions to release more than one reactive radical (mainly OH radicals) to realize a chain-branching. However, once the temperature gets higher than 600 K, the β -scission of the precursor CH_2OCH_2OOH radical is imposed to be dominant in the process of DME oxidation [48]. Therefore, the chain-branching reactions can be suppressed by the β -scission of the precursor (CH_2OCH_2OOH) on account of the sudden heat release of the weak flame. Thus, the weak flame represents the "self-inhibited behavior" that prohibits consuming the reactants completely.

The decomposition reaction of one CH_2OCH_2OOH radical into two HCHOs and one OH has been proposed as the main chain-propagation pathway, which occurs in the temperature range of 600-725 K [43, 48]. However, we have detected non-negligible amount of HCHO, HCOOH, and CH_3OCHO in the mild oxidation period (see Fig. 2.8-b), suggesting that there should be other chain-propagation pathways under 500 K. The model of Curran et al. [48] invokes the species hydroperoxymethyl formate (HPMF, HO_2CH_2OCHO) to be responsible for the second OH radical release of chain-branching pathway. However, Liu et al. failed to

detected HPMF and indicated that HPMF is less thermally stable than assumed or there are other reactions of HPMF [46]. Moreover, Anderson and Carter showed that the fate of HPMF is potentially very complicated and proposed several possible decomposition paths of HPMF [69]. Once the HPMF follows the decomposition reactions that release no OH radical, it turns to be a new chain-propagation pathway. The ambiguity of reactions related to HPMF also can be one of the important reasons that cause the strong temperature dependency of the auto-ignition regime as shown in Fig. 2.2.

According to the gas analysis results, CH_4 is found to be one of the key products of the low-temperature ignition, which is consistent with the experimental and numerical results of Oshibe et al. [56]. Moreover, the results indicate C_2H_2 to be another product formed through the explosive reactions. Traditionally, the transition from steady state to explosive kinetics often results in cool flame. Again, the cool flame does not reach the adiabatic flame temperature, and, therefore, the fuel is not fully consumed. Thus, it is considered that the weak flame captured in present study might correspond to the transition state between mild oxidation and low-temperature explosion (hot flame in this study). According to the models established by Dagaut et al. [43] and Curran et al. [48], one DME molecule needs one oxygen molecule to complete the chain-propagation pathway:

$$CH_3OCH_3 \xrightarrow{-H} CH_3OCH_2 \xrightarrow{+O_2} CH_3OCH_2OO \rightarrow \ldots + OH.$$

However, it needs two oxygen molecules to complete the chain-branching pathway:

$$CH_3OCH_3 \xrightarrow{-H} CH_3OCH_2 \xrightarrow{+O_2} CH_3OCH_2OO$$
$$\rightarrow CH_2OCH_2OOH \xrightarrow{+O_2} \ldots + 2OH$$

Thus the optimum equivalence ratio to complete the chain-branching pathway should be smaller than that of the chain-propagation pathway. Therefore, as the equivalence ratio

decreases, it is transited from the weak flame to the hot flame, as shown in Fig. 2.3 and Table 2-1.

2.6 Conclusions

Two kinds of flames (weak and hot) in DME/air mixture are captured when the temperature and equivalence ratio were finely controlled in certain narrow range under atmospheric pressure. During the specific narrow ignition regime, weak flames transit to the hot flames with decreasing of equivalence ratio from 3.20 to 1.38. It is concluded that the enhancement on chain-branching reaction pathway by relatively sufficient oxygen should be responsible for this transition. A specific case at equivalence ratio of 1.73, which includes both weak flames and hot flames, appears as a transition state between the weak flame and the hot flame. Time-sequential gas analyses are conducted against this specific case, indicating CH_4 and C_2H_2 act as two kinds of species formed due to the low-temperature ignition. On the other hand, the intermediates HCHO, HCOOH, and CH_3OCHO, formed due to the mild oxidation, are completely consumed by the hot flame. The observed auto-ignition behaviors should be induced by the well-known chain-branching precursor CH_2OCH_2OOH radical, which may accumulate in a relatively longer exposure time.

The periodic ignition behavior would be a preferrable scenario to investigate the ignition kinetics. However, some limitations are encountered in the present system. First, the chemical property of the weak flame is still questionable: is the weak flame a cool flame? Moreover, the detailed flame motions in the reactor are not clear and waited to be clarified. Updating of the flow reactor system is necessary and further experimental work is needed to make the story clear.

Chapter 3: Transition from Cool Flame to Hot flame and the NTC behavior

In Chapter 2, periodic ignition events involved with two kinds of flames, which were named as “weak flame” and “hot flame”, were captured in a preheated flow reactor. However, although the small slits were made for observation purpose, the precise dynamic behaviors of the flames were not clearly identified. On the other hand, the reactor temperature was controlled by an on-off controller (Omron E5CN-RT). Although temperature uniformity along the reactor could be realized, it frequently switched between heating (on) and cooling (off) states. According to a recent study [15], heating rate may strongly affect the ignition of hydrocarbon/air mixtures at low-temperatures (< 600 K). Hence, the temperature control method should be improved.

To overcome the above mentioned problems, in this chapter, we newly develop a “transparent” flow reactor with well-controlled temperature profiles to further investigate the low-temperature ignition regime of DME/air mixture at atmospheric pressure. First, the conditions to appear flame and the NTC behavior are identified at various combinations of temperature and equivalence ratio (T - ϕ) and the stability map (consisting of “ignition” and “stable oxidation”) is depicted in the T - ϕ plane. Within the ignition zone, detailed flame (weak flame and hot flame) behaviors are interpreted. For the first time, we report a periodic weak flame behavior of DME/air mixture in a well-controlled flow reactor system. Additionally, GC analyses toward the ignition conditions, as well as the stable oxidation conditions in the NTC zone are conducted. Finally, the chemical kinetics related to cool flame and NTC behavior are further discussed.

3.1 Updated flow reactor

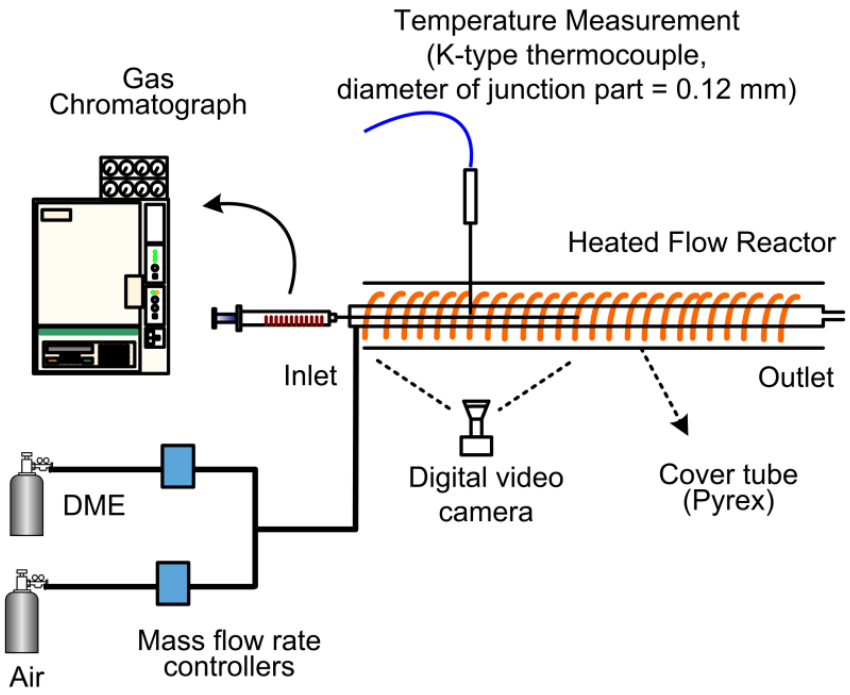

Figure 3.1 Schematic of the updated experimental set-up

Figure 3.1 shows the updated flow reactor. In order to obtain clear observation, a 60 cm transparent straight Pyrex tube (inner diameter 12 mm and outer diameter 15 mm) is used as a flow reactor, in which premixed DME/air mixture continuously flows. A Wire heater (Sakaguchi KAF065, diameter of 0.65 mm, 4.189 Ω/m) wraps uniformly around the flow reactor from 5 cm to 55 cm and is used to control the reactor temperature. The reactor is placed inside another Pyrex tube (inner diameter 35 mm and outer diameter 40 mm) to prevent heat losses to environments. A DC power supply (Kikusui PWR800L) with a resolution of 0.01 V is employed to control the voltage over the wire heater in order to exclude the possible heating rate effects caused by the on/off controller used in the previous work. A digital video camera (Sony HDR-XR500, 30 frames per second) is used to record the flame images. Gas is sampled using a 2-ml-volume Pyrex syringe (TOP type-0310) with a chromium plated needle (inner diameter of 0.7 mm and out diameter of 1.0 mm), and analyzed by direct injection of 1.0

ml sample into a gas chromatograph (Shimadzu GC-14B) with a thermal conductivity detector (TCD). The Syringe is preheated to 383 K to prevent possible condensations of the gaseous sample prior to injection. The gas GC analysis method is same as previous in chapter 2. The supplied gas mixture flow rate here is fixed to 24.5 ml/min (~ 3.6 mm/s at inlet).

Prior to the experiments, the potential species concentration gradient along the radial direction is carefully checked. It is confirmed that, at the same axial position, the mole fractions of the reactant species (e.g. O_2) are slightly higher on the centerline than that near the reactor surface, and the discrepancy is at most 3.0 %. On the contrary, the mole fractions of the product species (e.g. CO) are slightly higher near the reactor surface than that on the centerline, and the discrepancy is at most 6.7 %. During the experiments, gases are sampled on the centerline.

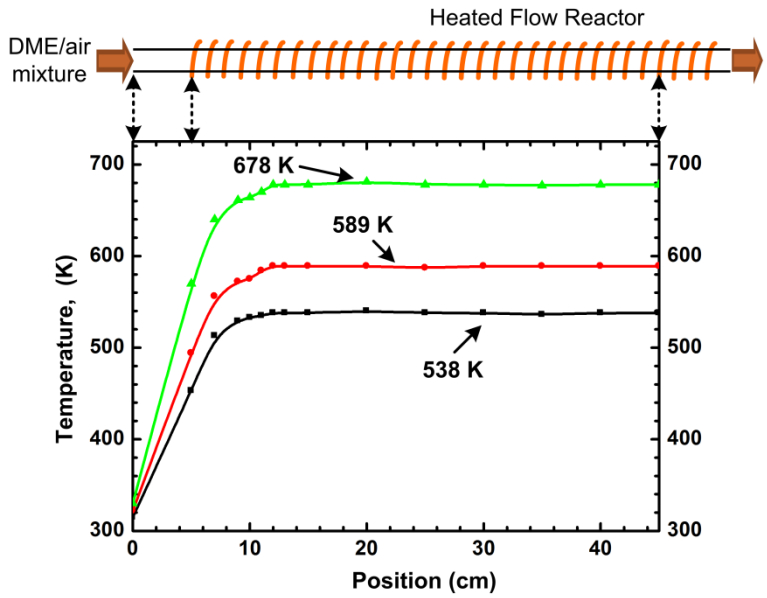

Figure 3.2 Controlled temperature profiles of the flow reactor

Prior to the experiments, the temperature profiles at the reactor centerline are measured for a 24.5 ml/min air-only condition, which are defined as “reactor temperature profiles”, as shown in Fig. 3.2. Note that the temperature reaches an equilibrium value around 12 cm and remains uniform (< 3 K) through the left length of the reactor. We define this equilibrium temperature

as the “reactor temperature, $T_{R,\ ex}$” hereafter. Temperature is measured by K-type thermocouples (junction diameter of 0.12 mm).

3.2 Ignition regime

3.2.1 Ignition limit

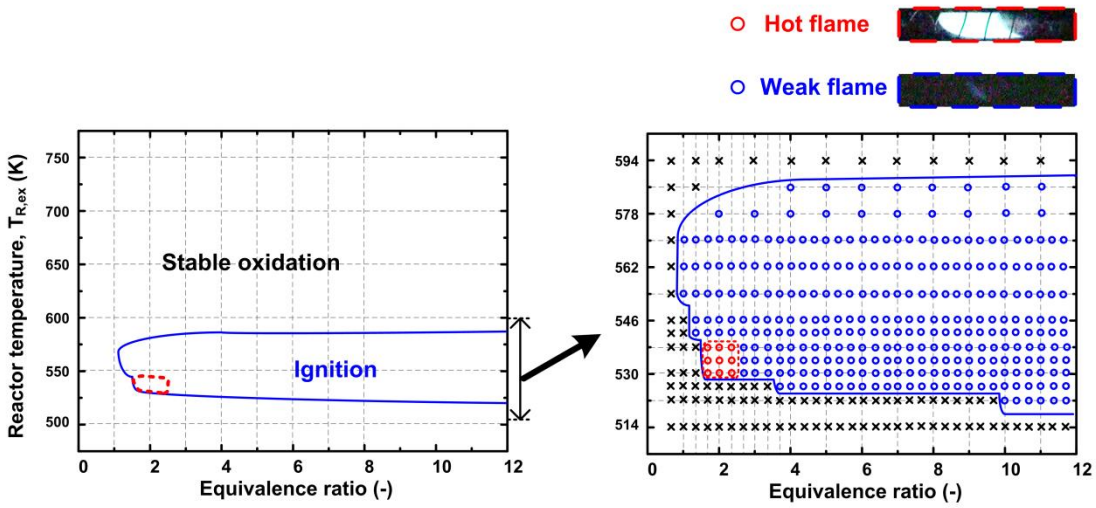

Figure 3.3 Low-temperature ignition limit of DME/air mixture

Figure 3.3 shows the ignition limit in the reactor temperature-equivalence ratio ($T_{R,ex}$ - ϕ) plane based on the definitions above. Here, the ignition is defined as the local event which sudden temperature rising larger than 15 K/s. Open/closed circles indicate ignition conditions, while crossed symbols indicate stable oxidation (non-ignition) conditions. As post-ignition event, two distinct types of flaming are followed: the one is that a dim blue flame locally propagates and quenches somewhere inside the reactor, is defined as "weak flame", as indicted by open cycles; and the other is that a much brighter flame propagates till the inlet, is defined as "hot flame", as indicated by closed cycles.

It is seen that the ignition tends to occur at fuel rich conditions (ϕ > 1.0) between 520 K and 590 K. According to the previous studies at atmospheric pressure [57, 58], the typical cool flame zone of DME is located between 525 K and 590 K. Under most conditions within the ignition zone in this study, the weak flame is always associated. The weak flame, therefore, might correspond to cool flame or the flame fails to transit to the subsequent hot flame. On

the other hand, the hot flame appears only in the narrow range of relatively low temperature (530 K - 540 K) and low equivalence ratio (1.5 - 2.5), implying that the cool flame successfully transits to the hot flame.

3.2.2 Distinct motions of weak flame and hot flame

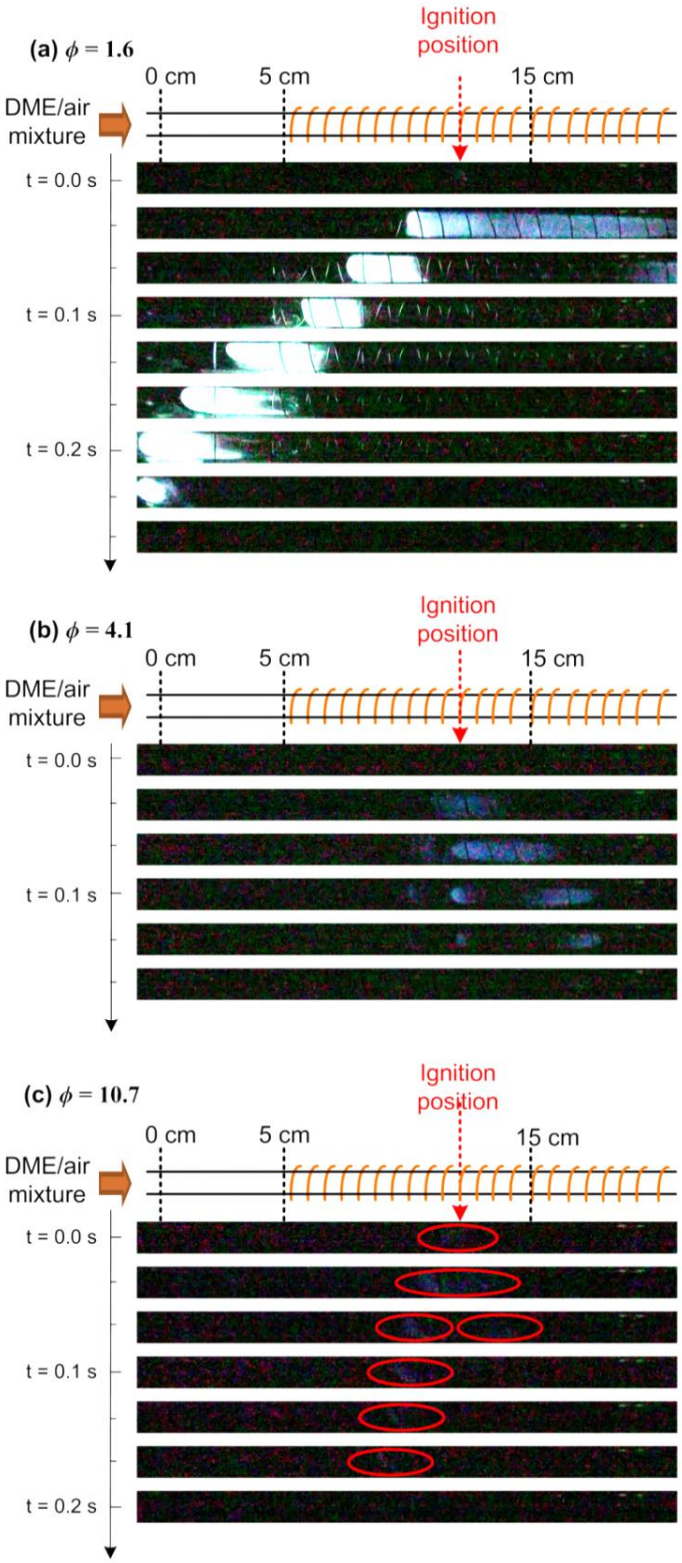

Figure 3.4 Flame propagation images after ignition at $T_{R,\,ex}$ = 538 K, (a) ϕ = 1.6, (b) ϕ = 4.1, and (c) ϕ = 10.7

In the post-ignition event, the subsequent weak flame and hot flame propagate in various ways. Fig. 3.4 shows typical flame behaviors at different equivalence ratios (ϕ = 1.6, ϕ = 4.1, and ϕ = 10.7) at the same controlled temperature of 538 K. The ignition occurs at 12.2 cm from the inlet, followed by a main flame propagates upstream and a bifurcated flame propagates downstream. The main flame quenches somewhere inside the reactor (for weak flames) or at the inlet of the reactor (for hot flames). Then, the incoming fresh mixture mixes with the product gas remained in the reactor and flows downward in turn. After a certain time delay, re-ignition occurs at the same location where the first ignition is identified. In this way, we can observe the periodic behaviors with ignition, flame propagation and extinction. Fig. 3.4-a shows a typical hot flame propagation at ϕ = 1.6, and Fig. 3.4-c shows a typical weak flame propagation at ϕ = 10.7. It clearly shows that the hot flame is much brighter than the weak flame. After the ignition, the hot flame propagates to the inlet and quenches there, while the weak flame is too weak to sustain the propagation, therefore, it quenches at around 9 cm from the inlet. Moreover, the estimated propagation speeds by the images are remarkably different: it is about 62 cm/s for the hot flame, while lower than 18 cm/s for the weak flame. Such large discrepancy indicates that the dominant chemical kinetics must be different.

When the equivalence ratio is set at ϕ = 4.1, an interesting "triple weak flames" mode is observed, as shown in Fig. 3.4-b. In this flaming mode, the flame bifurcates into three flames immediately after the ignition: one flame propagates upstream, another one keeps (almost) stagnant, and another one propagates downstream. Since the flame in the upstream side does not consume out the fuel or oxygen, unreacted fuel (or produced intermediates) and oxygen are remained at around the ignition position, and forms a stagnant flame there. The flame propagation speed relative to the local mixture flow velocity, $S = u - v$, where u is the local mixture flow velocity and v is the velocity of flame front. Flame stagnation indicates $v = 0$, therefore we have $S = u$ = 6.8 mm/s (u is calculated from the inlet velocity = 3.6 mm/s). Such

low propagation speed is another evidence to reveal that the reaction rate is extremely low for weak flame therefore readily to quench.

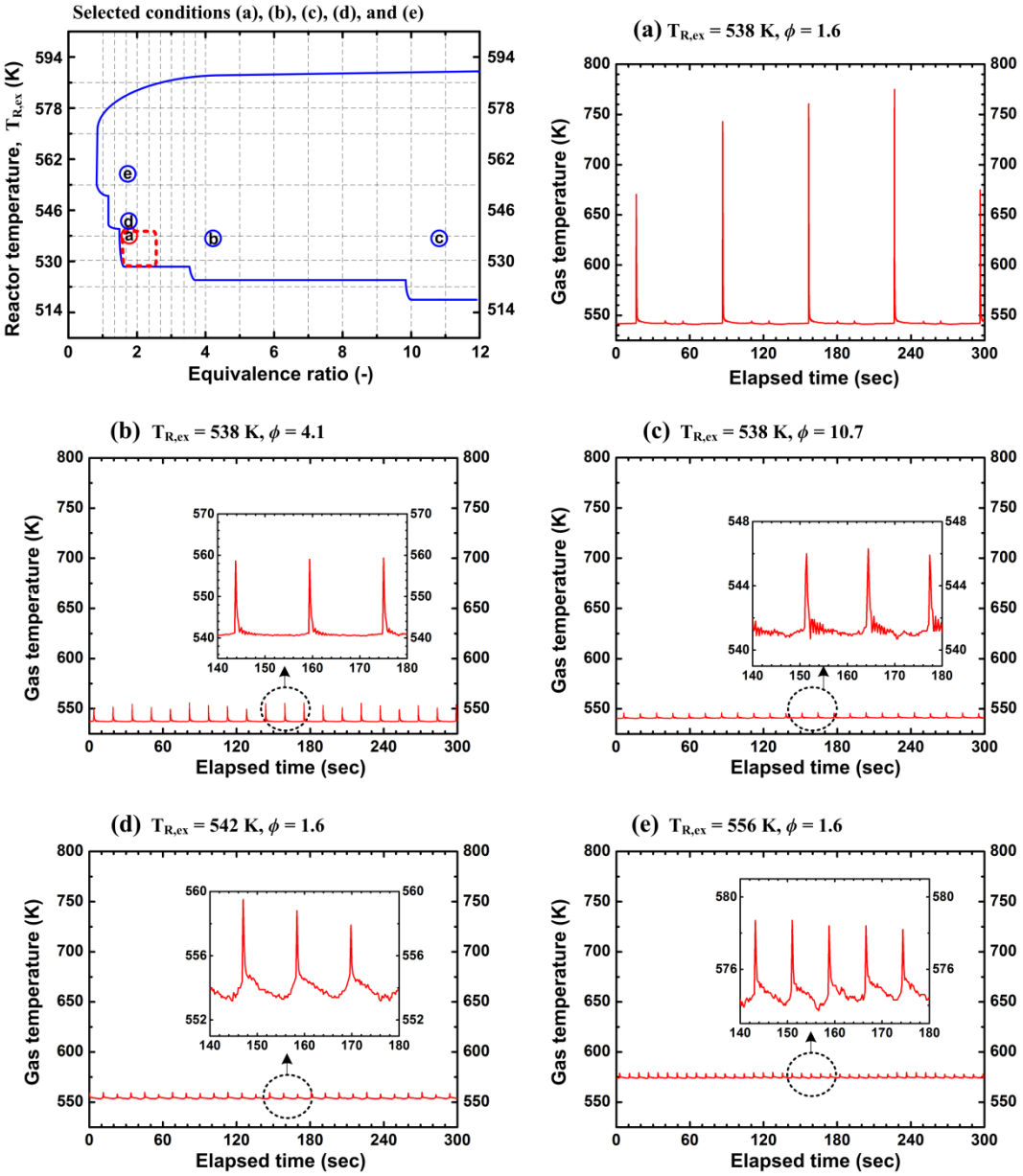

Figure 3.5 Gas temperature histories of the periodic ignition behaviors

As shown in Fig. 3.4, the ignition and the subsequent flame propagation is accomplished within less than 0.3 s, while, the period of cyclic behavior for achieving the ignition is much longer (tens of seconds). In order to clearly show the periodic ignition behaviors, a K-type thermocouple (diameter of junction part = 0.12 mm) is set at 12.2 cm to capture the gas

temperature there. Fig. 3.5 shows the selected conditions and the corresponding temperature histories. Condition (a) corresponds to a periodic hot flame behavior, while the others (b, c, d, and e) correspond to periodic weak flame behaviors. It is observed that periodic duration remains constant from event to event. The periodic duration for achieving one hot flame (about 70 sec) is much longer than that of a weak flame. This is because the hot flame propagates till the inlet, while the weak flame only locally propagates, and therefore the mixture needs a longer time to reach the condition to achieve the next ignition after the hot flame propagation. Moreover, the measured temperature increment due to the occurrence of a hot flame (more than 200 K) is much larger than that due to a weak flame (tens of K or less), indicating the heat release of a hot flame is much larger than that of a weak flame. Note that similar repetitive phenomenon with frequent flames due to low-temperature ignitions have been captured in the propane oxidation [70], DEE oxidation [10] and the acetaldehyde oxidation [11] by using jet-stirred reactors, which were named as "oscillatory cool flames". The present study shows that similar behavior is able to be achieved in a laminar flow reactor configuration.

However, identifications between the weak flames (again, this might be the cool flames) and the hot flames based only on visual observations or temperature measurements are not enough. In the following sections, we shall present the additional results of gas analyses toward these periodic flame behaviors.

3.3 Mechanism of the periodic weak flame behavior

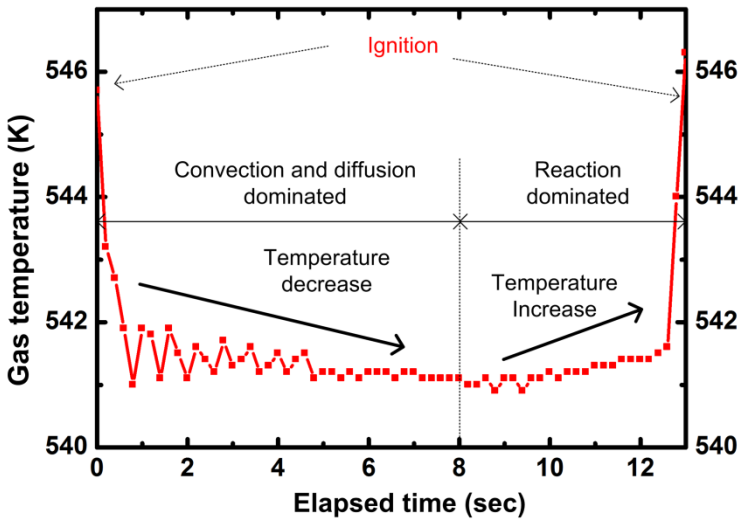

Figure 3.6 Gas temperature history during one cycle of the periodic weak flame behavior at $T_{R,\,ex}$ = 538 K and ϕ = 10.7

The ignition and propagation related to the hot flames are very normal and easily to find in other studies [66, 71], however, it is rare for the weak flames. Here, let us pay special attention to the periodic weak flame behavior. A typical case at $T_{R,\,ex}$ = 538 K and ϕ = 10.7 is to be detailed here. The corresponding flame images are shown in Fig. 3.4-c and the gas temperature history at the ignition position is shown in Fig. 3.5-c. In Fig. 3.6, the gas temperature history along one cycle is depicted for convenience purpose. One cycle is defined as the process between the two neighboring ignitions. As shown, the period of cyclic behavior is 13 s. The temperature suddenly increases at the ignition moment, and then gradually decreases as time goes by until 8 s. Then, the temperature starts to gradually increase from 8 s until the next ignition occurs.

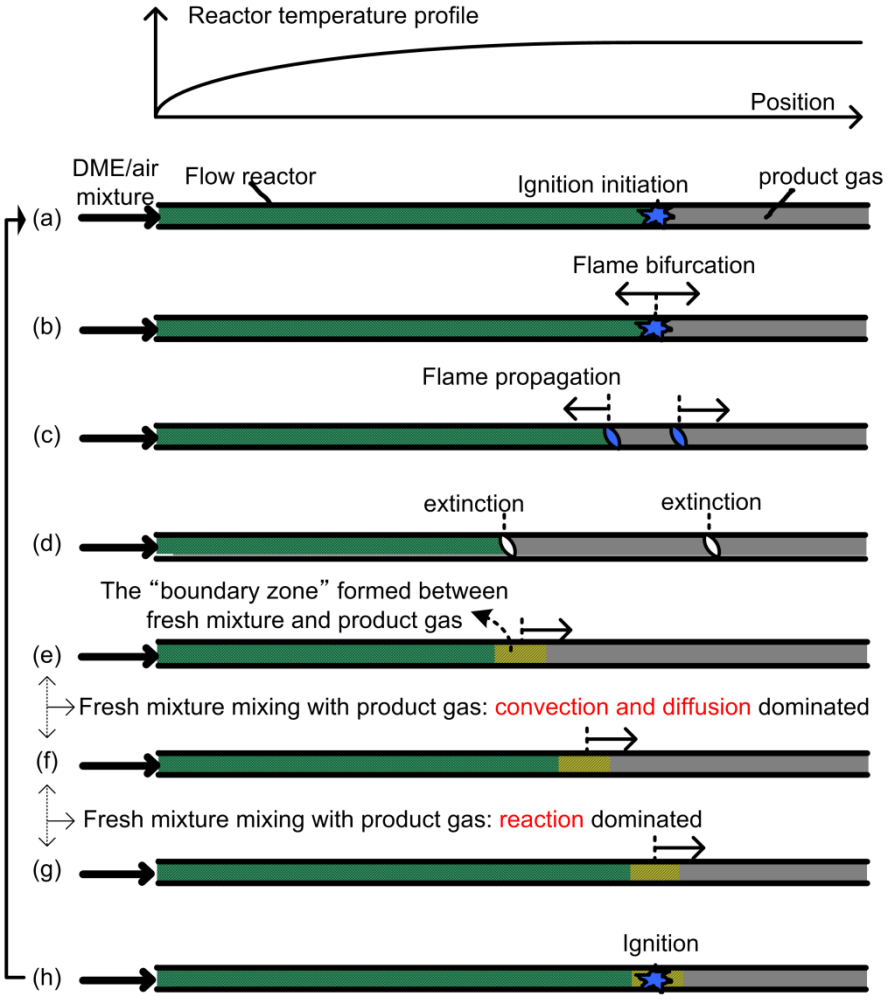

Figure 3.7 Schematic mechanism of the periodic weak flame behavior

Fig. 3.7 illustrates schematically the mechanism of the appearance of the periodic weak flame behavior. After flame propagation and quenching, the incoming fresh mixture gas slowly mixes with the product gas in the upstream side. Therefore, a "boundary zone" is formed between the fresh mixture gas and the product gas. As the mixture flows, the ignition occurs again when the gas composition of the boundary zone satisfies the ignition criterion. According to the temperature history at the ignition position shown in Fig. 3.6, it is suggested that one cycle can be divided into two phases: one is that the temperature decreasing phase, which should be dominated by convection and diffusion, and the other is that the temperature

increasing phase, which should be dominated by chemical reaction ready to trigger the following ignition.

In order to examine the ignition kinetics, gas analyses are made toward the periodic weak flame behavior. Gases are sampled at multi moments along one cycle (right after ignition, 2 s, 4 s, 6 s, 8 s, and 10 s after ignition) at the ignition position (at 12.2 cm). With regard to the gas sampling process, rapid extraction is accomplished within one second (< 1.0 s) so that any slow reaction within the syringe would be terminated. Fig. 3.8 shows the results, including the mole fractions of fuel (DME), oxygen, major product species (CO and CO_2), and intermediate product species (HCHO, CH_3OCHO, HCOOH and CH_4). Three to five measurements are made to form each result in the figure. The measurement errors might be caused by the fact that the periodic flame behavior is the results of the complicated transient processes, such as ignition, flame propagation, flame extinction and gas mixing.

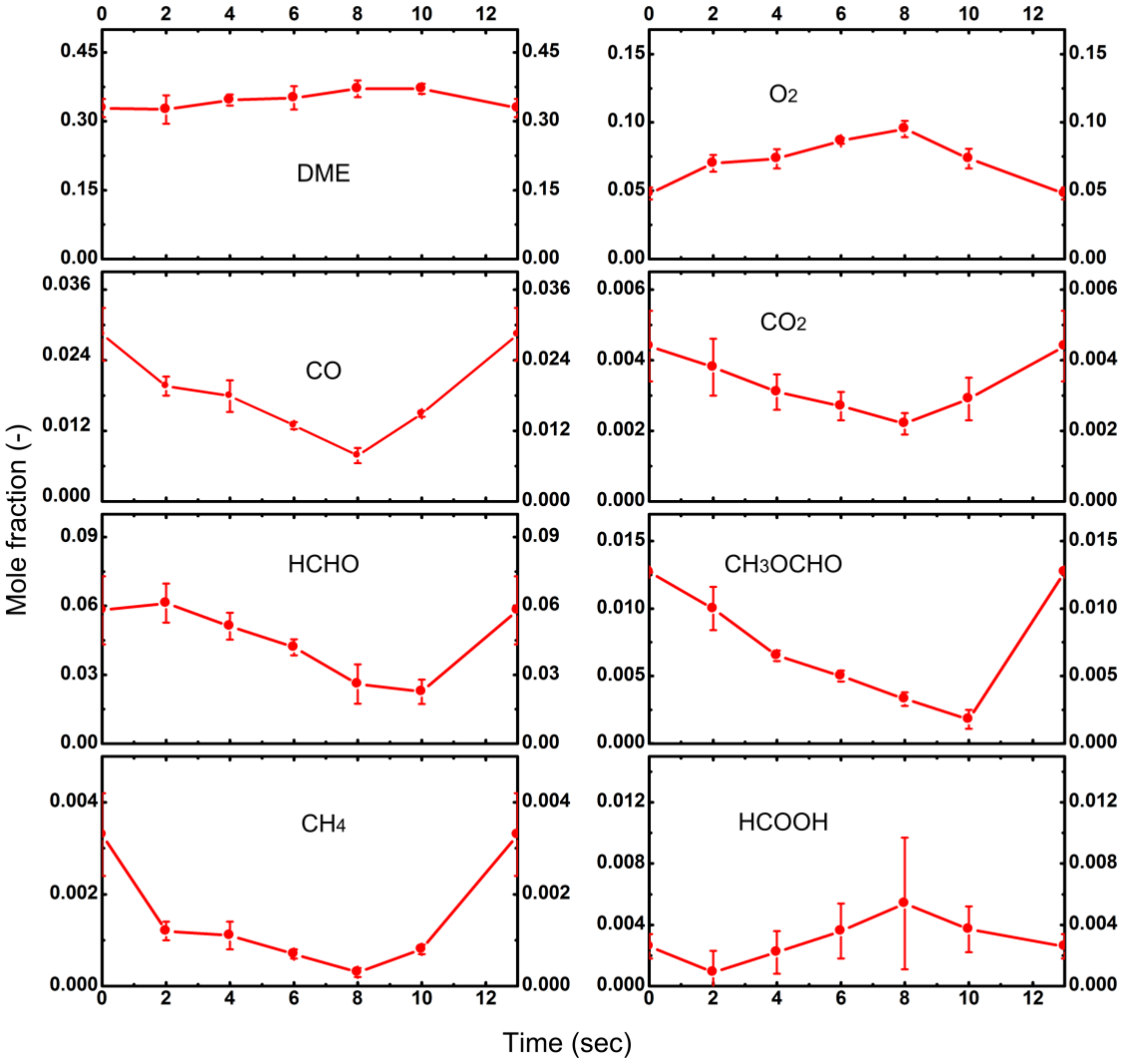

Figure 3.8 Time-dependent species mole fractions toward the periodic weak flame behavior at $T_{R,\,ex}$ = 538 K and ϕ = 10.7

As expected, during the temperature decreasing phase (0 ~ 8 s) dominated by convection and diffusion, the mole fractions of the product species (CO, CO_2, HCHO, CH_3OCHO, and CH_4) gradually decrease, whereas the mole fractions of fuel (DME) and oxygen gradually increase. This is because the fresh gas slowly flows downward and the product gas is then slowly diluted. In the following temperature increasing phase (8 ~ 13 s), the trend turns into opposite. The chemical reaction starts to become dominant, thus the major products (such as

CO and CO_2) as well as the intermediates (such as HCHO, CH_3OCHO, and CH_4) start to form and accumulate there. However, it is interesting to notice that HCOOH shows different trend compared with other product species. Additionally, it should be noted that either fuel or oxygen is never consumed out, therefore always exist even just after ignition.

3.4 Speciation of weak flame and hot flame

As described in the previous sections, at $T_{R, ex}$ = 538 K, the ignition induces the subsequent weak flame propagation at the higher equivalence ratios (ϕ = 4.1 and ϕ = 10.7) and the hot flame propagation at the lower equivalence ratio (ϕ = 1.6). Here, let us compare the gas composition reforming due to the weak flame propagation and the hot flame propagation. Fig. 3.9 and Fig. 3.10 show the gas analysis results at multi positions along the reactor before and after the flame propagations toward the weak flame condition at ϕ = 10.7 and the hot flame condition at ϕ = 1.6, respectively. The vertical dashed lines indicate the ignition position (at 12.2 cm from the inlet).

For the weak flame condition (Fig. 3.9), gases are sampled at the moments of "3 s before flame propagation" and "right after flame propagation". As shown in the figure, DME and oxygen are partially consumed at 10 cm and 12.2 cm due to the weak flame propagation. It is understood that the major and intermediate product species mole fractions increase due to the flame propagation except for HCOOH. It seems that the weak flame propagation does not make apparent change to the amount of HCOOH. In the upstream side at 5 cm, the mixture composition shows little difference before and after the flame propagation, indicating the flame does not reach there. This is consistent with the observation that the weak flame quenches at around 9 cm, as shown in Fig 3.4-c.

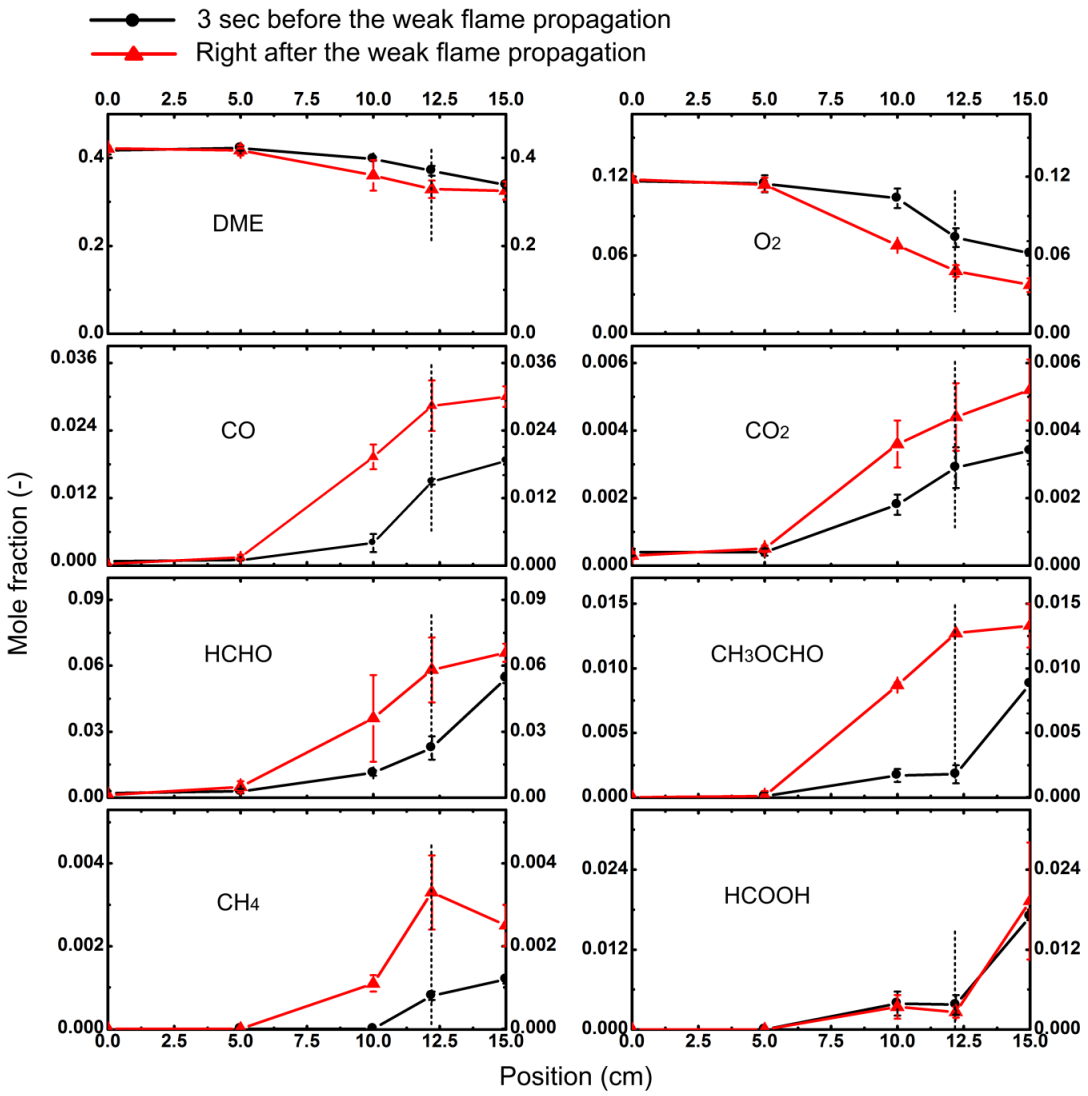

Figure 3.9 Position-dependent species mole fractions toward the weak flame propagation at $T_{R,ex}$ = 538 K and ϕ = 10.7

On the other hand, for the hot flame condition (Fig. 3.10), the samplings are conducted at "5 s before flame propagation" and "right after flame propagation". As a result of the hot flame propagation, DME and oxygen are remarkably consumed and large quantities of major product species (CO and CO2) are produced. Interestingly, although the equivalence ratio is fuel rich (ϕ = 1.6), DME are almost consumed out, and a certain amount of oxygen is remained as unreacted species. With regard to the intermediate species, CH_3OCHO and HCOOH are not detected either before or after the hot flame propagation. A certain amount of HCHO is

detected at 5 s before the hot flame propagation along the reactor, and then it is remarkably consumed by the hot flame propagation.

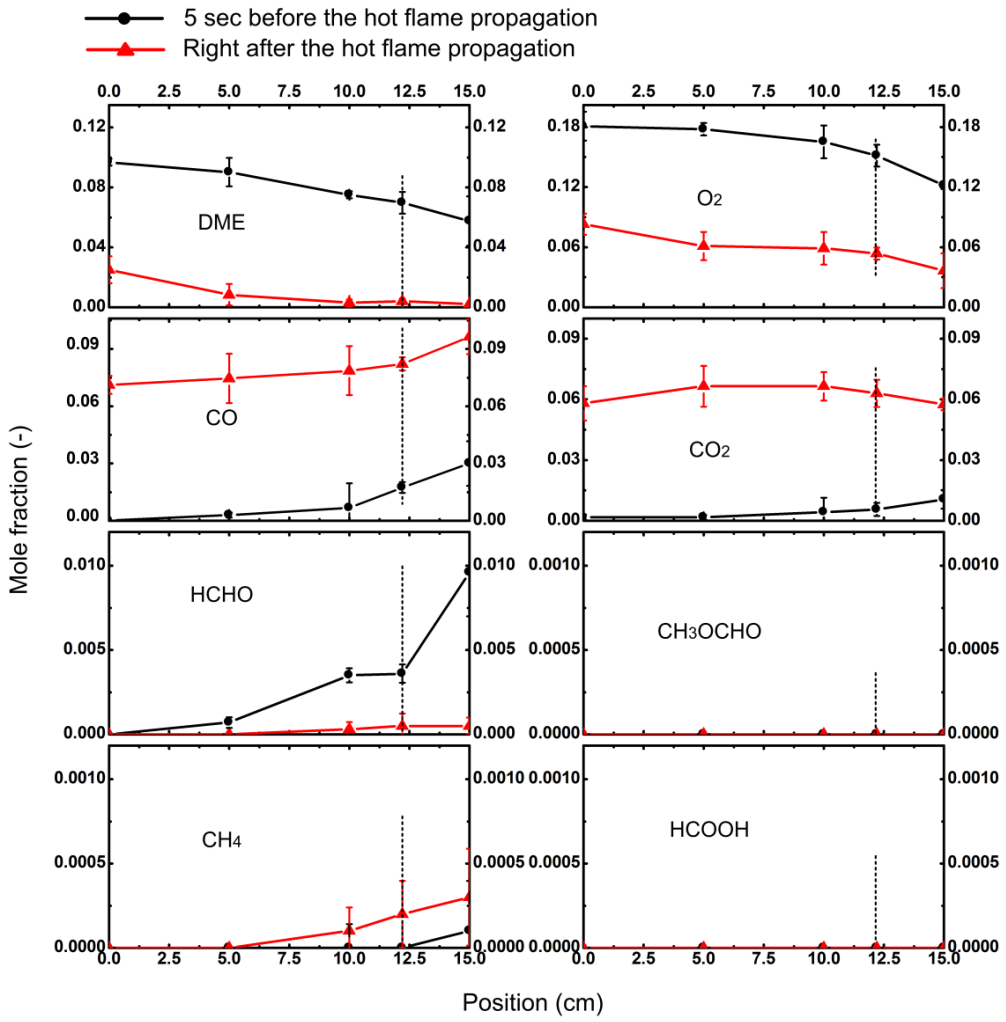

Figure 3.10 Position-dependent species mole fractions toward the hot flame propagation at $T_{R,ex}$ = 538 K and ϕ = 1.6

3.5 NTC behavior

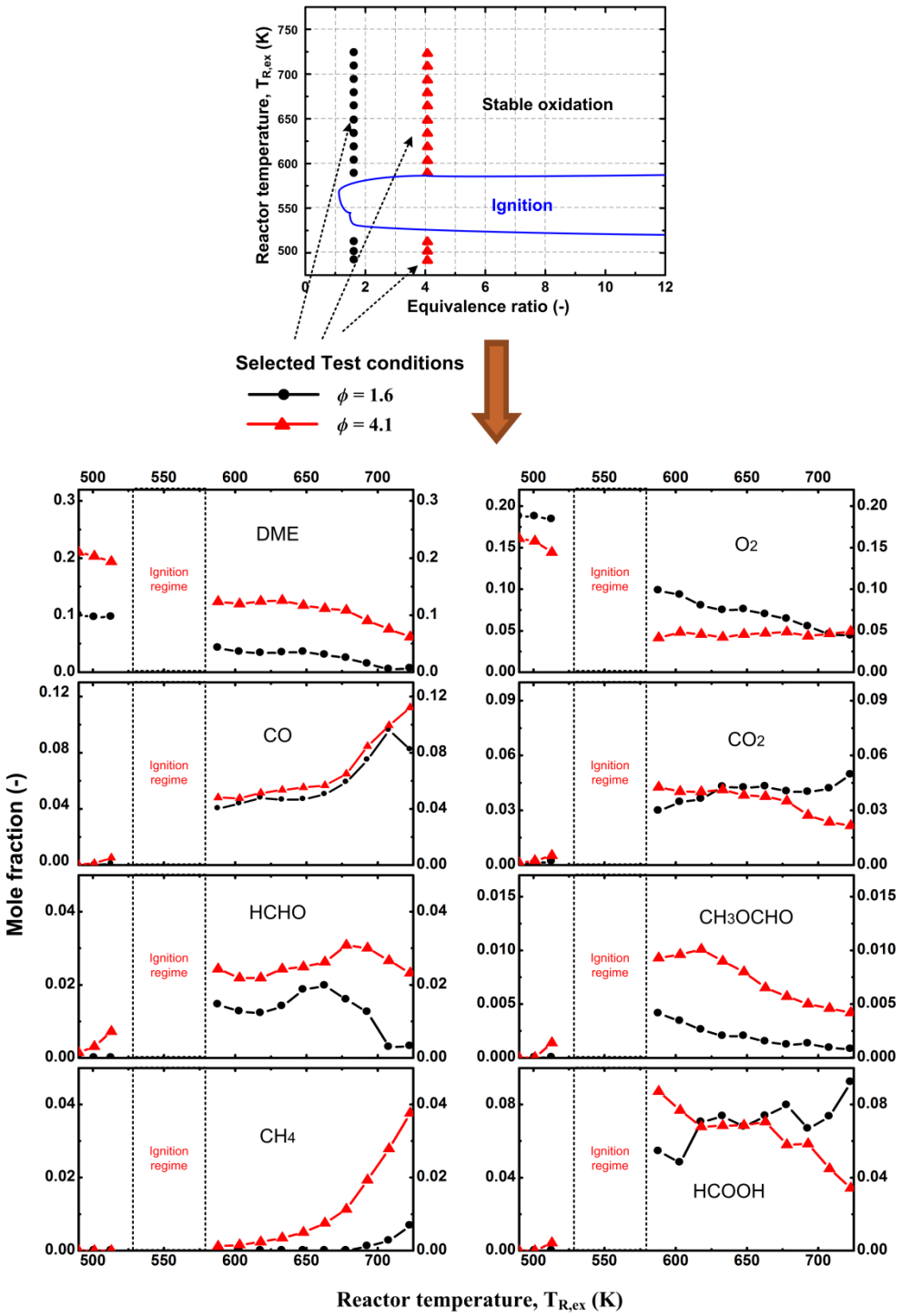

Figure 3.11 Temperature-dependent species mole fractions toward the stable oxidation conditions

At temperatures above 590 K, the ignition does not occur, indicating the NTC zone is encountered, thus stable oxidation is progressed. Gas analyses are made to investigate the NTC behavior. The measured species mole fractions as a function of controlled temperature are showed in Fig. 3.11, including the selected conditions in the T - ϕ plane and the corresponding gas analysis results. Gases are sampled at 45 cm from the inlet. Note that the corresponding residence time here is much longer (e.g. about 60 s at 680 K) than that in the typical flow reactors [47, 48, 57, 58] or jet-stirred reactors [43, 44] in the previous studies. In the present system, the NTC behavior is most pronounced in the range of 590 K - 680 K, which is consistent with the recent study [58]. The mole fractions of DME, CO, and CO_2 do not change too much as the temperature increases in this range. On the contrary, the mole fraction of oxygen does not vary much at ϕ = 4.1 in the whole range (590 K - 725 K) considered here, however, it continuous decreases at ϕ = 1.6 as the imposed temperature increases. This fact indicates that the NTC effect is more significant at fuel-richer conditions. It is found that the formations of HCHO, CH_3OCHO, and HCOOH are remarkably influenced by the NTC behavior, especially, CH_3OCHO is found to be a good marker to clearly reflect the NTC behavior. At ϕ = 1.6, the mole fraction of CH_3OCHO decreases as temperature increases, while at ϕ = 4.1, it slightly increases till 620 K and then decreases till 725 K. The temperature dependency of HCHO formation shows complex behavior: it slightly decreases till 610 K, then increases till 670 K, and finally decreases till 725 K. This complexity should be caused by the fact that HCHO is involved in both chain-branching and chain-propagation pathways. Moreover, it is interesting to see that the temperature dependency of HCOOH formation (so as CO_2) shows reversed trends between at ϕ = 1.6 and at ϕ = 4.1. This implies that the low-temperature oxidation kinetics is very sensitive to equivalence ratio. In low-temperature region, a number of reaction pathways are “opened” so that the dominated chemistry could be remarkably different at varied equivalence ratios. Here, at least the reactions related to HCOOH and CO_2 formation are significantly affected by equivalence ratio.

3.6 Further discussion on the kinetics related to cool flame and NTC behavior

3.6.1 On cool flame

In the following part, we shall discuss the obtained results based on the detailed kinetics proposed by Fischer et al. [47, 48]. As summarized in Fig. 1.4, in the low-temperature (< 800 K) region, oxidation of DME is dominated by the competition between the chain-branching and the chain-propagation pathways. The CH_3OCH_2 radical, reacts with O_2 to form a CH_3OCH_2OO radical, which isomerize to form a CH_2OCH_2OOH radical. Then, CH_2OCH_2OOH radicals combine with O_2 to lead the chain-branching pathway, which would give rise to cool flames. As temperature increases, the β-scission of CH_2OCH_2OOH radicals is enhanced to lead the chain-propagation pathway. While at above 800 K, the DME oxidation is dominated by the β-scission of the CH_3OCH_2 radicals and the following steps.

As shown in Fig. 3.11, product species firstly appear at 490 K, indicating the low-temperature oxidation is initialed although the reaction is very weak. Then, according to the ignition limit showed in Fig. 3.3, the weak flame is firstly observed at around 520 K, suggesting the chain-branching pathway starts:

$CH_2OCH_2OOH + O_2 \rightarrow OOCH_2OCH_2OOH$ (R3.1)

$OOCH_2OCH_2OOH \rightarrow HPMF\ (HOOCH_2OCHO) + OH$ (R3.2)

$HPMF(HOOCH_2OCHO) \rightarrow OCH_2OCHO + OH$ (R3.3)

Within the obtained ignition regime located between 520 K and 590 K, the chain-branching pathway competes with the chain-propagation pathway, which starts from the decomposition reaction of CH_2OCH_2OOH radicals:

$CH_2OCH_2OOH \rightarrow HCHO + HCHO + OH$ (R3.4)

This decomposition reaction is enhanced as the temperature increases. Therefore, once the cool flame occurs, the heat release will enhance the decomposition of CH_2OCH_2OOH radicals, then enhance the chain-propagation to suppress the chain-branching, resulting that the cool flame is quenched. This is so called "self-restrained" feature of the cool flame. As showed in Figs. 3.8 and 3.9, the observed weak flame shows this feature: both fuel and oxygen are remained in the product species, and intermediate species (e.g., HCHO, CH_3OCHO) are produced due to the weak flame appearance. Hence, it is suggested that the weak flame might be the cool flame, or the flame formed due to the fact that the transition from the cool flame to the hot flame is significantly suppressed. It should be further noted that the mole fraction of HCOOH is not affected apparently by the weak flame propagation, as shown in Fig. 3.9. This is probably because HCOOH locates at the end of the chain-branching pathway, while the chain-branching reactions are highly restrained at higher equivalence ratios (e.g. ϕ = 10.7).

3.6.2 On the transition from cool flame to hot flame

What newly captured in the ignition zone through this study is, in a specific narrow range (530 K < T < 540 K, 1.5 < ϕ < 2.5), the cool flame successfully transits to the hot flame. This transition might be explained as follows. Apparently, compared with the chain-propagation pathway via R3.4, the chain-branching pathway favors more O_2 (i.e. low equivalence ratio) to promote the O_2 addition reaction R3.1. When we apply a "suitable" lower equivalence ratio (e.g. ϕ = 1.6), sufficient O_2 is supplied to complete the chain-branching pathway. Thus, the

chain-branching pathway is repetitively progressed, and the temperature continuously increases till the critical value of 730 K. Then, the decomposition of H_2O_2, accumulated in the chain-branching stage (cool flame stage), is to induce the sequent hot flame stage by producing two active OH radicals by the following reaction [30]:

$$H_2O_2 + M \rightarrow 2OH + M \qquad \text{(R3.5)}$$

The released OH radicals again enhance the reaction rate of the whole system. Finally, the cool flame would transit to the hot flame. As shown in Fig. 3.10, major product species are dominant in the product gas of the hot flame, while the amounts of the intermediate product species are very small. Especially, it is clearly shown that HCHO is formed due to the weak flame appearance, and then consumed by the hot flame appearance.

Furthermore, the transition from the cool flame to the hot flame is sensitive not only to equivalence ratio but also to temperature. At temperatures higher than 540 K, the cool flame never transit to the hot flame whatever the equivalence ratio is, as a result, weak flames are captured there. Here, we propose that this is because another chain-propagation pathway is "hidden" in the chain-branching pathway. With regard to the chain-branching pathway, the steps till reaction R3.2 to release the first OH radical are relatively clear, however, the formation of the second OH radical related to the decomposition of HPMF (hydroperoxy-methyl formate, $HOOCH_2OCHO$) is complicated and still ambiguous. Liu et al. [46] tried to experimentally detect HPMF by FTIR but unfortunately failed. They suggested that the HPMF was less thermally stable than assumed or there were other reactions between HPMF and OH radicals. Assume that if HPMF easily reacts with OH radicals, the second OH radical should fail to release, therefore, the chain-branching pathway becomes a chain-propagation pathway. Andersen et al. [69] conducted theoretical analysis focused on

the decomposition of HPMF. They predicted that at least six paths should be concerned for HPMF decomposition:

$HPMF \rightarrow HCO + HCOOH + OH$ (R3.6)

$HPMF \rightarrow H_2O + HCOOCHO$ (R3.7)

$HPMF \rightarrow CH_2OO + HCOOH$ (R3.8)

$HPMF \rightarrow HCOOOH + CO + H_2$ (R3.9)

$HPMF \rightarrow (HO)_2HCOCHO$ (R3.10)

$HPMF \rightarrow OCH_2OCHO + OH$ (R3.11)

The reactions R3.6 and R3.11 directly form OH radicals could contribute to lead the chain-branching. However, if any other reaction without OH radical formation is favored, the chain-branching pathway will become a chain-propagation pathway. Therefore, due to the observation that the cool flame fails to transit to the hot flame at temperature higher than 540 K, we suggest that some chain-propagation steps through HPMF should be pronounced there to compete with the chain-branching steps, resulting in suppressing the transition from the cool flame to the hot flame.

3.6.3 On NTC behavior

As temperature increases, the chain-propagation pathway via decomposition of CH_2OCH_2OOH becomes more dominant as compared with the chain-branching pathway. Since the chain-propagation way produces only one reactive OH radical, the overall reactivity of the system decreases, thus the ignition disappears and negative temperature coefficient

(NTC) zone is encountered at above 590 K. As shown in Fig. 3.11, due to The NTC behavior, the mole fractions of the major product species (CO and CO_2) do not increase as temperature increases in the range of 590 - 680 K. The temperature dependency of HCHO formation shows complex behavior because the formation of HCHO is involved in both chain-branching and chain-propagation pathways through the decompositions of OCH_2OCHO radicals and CH_2OCH_2OOH radicals, respectively. While the mole fraction of CH_3OCHO decreases as temperature increases. This is because the formation of CH_3OCHO is only through:

$CH_3OCH_2O_2 \rightarrow CH_3OCH_2O \rightarrow CH_3OCHO$

As the temperature increases, the decomposition of $CH_2OCH_2O_2H$ (isomer of $CH_3OCH_2O_2$) via reaction R3.4 is enhanced, therefore reaction (12) is restrained and the concentration of CH_3OCHO decreases.

At above 680 K, the consumption of DME as well as the formations of HCHO and CO is enhanced as the temperature increases. This might be because the system reactivity is increased due to the enhancement of reaction R3.5 to release OH radicals. It should be noticed that, in the temperature range of 680 - 725 K, the mole fraction of HCOOH (so as to CO_2) increases as temperature increases at ϕ = 1.6, while decreases as temperature increases at ϕ = 4.1. Again, this reflects the significant sensitivity to equivalence ratio in low-temperature oxidation. Note that HCOOH locates at the end of the chain-branching pathway. At ϕ = 1.6, the chain-branching pathway is potentially available there, therefore, once the system reactivity increases (again, due to the released OH radicals via reaction R3.5), the chain-branching pathway is enhanced producing more HCOOH. On the other hand, at ϕ = 4.1, the chain-branching pathway is relatively less dominant, therefore, once the system reactivity increases, the chain-propagation pathway is more remarkably enhanced, and thus the formation

of HCOOH is suppressed. From 590 K to 725 K, the mole fraction profile of CO_2 shows similar trend with HCOOH either at ϕ = 1.6 or at ϕ = 4.1, indicating that it is an important (maybe dominant) way to form CO_2 via HCOOH.

3.7 Conclusions

Low-temperature (< 730 K) oxidation of DME is investigated by using a newly developed laminar flow reactor with very low flow velocities. The ignition regime and the stable oxidation regime are identified in the temperature-equivalence ratio (T - ϕ) plane. It shows that the ignition zone locates between 520K and 590 K. At temperatures above 590 K, the ignition disappears, then stable oxidation takes over the reaction status in the tube, indicating the NTC zone is encountered. Importantly, the ignition triggered weak flames and hot flames are clearly observed. A periodic weak flame behavior of DME with low-temperature ignition, flame propagation, and extinction is captured for the first time at atmospheric pressure. The gas analysis results confirm that the weak flame appearance is accompanied by the formation of intermediate product species, such as HCHO, CH_3OCHO, and CH_4. Due to the self-restrained feature, either fuel or oxygen cannot be consumed out thus remained in the product gas of the weak flame. Therefore, the weak flame is suggested to be cool flame, or the flame formed due to the suppression of transition from the cool flame to the hot flame.

It is found that the cool flame transits to the hot flame in a specific range (530K < T < 540 K, 1.5 < ϕ < 2.5), indicating this is an optimal range to realize the chain-branching pathway. It is proposed that there should be another chain-propagation pathway via decomposition of HPMF without forming any OH radical. This reaction path gets pronounced at above 540 K, where the transition from cool flame to the hot flame cannot be achieved whatever the equivalence ratio is.

The low-temperature oxidation is sensitive to equivalence ratio because many possible reaction channels are simultaneously opened in the low-temperature range. It is found that the formation of HCOOH shows the reversed temperature dependency in the NTC zone at different equivalence ratios. This implies that validations in a wide range of equivalence ratio

are quite necessary in oxidation kinetic modeling studies, especially in the low-temperature range.

The flow reactor system developed in the present study enables us to capture the low-temperature ignition phenomenon as well as the NTC behavior.

Chapter 4: Numerical Investigations on Ignition Limit and Ignition Regime

As described in Chapter 3, ignition limit is depicted in the temperature-equivalence ratio (T - ϕ) plane. Dramatic effect of equivalence ratio on the transition from a cool flame to a hot flame was observed. In order to better understand the ignition kinetics, computations with detailed chemical kinetics are performed in this chapter. Special attention is paid to ignition limit as well as ignition regime.

The computations are conducted using the plug-flow reactor model. Interestingly, the ignition limit in experiments is well predicted, while apparent discrepancy exists in terms of ignition regime, to say, the observed transition from a cool flame to a hot flame cannot be predicted numerically. Then, reaction pathway analyses are conducted against a typical ignition case to find the potential reason caused the discrepancy. The competition reactions related to the CH_3OCH_2 radical are found to be important in the transition from a cool flame to a hot flame. It is further found that, based on a slight modification of the activation energy (E_{R248}) of the β-scission reaction of the CH_3OCH_2 radical, both ignition limit and ignition regime are well predicted. Finally, the effect of E_{R248} is further interpreted via comparing the computed ignition delay results with the experimental results.

4.1 Numerical method

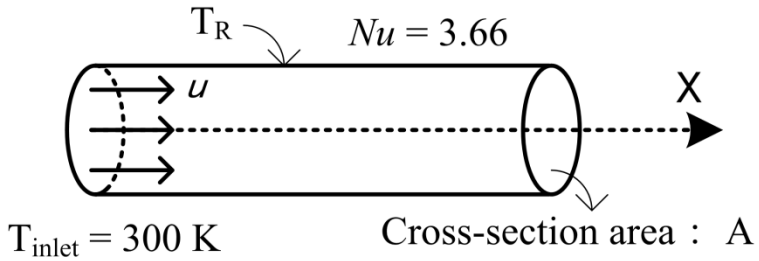

Figure 4.1 Schematic of the flow reactor in the numerical computation

Although mass and heat transports are important in the low velocity reacting flow, in the present study, we limit our focus to understanding the ignition kinetics. Numerical computations are conducted using the plug-flow reactor model (as shown in Fig. 4.1) neglecting mass and heat transport effects. The governing equations are as follows:

$$M = \rho u A$$

$$M\frac{dY_k}{dx} - A\dot{\omega}_k W_k = 0$$

$$M\frac{dT}{dx} + \frac{A}{c_p}\sum_{K=1}^{K}\dot{\omega}_k h_k W_k - \frac{A}{c_p}\frac{4\lambda Nu}{d^2}(T_R - T_g) = 0$$

The heat transfer between the reactor (wall) and the gas mixture is considered. The inlet gas temperature is set to 300 K, and the flow velocity is set to the same value in experiments (3.6 mm/s at inlet). The reactor wall temperature (T_R) is set to constant values and therefore the Nusselt number (*Nu*) is set to 3.66 [72]. Thermal conductivities of DME are determined by [73], and the details could be found in Appendix-A. Computations are conducted using the CHEMKIN-Pro software [74]. Current calculations are conducted with even grid size of Δx = 0.5 μm. Reducing the grid size by a factor of 2 gives no significant difference in results, indicating the computation is sufficiently resolved. The model DME-2007 is employed for the detailed chemical kinetics.

4.2 Experimental results

The focuses in this chapter are ignition limit and ignition regime associated with the transition from a cool flame to a hot flame. For readers' convenience, the ignition limit obtained in Chapter 3 is shown Fig. 4.2, and mole fractions of DME, CO and HCHO in the flame product gases are shown in Fig. 4.3. Again, at T_R = 538 K and ϕ = 10.7, DME is partially consumed and a certain amount of HCHO is formed due to the weak flame propagation (the concentrations of HCHO are very low at 0 cm and 5 cm because the upward propagating weak flame quenches at around 9 cm). On the other hand, at T_R = 538 K and ϕ = 1.6, DME is almost consumed out, and only a small amount of CO is formed through the reactor.

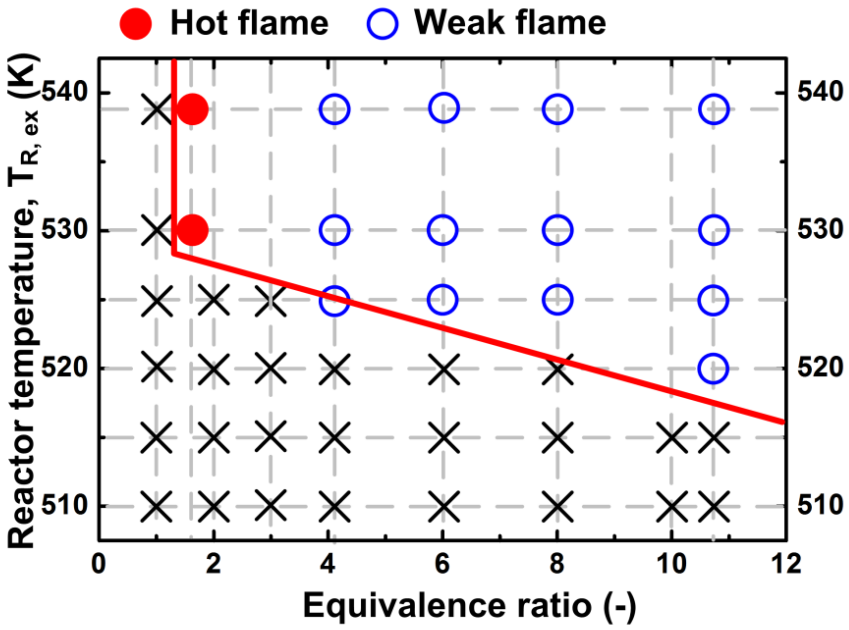

Figure 4.2 Low-temperature ignition limit of DME/air mixture (experimental).

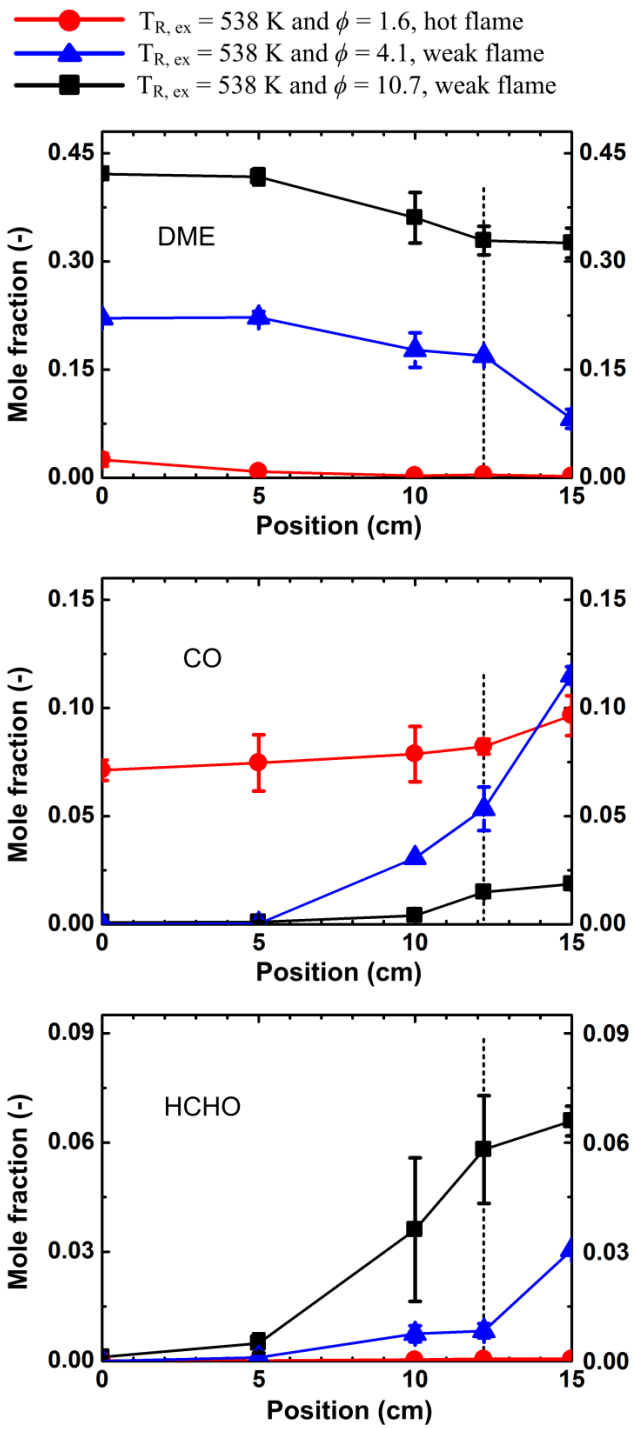

Figure 4.3 Position-dependent flame product analysis results of a hot flame for ϕ = 1.6, and weak flames for ϕ = 4.1 and ϕ = 10.7, T_R = 538 K.

4.3 Numerical predictions of ignition limit and ignition regime

4.3.1 Ignition limit

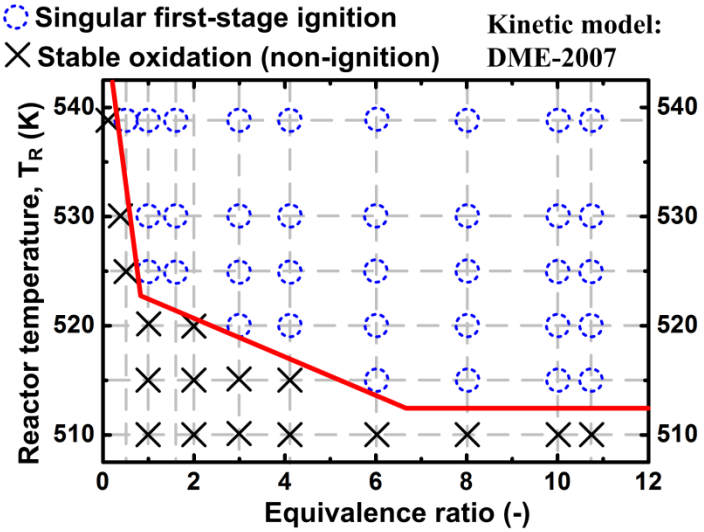

Figure 4.4 Prediction of low-temperature ignition limit of DME/air mixture with DME-2007.

In computations, ignition is defined as a rapid temperature increase accompanied by a heat release rate larger than 10^8 J/(m^3-sec), otherwise, it is defined as stable oxidation (non-ignition). The predicted ignition limit is shown in Fig. 4.4. It shows good agreement with the experimental results showed in Fig. 4.2. Ignition tends to occur at fuel rich conditions, and the lowest temperature to achieve ignition increases as equivalence ratio decreases in the noted range.

4.3.2 Stable oxidation (non-ignition)

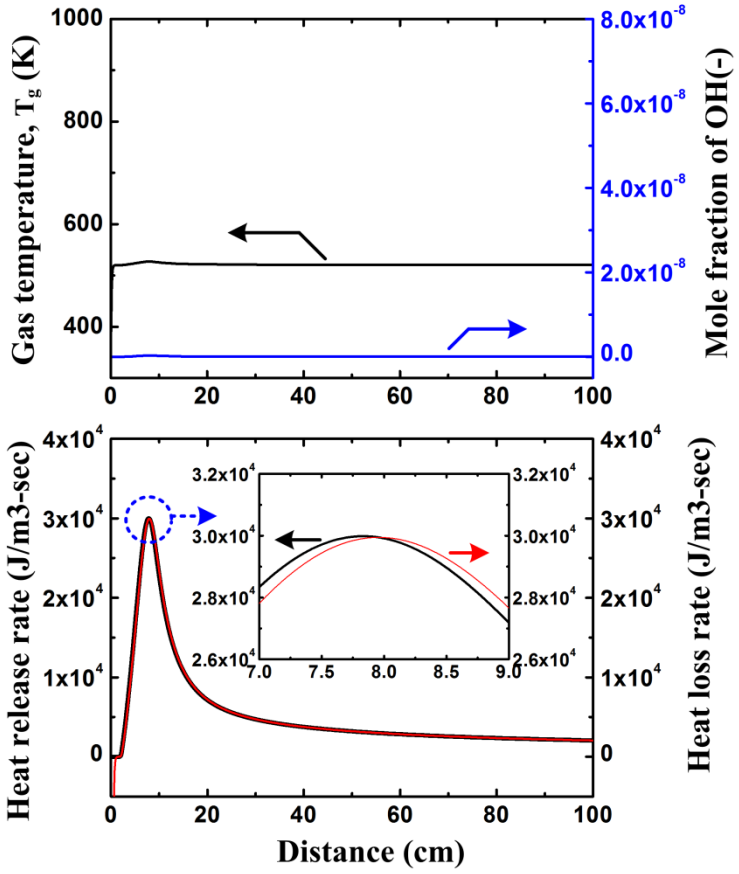

Figure 4.5 Profiles of gas temperature, OH mole fraction, heat release rate, and heat loss rate (T_R = 520 K and ϕ = 1.6)

As shown in Fig. 4.4, stable oxidation is experienced at T_R = 520 K and ϕ = 1.6. The profiles of gas temperature, OH mole fraction, heat release rate, and heat loss rate are shown in Fig. 4.5. The profiles of mole fractions of the selected species (DME, O_2, CO, CO_2, HCHO, and H_2O_2) are shown in Fig. 4.6. No significant rapid temperature increase could be found although sufficient residence time is given, and the mole fraction of OH radical keeps lower than 10^{-8}. The heat release rate reaches its peak value at around 10 cm, then becomes lower than the heat loss rate, resulting in a gradual decrease of the gas temperature until same with the reactor temperature (520 K). Simultaneously, as shown in Fig 4.6, reactants (DME and

oxygen) are gradually consumed, and the major products (such as CO and CO_2) are gradually produced as the gas mixture flows downward.

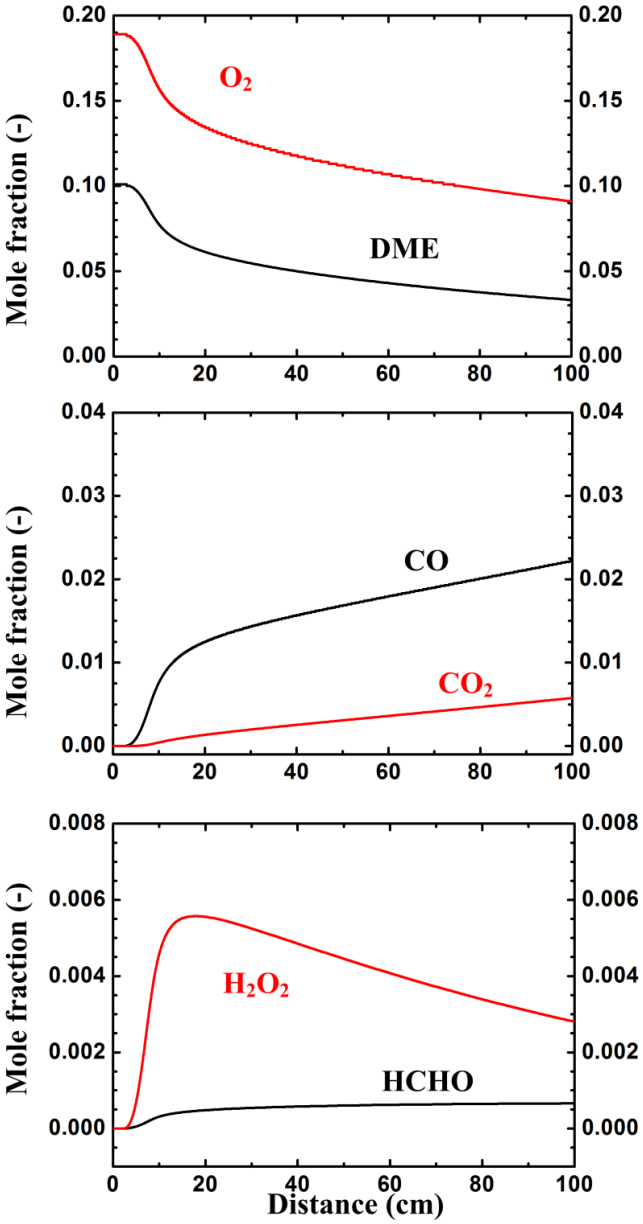

Figure 4.6 Profiles of mole fractions of DME, O_2, CO, CO_2, HCHO, and H_2O_2 (T_R = 520 K and ϕ = 1.6)

4.3.3 Singular first-stage ignition

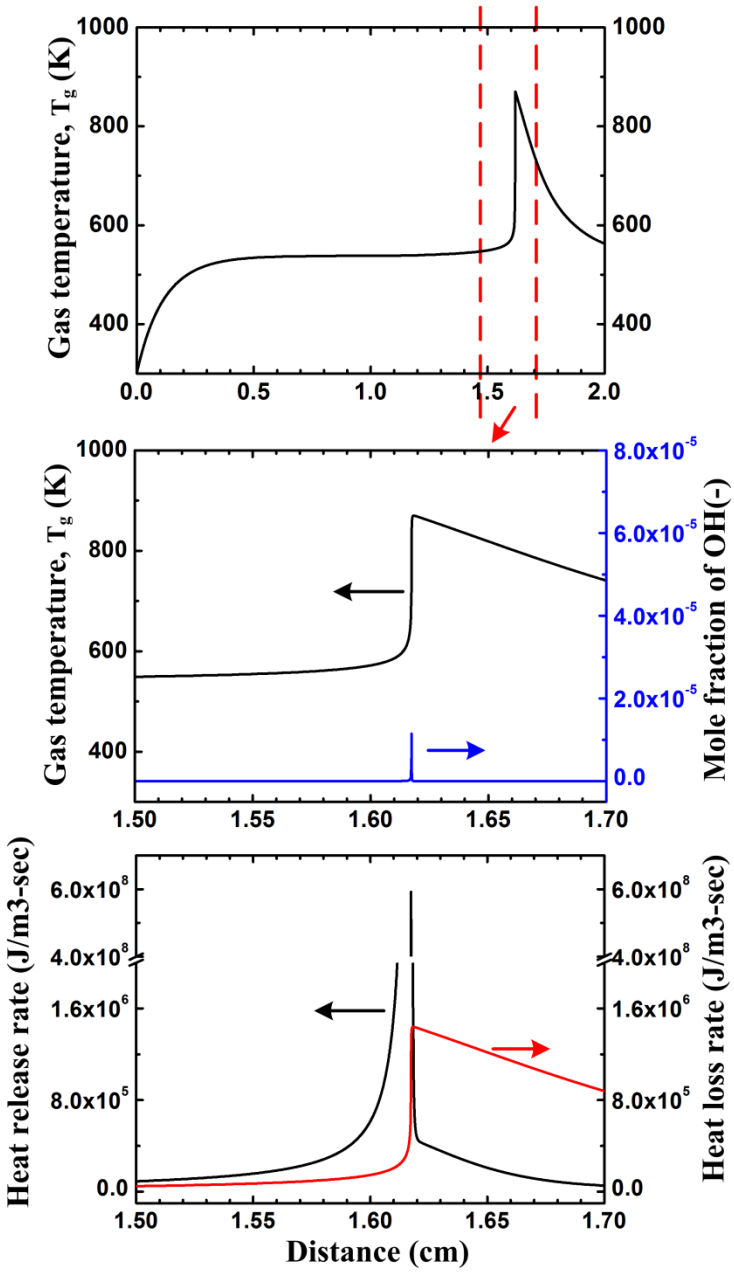

Figure 4.7 Profiles of gas temperature, OH mole fraction, heat release rate, and heat loss rate (T_R = 538 K and ϕ = 1.6)

There exist sigular first-stage ignition regimes at ignition conditions. Typically, at T_R = 538 K and ϕ = 1.6, the profiles of gas temperature, OH mole fraction, heat release rate, and heat loss rate are shown in Fig. 4.7, and the selected species (DME, O_2, CO, CO_2, HCHO, and H_2O_2)

mole fractions are shown in Fig. 4.8. It is seen that, a rapid temperature increase occurs at around 1.62 cm, accompanied by rapid consumptions of the reactants (DME and O_2) and rapid formations of the product species such as CO, CO_2, HCHO, and H_2O_2.

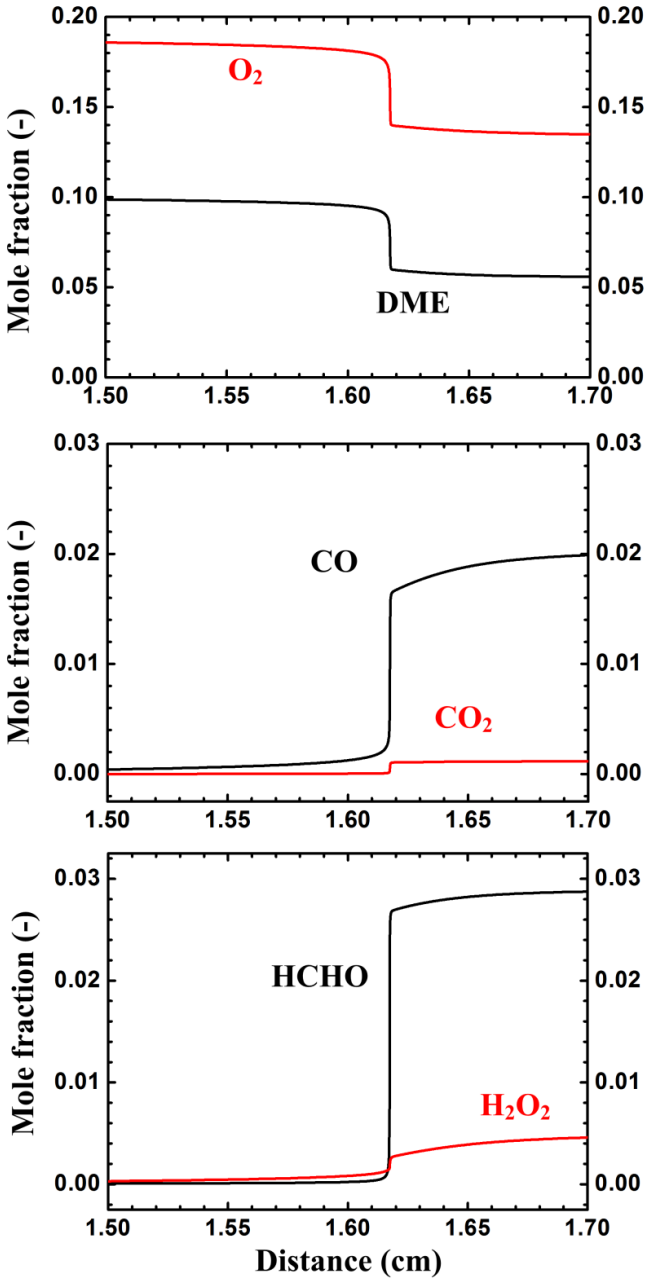

Figure 4.8 Profiles of mole fractions of DME, O_2, CO, CO_2, HCHO, and H_2O_2 (T_R = 538 K and ϕ = 1.6)

The first-ignition stage is characterized by the formation of HCHO and H_2O_2, indicating the cool flame chemistry is dominant in this stage. Then, the formed HCHO and H_2O_2 are not consumed after the first-stage ignition, indicating the second-stage ignition is not induced. Compared to the experimental results in Fig. 4.2, apparent discrepancy is found in ignition regime: numerically, singular first stage ignitions are experienced at all ignition conditions, to say, the cool flame never transits to hot flame; experimentally, hot flame at $\phi = 1.6$ has been clearly observed.

4.4 Reaction pathway analyses

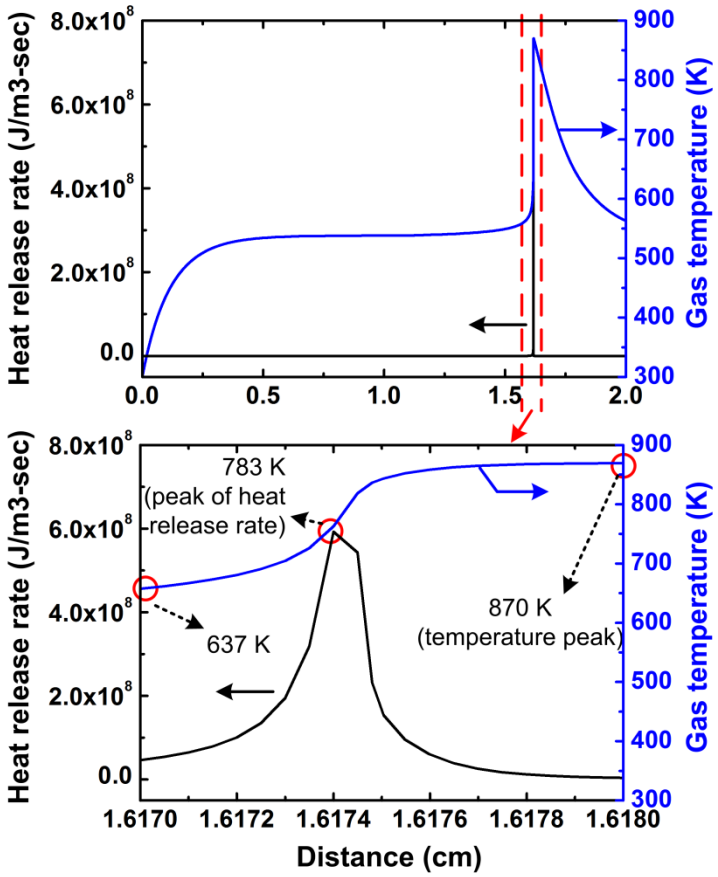

Figure 4.9 Profiles of temperature and heat release rate (T_R = 538 K and ϕ = 1.6)

To find the reactions responsible for the transition from a cool flame to a hot flame, reaction pathway analyses are performed against the ignition case at T_R = 538 K and ϕ = 1.6. Detailed temperature and heat release rate profiles close to the ignition moment are shown in Fig. 4.9. It shows that the heat release rate is very low at 637 K, and then rapidly reaches its peak value at 783 K. The gas temperature attains its peak at 870 K and then decreases, because the heat release rate is lower than heat loss rate at 870 K.

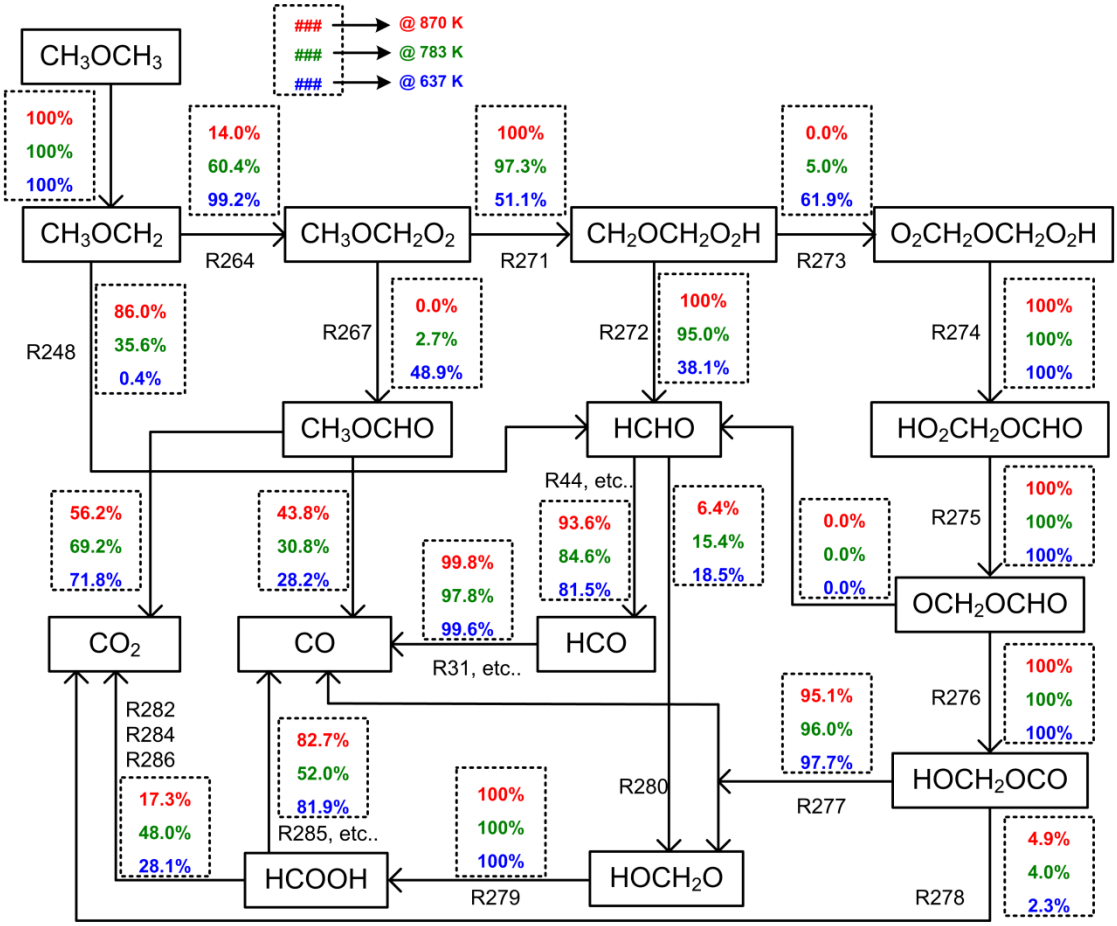

Figure 4.10 Reaction pathway analysis for the singular first-stage ignition regime (T_R = 538 K and ϕ = 1.6)

The reaction pathway analyses performed at these three moments are shown in Fig. 4.10. At 637 K, 99.2% of the resulting CH_3OCH_2 radicals react with oxygen to form $CH_3OCH_2O_2$ radicals. One consumption path of $CH_3OCH_2O_2$ radicals produces CH_3OCHO (48.9%). Other $CH_3OCH_2O_2$ radicals (51.1%) isomerize into $CH_2OCH_2O_2H$ radicals, followed by the chain-propagation pathway via the decomposition of $CH_2OCH_2O_2H$ radicals, and the chain-branching pathway via the molecular oxygen addition reaction of $CH_2OCH_2O_2H$ radicals. As temperature reaches 783 K, the path to CH_3OCHO is almost closed (2.7%). Moreover, the chain-propagation pathway becomes dominant (95.0 %) consuming $CH_2OCH_2O_2H$ radicals, while the chain-branching pathway is almost closed (5.0%). More importantly, from this

moment on, the consumption of the CH_3OCH_2 radical is dominated by the competition between the β-scission reaction:

R248: $CH_3OCH_2 \rightarrow CH_3 + HCHO$

and the molecular oxygen addition reaction:

R264: $CH_3OCH_2 + O_2 \rightarrow CH_3OCH_2OO$

As temperature increases from 783 K to 870 K, R248 becomes more dominant (from 35.6% to 86.0%), while R264 is significantly suppressed (from 60.4% to 14.0%). Simultaneously, the heat release rate sharply decreases (Fig. 4.9). At 870 K, the heat release rate becomes lower than the heat loss rate, thus, the temperature starts to decrease, failing to induce the transition from a cool flame to a hot flame. Therefore, it is understood that the transition is strongly affected by the competition between the reactions R248 and R264.

4.5 Numerical predictions based on the modification of E_{R248} = 28.00 kcal/mol

4.5.1 Ignition limit

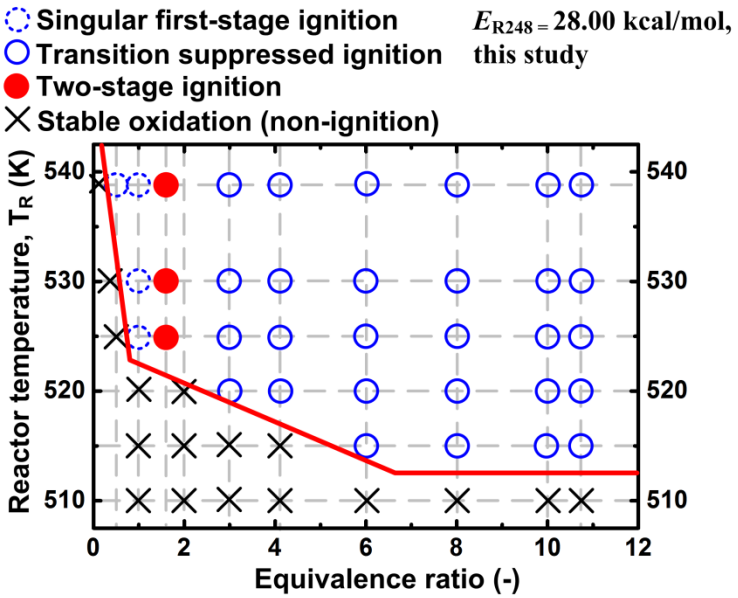

Figure 4.11 Low-temperature ignition limit of DME/air mixture (computational results with E_{R248} = 28.00 kcal/mol)

Regarding the reactions R248 and R264, R264 is a barrier-less reaction that is relatively well understood. However, experimental studies determining the reaction rate constants of R248 are rare. The reaction rate constants of R248 (A = 1.6E13 and E_{R248} = 25.50 kcal/mol) were originally taken from the study of Loucks and Laidler [75] in 1967. Sehested et al. [38] found a good consistence with this work in a narrow temperature range of 573–666 K, and indicated that confirmation at high temperatures is needed. However, no further experimental studies could be found till now. Zhao et al. [49] revised these constants into A = 1.2E13 cm^3/mol/s and E_{R248} = 25.75 kcal/mol to get good agreements with experiments.

Here, we shall show the ignition regimes based on a modified activation energy of E_{R248} = 28.00 kcal/mol, and an unchanged A factor. The ignition limit based on E_{R248} = 28.00

kcal/mol is shown in Fig. 4.11. Comparing Fig. 4.11 to Fig. 4.2, a good agreement, both in terms of ignition limit and ignition regimes against equivalence ratio, is obtained. Three kinds of ignition regimes exist at T_R = 538 K: singular first-stage ignition at ϕ = 1.0, two-stage ignition regime at ϕ = 1.6, and transition suppressed ignition regime at higher equivalence ratios (e.g., ϕ = 4.1, ϕ = 10.7). Details of different ignition regimes are shown in the following sections.

4.5.2 Ignition regime-1: singular first-stage ignition

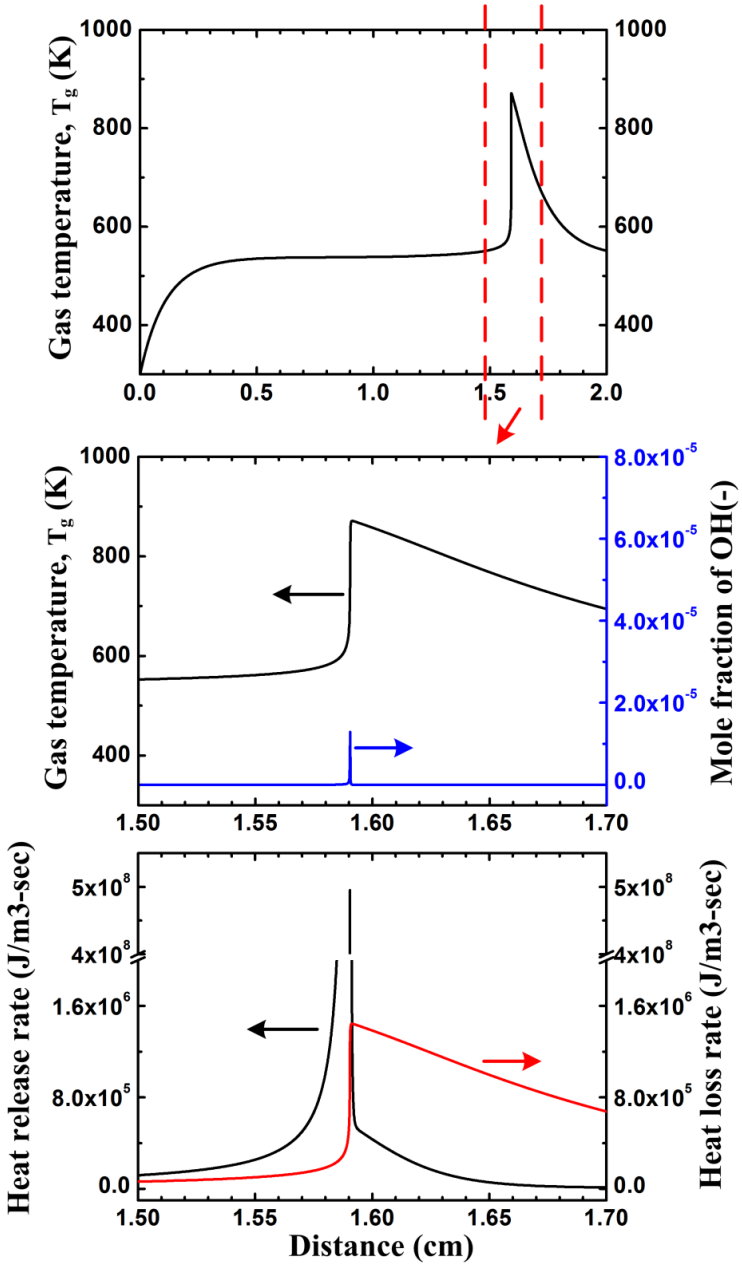

Figure 4.12 Profiles of gas temperature, OH mole fraction, heat release rate, and heat loss rate

(T_R = 538 K and ϕ = 1.0)

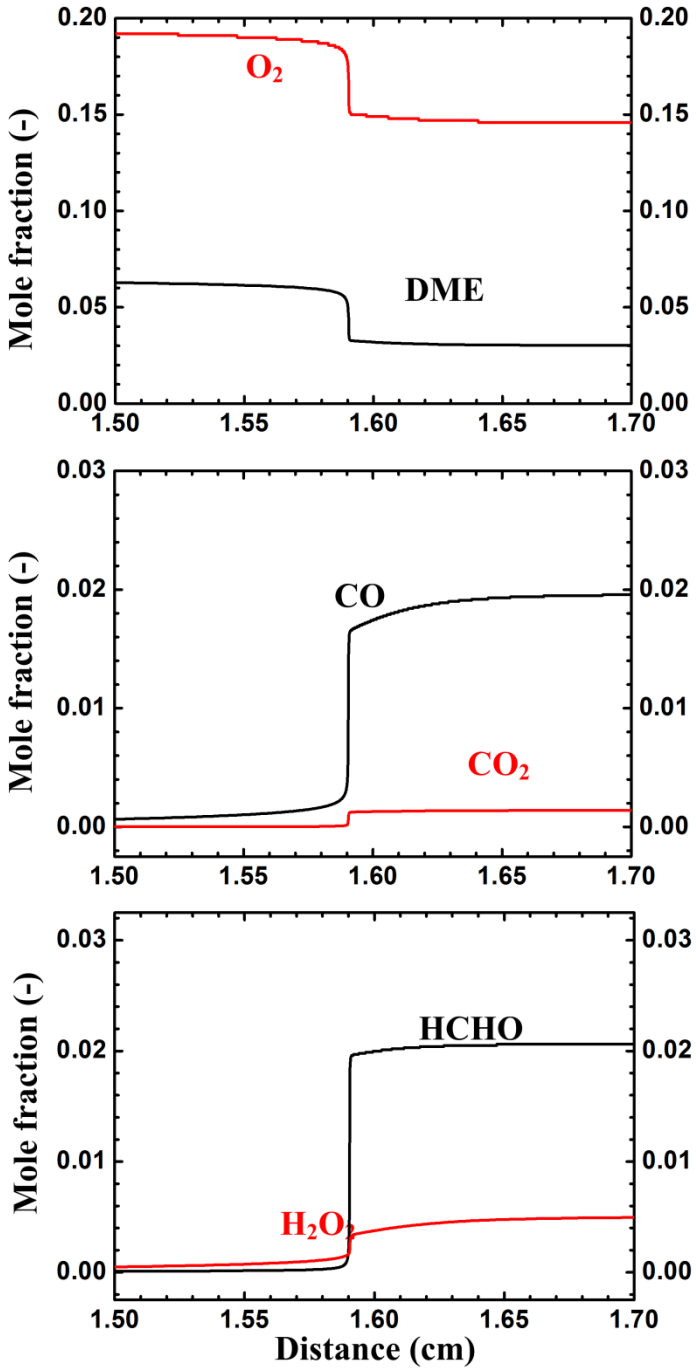

Figure 4.13 Profiles of mole fractions of DME, O_2, CO, CO_2, HCHO, and H_2O_2 (T_R = 538 K and ϕ = 1.0)

First, a singular first-stage ignition regime exits at T_R = 538 K and ϕ = 1.0. The results are shown in Fig. 4.12 and Fig. 4.13. All the profiles show similarities to the singular first-stage ignition regime described in part 4.3.3. Notice that it is observed as stable oxidation at the

same condition in the experiments. Probably, this is because the resulting cool flame is too weak to detect.

4.5.3 Ignition regime-2: two-stage ignition

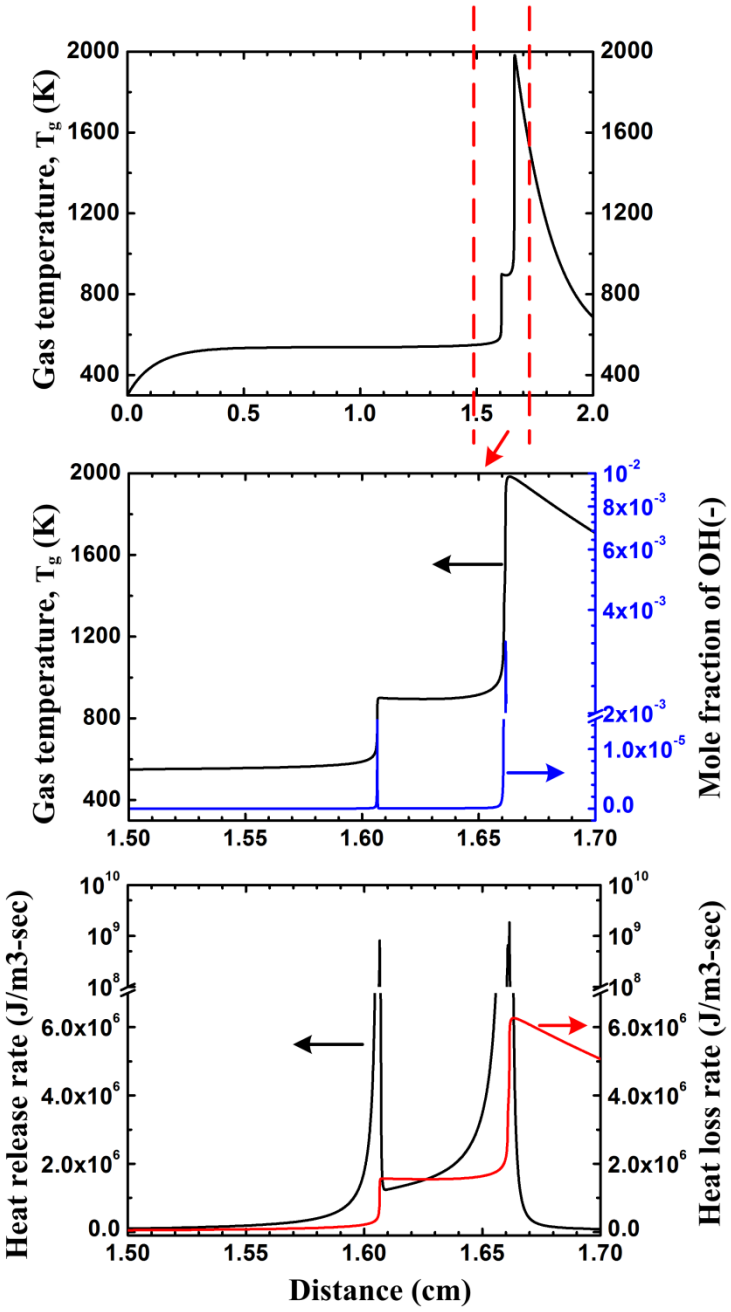

Figure 4.14 Profiles of gas temperature, OH mole fraction, heat release rate, and heat loss rate (T_R = 538 K and ϕ = 1.6)

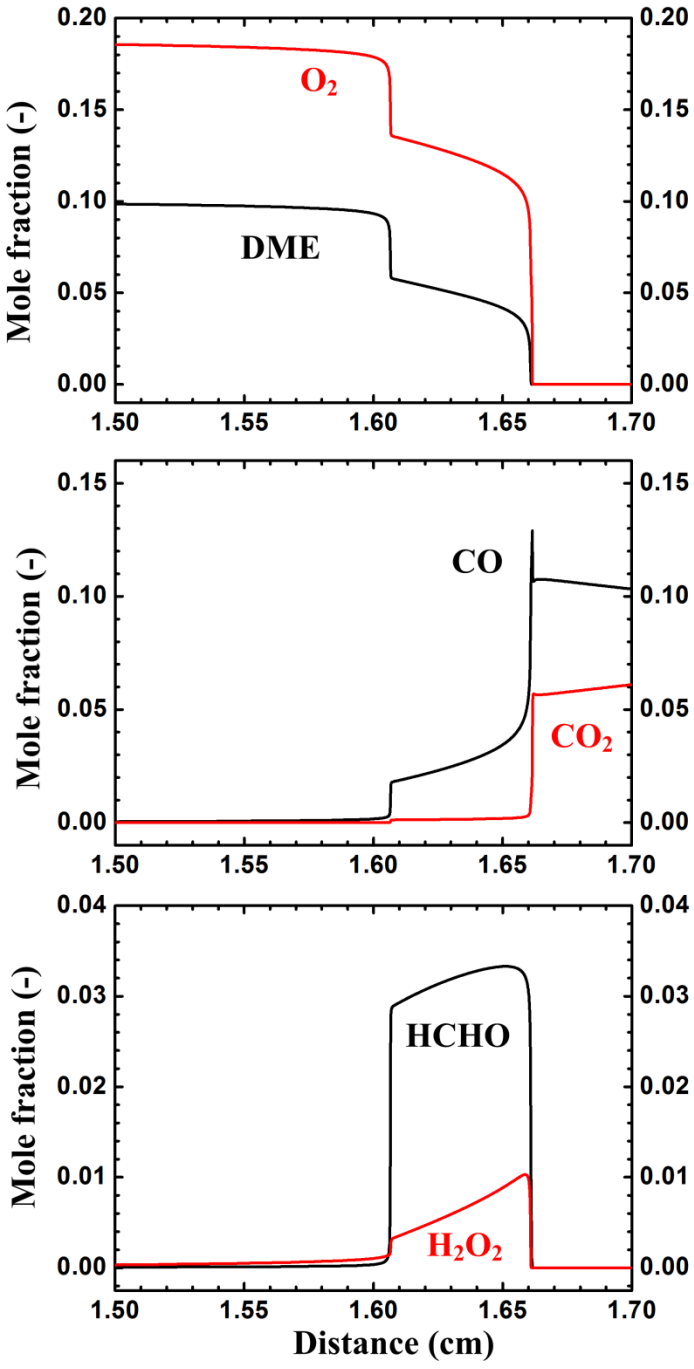

Figure 4.15 Profiles of mole fractions of DME, O_2, CO, CO_2, HCHO, and H_2O_2 (T_R = 538 K and ϕ = 1.6)

Secondly, a two-stage ignition regime exits at T_R = 538 K and ϕ = 1.6. The profiles of the results are shown in Fig. 4.14 and Fig. 4.15. Two rapid temperature increases appear in turn accompanied by two heat release peaks. Differently with that in the singular first-stage ignition regime, the temperature does not decrease, instead, gradually increases after the first-stage ignition until trigger the second-stage ignition. Heat release due to the second stage is much higher than that due to the first stage, and the gas temperature reaches about 2000K due to the large heat release rate from the second stage. This is observed as hot flame in the experiments, to say, the cool flame successfully transits to the hot flame.

Additionally, as shown in Fig. 4.15, HCHO, and H_2O_2 are produced in the first stage and then almost consumed out (mole fraction < 1E-7) in the second stage. DME and oxygen are partially consumed (about one third) in the first stage, and then almost consumed out by the second stage ignition. Regarding CO, it is formed in the first stage; while, in the second stage, it is firstly formed and then oxidized into CO_2. Eventually, both DME and oxygen are almost consumed out at this condition. Therefore, it is understood that equivalence ratio of 1.6 is an optimal condition to realize a complete two-stage ignition regime, which is consistent with the experimental findings in Chapter 3.

4.5.4 Ignition regime-3: transition suppressed ignition

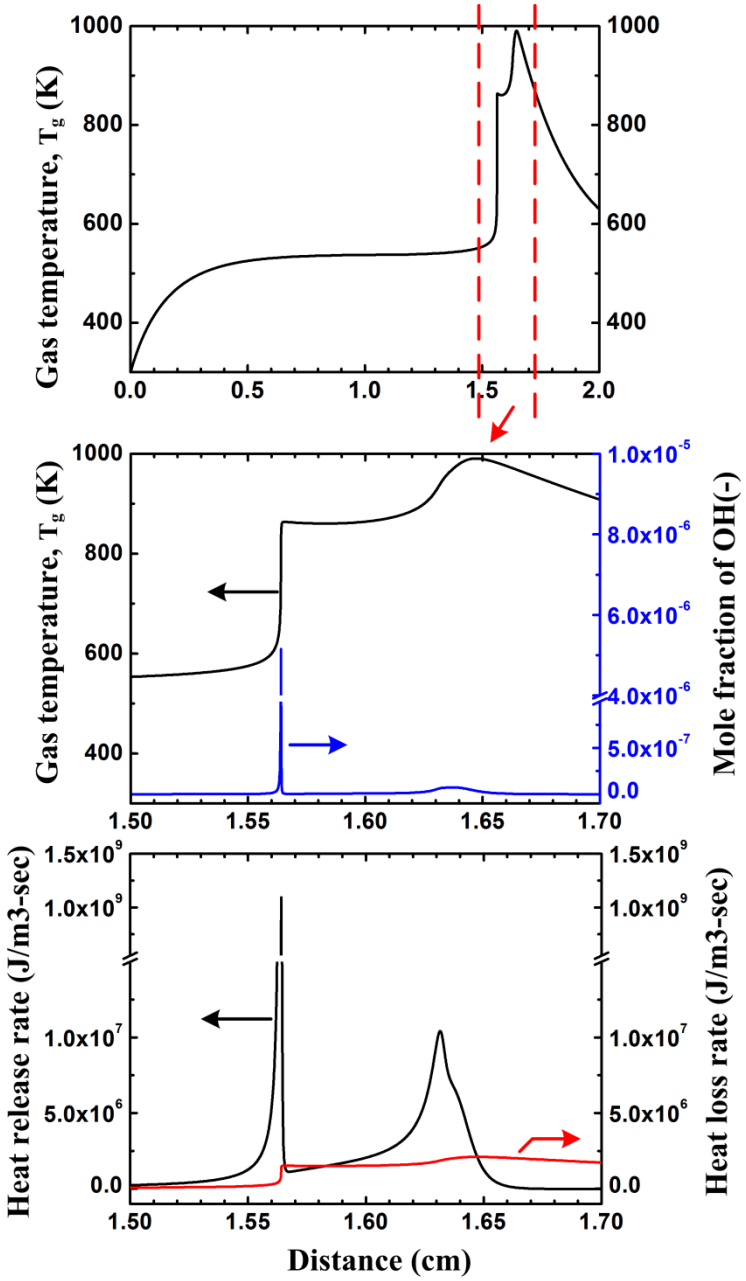

Figure 4.16 Profiles of gas temperature, OH mole fraction, heat release rate, and heat loss rate

(T_R = 538 K and ϕ = 10.7)

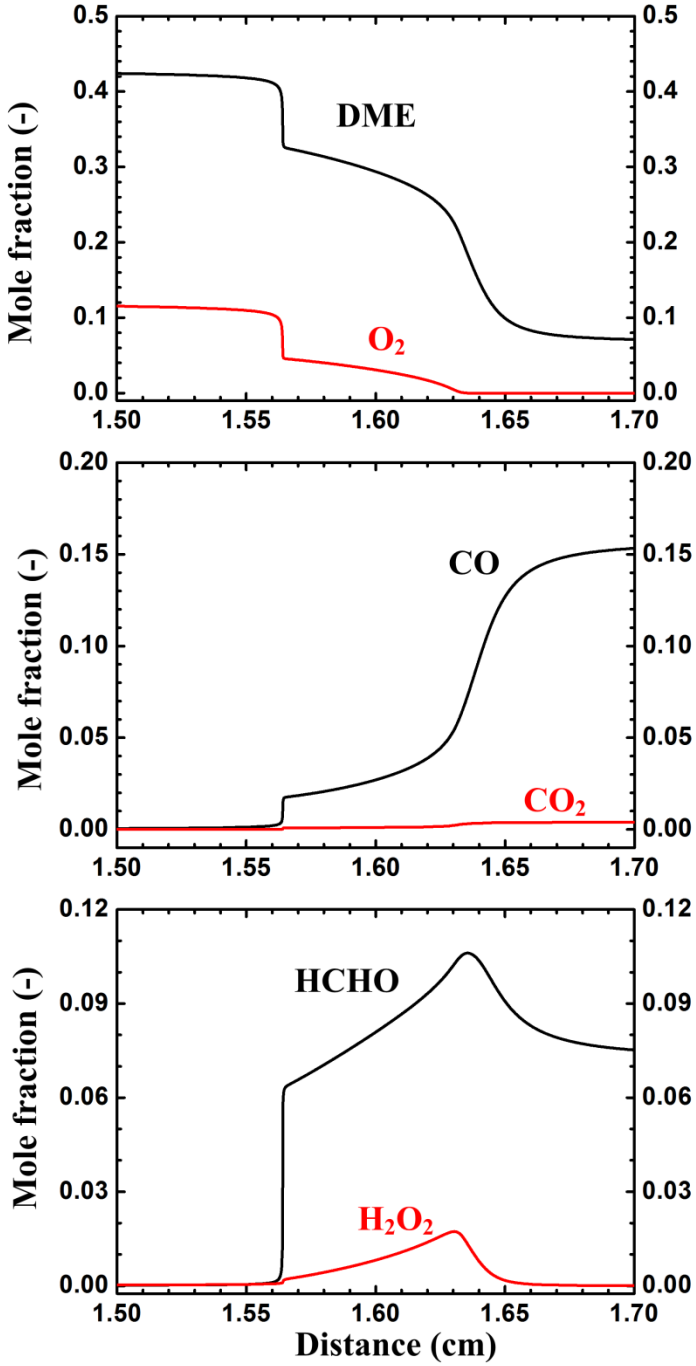

Figure 4.17 Profiles of mole fractions of DME, O_2, CO, CO_2, HCHO, and H_2O_2 (T_R = 538 K and ϕ = 10.7)

Finally, a transition suppressed regime appears at T_R = 538 K and ϕ = 10.7. The profiles of results are shown in Fig. 4.16 and Fig. 4.17. Although the temperature gradually increases

after the first-stage ignition, the second-stage ignition is remarkably suppressed. The marker species HCHO and H_2O_2 are formed due to the first stage ignition, however, only partially consumed by the second stage. This is because, the oxidation of HCHO and H_2O_2 are remarkably restrained due to the lack of oxygen at extremly high equivalence ratios. The heat release rate due to the second stage is therefore pretty low (< 10^7 J/m3-sec), and the tempeature reaches its peak only as low as 1000 K. That is to say, the transition from a cool flame to a hot flame is suppressed, and it is observed as a weak flame in the experiments.

4.6 The effect of E_{R248}

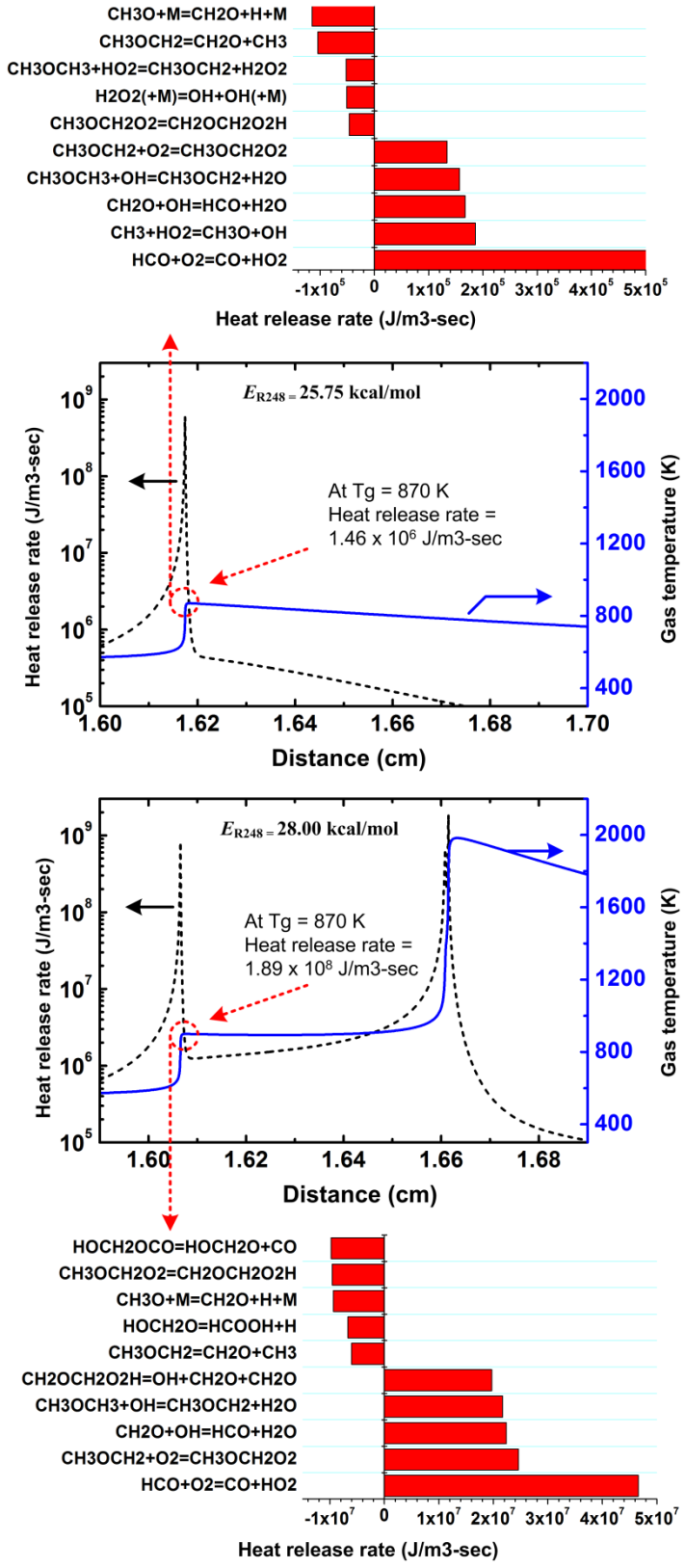

Figure 4.18 The effect of E_{R248} on heat release rates

In this section, we shall show the details how the activation energy of R248 affects the igntion regime. Fig. 4.18 compares the results with E_{R248} = 25.75 kcal/mol to that with E_{R248} = 28.00 kcal/mol. It is similar that gas temperature reaches about 870 K after accomplish the first-stage ignition. However, it is different that the heat release rates are different in order of magnitude at the same temperature (870K): the heat release rate is 1.46E6 J/m3-sec with E_{R248} = 25.75 kcal/mol and 1.89E8 J/m3-sec with E_{R248} = 28.00 kcal/mol. Note that same gas temperature implies same heat loss rate. Therefore, smaller heat release rate with smaller activation energy (E_{R248} = 25.75 kcal/mol) results in decrease of gas temperature after experiencing the first-stage ignition, failing to induce the second-stage ignition. While larger heat release rate with larger activation energy (E_{R248} = 28.00 kcal/mol) results in gradual increase of gas temperature after experiencing the first-stage ignition, eventually giving rise to the second-stage ignition.

The most contributed endothermic and exothermic elementary reactions are also shown in Fig. 4.18. The chain-propagation pathway is dominant at 870 K with the following reactions:

R264: $CH_3OCH_2+O_2=CH_3OCH_2O_2$

R272: $CH_2OCH_2O_2H=OH+HCHO+HCHO$

R44: $HCHO+OH=HCO+H_2O$

R31: $HCO+O_2=CO+HO_2$

It is shown that slight elevation of E_{R248} by 9% (from E_{R248} = 25.75 kcal/mol to E_{R248} = 28.00 kcal/mol) greatly increases the heat release rates of these reactions with about two orders of magnitude (from 10^5 J/m3-sec to 10^7 J/m3-sec). Moreover, it is noticed that the most contributed reaction is:

R31: $HCO+O_2=CO+HO_2$

in which O_2 is directly involved as a reactant. This could be an important reason why the equivalence ratio dramatically influences the ignition regime.

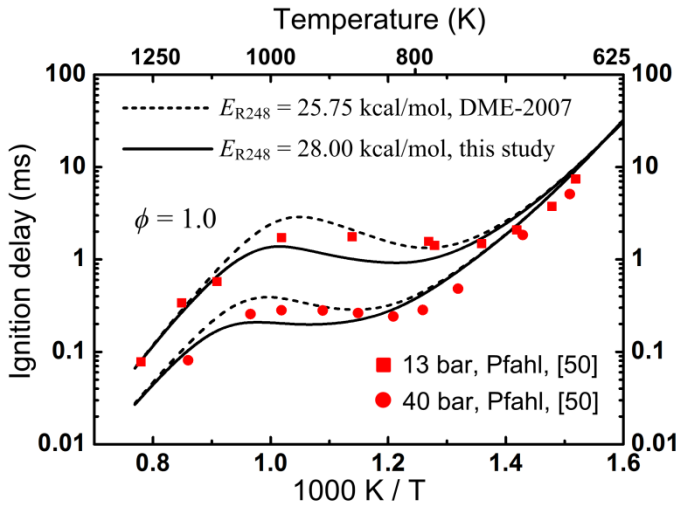

Figure 4.19 Comparison of experimental [50] and computational ignition delay times.

To further determine whether the modification of the activation energy is reasonable, simulations with the modified activation energy are compared to the shock tube ignition delay time results of Pfahl et al. [50], as shown in Fig. 4.19. It is seen that, the modification does not lead to difference at low-temperature (< 800 K) or at high-temperature (> 1100 K) region. This is because at low-temperature region oxidation is dominated by the chain-branching and chain-propagation pathways, which follow after R264; on the other hand, at high–temperature region, oxidation is dominated by the pathway following after R248. The competition between R248 and R264 mainly affects the performance at the mediate temperature region, where the NTC behavior exists. In the NTC region, the Zhao model over predicts the ignition delay times, while the modified activation energy model lower predicts the ignition

delay times. However, both show reasonable agreement with the experiments. It is understood that shorter ignition delay time essentially indicates higher reactivity in the NTC region, resulting in transition from a cool flame to a hot flame.

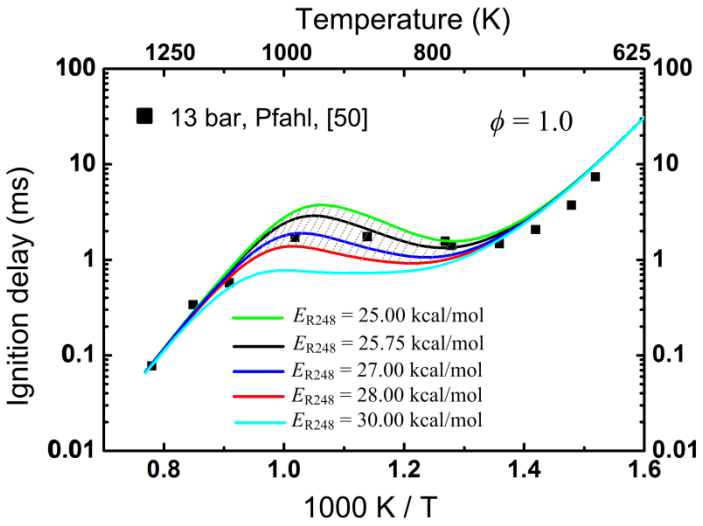

Figure 4.20 The effect of E_{R248} on ignition delay times.

One may wonder the igntion regime with other values of E_{R248}, such as slightly higher than 28.00 kcal/mol or slightly lower than 25.75 kcal/mol. Fig. 4.20 shows the ignition delay times with different values of E_{R248}. It is found that, the transition from a cool flame to a hot flame occurs with $E_{R248} \geq 28.00$ kcal/mol, while the transition fails to occur with $E_{R248} < 28.00$ kcal/mol. Again, the rate constants of R248 (or R264) dramatically influence the reactivity in the NTC region. More importantly, this effect cannot be captured in low-temperature (< 800 K) or high-temperature (> 1100 K) region. It is, therefore, very necessary to further determine the rate constants of these reactions via more specific experiments.

4.7 Conclusions

In this chapter, numerical computations are conducted using the plug-flow reactor model. Ignition limit is well predicted while discrepancy in predicting the transition from a cool flame to a hot flame is noticed. Reaction pathway analyses indicate that the competition between the β-scission reaction (R248) and the molecular oxygen addition reaction (R264) of the CH3OCH2 radical could strongly influence the transition from a cool flame to a hot flame.

It is further shown that based on a modified activation energy (ER248 = 28.00 kcal/mol), both ignition limit and ignition regime against equivalence ratio are predicted with good agreement. The two-stage ignition regime corresponds to the hot flame occurrence observed in the experiments, and the transition suppressed ignition regime corresponds to the weak flame occurrence in the experiments. Moreover, the model with the modification is able to predict the shock tube ignition delay results with reasonable agreement. The competition between the reactions R248 and R264 strongly influences the reactivity in the NTC region, therefore influences the transition from a cool flame to hot flame. It may need further and rigorous measurements of the rate constants of R248 and R264 to improve the DME ignition kinetics.

Chapter 5: Summary and Recommendations

5.1 Summary of conclusions

In this dissertation, low-temperature ignition of DME/air mixture is systematically investigated using flow reactor scenarios. Special attention is given to the low-temperature ignition limit and ignition regime associated with the transition from a cool flame to a hot flame.

Specifically, in Chapter 2, periodic behaviors with ignition, flame propagation, and extinction are interpreted. The weak flame is found to transit to the hot flame with decreasing equivalence ratio. A specific case, which includes both weak flames and hot flames, appears as a transition state between the weak flame and the hot flame. Time-sequential gas analyses were conducted, indicating that CH_4 and C_2H_2 act as two kinds of species formed due to low-temperature ignition. On the other hand, the intermediates HCHO, HCOOH, and CH_3OCHO, formed due to mild oxidation, are completely consumed by the hot flame. The observed ignition phenomenon, is suggested to be induced by the well-known chain-branching precursor CH_2OCH_2OOH radical, which could accumulate in a relatively longer exposure time.

In Chapter 3, thanks to the updated transparent flow reactor, phenomenological investigation on the two-stage ignition regime is conducted. Due to the NTC effect, both ignition regime and stable oxidation regime exist in the temperature-equivalence ratio (T - ϕ) plane. It shows that the ignition zone locates between 520K and 590 K. At temperatures above 590 K, ignition disappears while stable oxidation takes over the reaction status, indicating the NTC zone is encountered. Importantly, within the ignition zone, the detailed weak flame and hot flame motions are clearly observed. The gas analysis results against weak flame propagations confirm that the weak flame occurrence is accompanied by the formation of intermediate

product species, such as HCHO and CH_3OCHO. Due to the self-restrained feature, either fuel or oxygen cannot be consumed out thus remained in the product gas of the weak flame. Therefore, the weak flame is suggested to be cool flame, or the flame formed due to the suppression of the transition from a cool flame to a hot flame. Additionally, it is suspected that there might be another chain-propagation pathway via decomposition of HPMF without forming any OH radical. This reaction path gets pronounced at above 540 K, where the transition from a cool flame to a hot flame cannot be achieved whatever the equivalence ratio is.

In Chapter 4, numerical computation is conducted using the plug-flow reactor model to investigate the ignition kinetics. Ignition limit in the experiments is well predicted while discrepancy in predicting the transition from a cool flame to a hot flame is noticed. Thanks to reaction pathway analyses, it is indicated that the competition between the β-scission reaction and the molecular oxygen addition reaction of the CH_3OCH_2 radical could strongly influence the transition from a cool flame to a hot flame. It is further shown that based on a modified activation energy (E_{R248} = 28.00 kcal/mol), both the ignition limit and the ignition regimes against equivalence ratio are well predicted. The two-stage ignition regime corresponds to a hot flame observed in the experiments, and the transition suppressed ignition regime corresponds to a weak flame in the experiments. Moreover, the model with the modification is able to predict the shock tube ignition delay results with reasonable agreement. It is shown that the competition between the β-scission reaction and the molecular oxygen addition reaction of the CH_3OCH_2 radical strongly influences the reactivity in the NTC region, therefore influences the transition from a cool flame to hot flame. It is suggested that further measurements of the rate constants of the elementary reactions of the CH_3OCH_2 radical might be needed to improve the DME ignition kinetics.

5.2 Recommendations for future work

Based on the results of the present study, the following are some recommendations to pursue the studies on low-temperature ignition:

(1) The transparent flow reactor developed in the present study is proved to be a simple but efficient method to capture the phenomenon related to low-temperature ignition, especially the transition from a cool flame to a hot flame. However, the present study is limited to DME. The present work is waiting to be extended to many other practical fuels, such as (a) typical oxygenated fuels: diethyl ether (DEE), and ethanol; (b) typical alkanes: propane, n-butane, iso-butane,n-hexane, n-heptane. Note that ethanol and iso-butane may not possess the cool flame feature, however, they might be employed to conduct the comparison studies against DME and n-butane, respectively, due to the isomeric structures.

(2) In Chapter 4, to focus on the ignition kinetics, we conducted numerical simulation using the plug-flow model neglecting the mass and species transport effects. Actually, the periodic behavior capture in the experiments is an unsteady process with ignition, flame propagation and extinction. The realistic numerical simulation, which is complicated but possible, is expected to be performed in the future. Combined with the experimental results, it could be utilized to further validate and improve ignition kinetic models.

Reference

[1] T.A. Semelsberger, R.L. Borup, H.L. Greene, J. Power Sources, 156 (2006) 497-511.

[2] R.P. Verbeek, SAE Paper 941607, (1997).

[3] A.L. Boehman, Fuel Processing Technology, 89 (2008) 1243.

[4] C. Arcoumanis, C. Bae, R. Crookes, E. Kinoshita, Fuel, 87 (2008) 1014-1030.

[5] C.Y. Choi, R.D. Reitz, Fuel, 78 (1999) 1303-1317.

[6] M. Marchionna, R. Patrini, D. Sanfilippo, G. Migliavacca, Fuel Processing Technology, 89 (2008) 1255-1261.

[7] http://japan-dme.or.jp/english/index.html.

[8] M. Naito, C. Radcliffe, Y. Wada, T. Hoshino, X. Liu, M. Arai, M. Tamura, Journal of Loss Prevention in the Process Industries, 18 469-473.

[9] I. Glassman, R. Yetter, Combustion, Access Online via Elsevier, 2008.

[10] J.F. Griffiths, T. Inomata, Journal of the Chemical Society, Faraday Transactions, 88 (1992) 3153-3158.

[11] C. Gibson, P. Gray, J.F. Griffiths, S.M. Hasko, Symposium (International) on Combustion, 20 (1985) 101-109.

[12] O. Herbinet, F. Battin-Leclerc, S. Bax, H.L. Gall, P.-A. Glaude, R. Fournet, Z. Zhou, L. Deng, H. Guo, M. Xie, F. Qi, Physical Chemistry Chemical Physics, 13 (2011) 296-308.

[13] F. Battin-Leclerc, O. Herbinet, P.A. Glaude, R. Fournet, Z.Y. Zhou, L.L. Deng, H.J. Guo, M.F. Xie, F. Qi, Angewandte Chemie-International Edition, 49 (2010) 3169-3172.

[14] C. Bahrini, P. Morajkar, C. Schoemaecker, O. Frottier, O. Herbinet, P.-A. Glaude, F. Battin-Leclerc, C. Fittschen, Physical Chemistry Chemical Physics, 15 (2013) 19686-19698.

[15] P.A. Boettcher, R. Mével, V. Thomas, J.E. Shepherd, Fuel, 96 (2012) 392-403.

[16] M. Yahyaoui, N. Djebaïli-Chaumeix, P. Dagaut, C.E. Paillard, S. Gail, Combustion and Flame, 147 (2006) 67-78.

[17] A. Yamamoto, H. Oshibe, H. Nakamura, T. Tezuka, S. Hasegawa, K. Maruta, Proceedings of the Combustion Institute, 33 (2011) 3259-3266.

[18] D.M.A. Karwat, S.W. Wagnon, M.S. Wooldridge, C.K. Westbrook, Combustion and Flame, 160 (2013) 2693-2706.

[19] P. Dagaut, M. Reuillon, M. Cathonnet, Combustion and Flame, 101 (1995) 132-140.

[20] E. Ranzi, P. Gaffuri, T. Faravelli, P. Dagaut, Combustion and Flame, 103 (1995) 91-106.

[21] O. Herbinet, B. Husson, Z. Serinyel, M. Cord, V. Warth, R. Fournet, P.-A. Glaude, B. Sirjean, F. Battin-Leclerc, Z. Wang, M. Xie, Z. Cheng, F. Qi, Combustion and Flame, 159 (2012) 3455-3471.

[22] S. Jahangirian, S. Dooley, F.M. Haas, F.L. Dryer, Combustion and Flame, 159 (2012) 30-43.

[23] M.J. Pilling, Low-temperature combustion and autoignition, Access Online via Elsevier, 1997.

[24] J. Zádor, C.A. Taatjes, R.X. Fernandes, Progress in Energy and Combustion Science, 37 (2011) 371-421.

[25] R.S. Sheinson, F.W. Williams, Combustion and Flame, 21 (1973) 221-230.
[26] H. Yamada, K. Suzaki, A. Tezaki, Y. Goto, Combustion and Flame, 154 (2008) 248-258.
[27] H. Yamada, K. Suzaki, H. Sakanashi, N. Choi, A. Tezaki, Combustion and Flame, 140 (2005) 24-33.
[28] Y. Ju, W. Sun, M.P. Burke, X. Gou, Z. Chen, Proceedings of the Combustion Institute, 33 (2011) 1245-1251.
[29] H. Yamada, M. Yoshii, A. Tezaki, Proceedings of the Combustion Institute, 30 (2005) 2773-2780.
[30] C.K. Westbrook, Proceedings of the Combustion Institute, 28 (2000) 1563-1577.
[31] C.K. Law, Combustion physics, Cambridge University Press, 2006.
[32] R. Shan, T. Lu, Combustion and Flame, 159 (2012) 2069-2076.
[33] P. Zhao, C.K. Law, Combustion and Flame, 160 (2013) 2352-2358.
[34] C.K. Law, P. Zhao, Combustion and Flame, 159 (2012) 1044-1054.
[35] V. Nayagam, D.L. Dietrich, P.V. Ferkul, M.C. Hicks, F.A. Williams, Combustion and Flame, 159 (2012) 3583-3588.
[36] O. Moriue, Y. Nishiyama, Y. Yamaguchi, H. Hashimoto, E. Murase, Proceedings of the Combustion Institute, 34 (2013) 1585-1592.
[37] T.I. Farouk, F.L. Dryer, Combustion and Flame, 161 (2014) 565-581.
[38] J. Sehested, K. Sehested, J. Platz, H. Egsgaard, O.J. Nielsen, International Journal of Chemical Kinetics, 29 (1997) 627-636.
[39] J. Sehested, T. Mogelberg, T.J. Wallington, E.W. Kaiser, O.J. Nielsen, Journal of Physical Chemistry, 100 (1996) 17218-17225.
[40] M.M. Maricq, J.J. Szente, J.D. Hybl, The Journal of Physical Chemistry A, 101 (1997) 5155-5167.
[41] M.E. Jenkin, G.D. Hayman, T.J. Wallington, M.D. Hurley, J.C. Ball, O.J. Nielsen, T. Ellermann, The Journal of Physical Chemistry, 97 (1993) 11712-11723.
[42] S.M. Japar, T.J. Wallington, J.F.O. Richert, J.C. Ball, International Journal of Chemical Kinetics, 22 (1990) 1257-1269.
[43] P. Dagaut, C. Daly, J.M. Simmie, M. Cathonnet, Symposium (International) on Combustion, 27 (1998) 361-369.
[44] P. Dagaut, J.-C. Boettner, M. Cathonnet, Symposium (International) on Combustion, 26 (1996) 627-632.
[45] H.J. Curran, W.J. Pitz, C.K. Westbrook, P. Dagaut, J.C. Boettner, M. Cathonnet, International Journal of Chemical Kinetics, 30 (1998) 229-241.
[46] I. Liu, N.W. Cant, J.H. Bromly, F.J. Barnes, P.F. Nelson, B.S. Haynes, Chemosphere, 42 (2001) 583-589.
[47] S.L. Fischer, F.L. Dryer, H.J. Curran, International Journal of Chemical Kinetics, 32 (2000) 713-740.

[48] H.J. Curran, S.L. Fischer, F.L. Dryer, International Journal of Chemical Kinetics, 32 (2000) 741-759.
[49] Z. Zhao, M. Chaos, A. Kazakov, F.L. Dryer, International Journal of Chemical Kinetics, 40 (2008) 1-18.
[50] U. Pfahl, K. Fieweger, G. Adomeit, Symposium (International) on Combustion, 26 (1996) 781-789.
[51] X. Qin, Y. Ju, Proceedings of the Combustion Institute, 30 (2005) 233-240.
[52] A. McIlroy, T.D. Hain, H.A. Michelsen, T.A. Cool, Proceedings of the Combustion Institute, 28 (2000) 1647-1653.
[53] C.A. Daly, J.M. Simmie, J. Würmel, N. DjebaÏli, C. Paillard, Combustion and Flame, 125 (2001) 1329-1340.
[54] E.W. Kaiser, T.J. Wailington, M.D. Hurley, J. Platz, H.J. Curran, W.J. Pitz, C.K. Westbrook, J. Phys. Chem. A, 104 (2000) 8194-8206.
[55] Z. Zhao, A. Kazakov, F.L. Dryer, Combustion and Flame, 139 (2004) 52-60.
[56] H. Oshibe, H. Nakamura, T. Tezuka, S. Hasegawa, K. Maruta, Combustion and Flame, 157 (2010) 1572-1580.
[57] F. Herrmann, P. Oßwald, K. Kohse-Höinghaus, Proceedings of the Combustion Institute, 34 (2013) 771-778.
[58] H. Guo, W. Sun, F.M. Haas, T. Farouk, F.L. Dryer, Y. Ju, Proceedings of the Combustion Institute, 34 (2013) 573-581.
[59] G. Mittal, M. Chaos, C.-J. Sung, F.L. Dryer, Fuel Processing Technology, 89 (2008) 1244-1254.
[60] F.L. Dryer, M. Chaos, Combustion and Flame, 152 (2008) 293-299.
[61] M. Chaos, F.L. Dryer, Combust. Sci. Technol., 180 (2008) 1053-1096.
[62] C.T. Bowman, D.M. Golden, R.K. Hanson, H. Pitsch, D.F. Davidson, A. Bardos, R. Cook, Z. Hong, P. Iyengar, S. Shashank, S. Vasu, K. Walters, R. Malhotra, GCEP Technical Report http://gcep.stanford.edu/pdfs/QeJ5maLQQrugiSYMF3ATDA/2.6.5.bowman_06.pdf.
[63] Y. Nakamura, D. Tsukanaka, H. Ito, S. Sagawa, in: 6th Asian DME Conference 2009.
[64] Y. Nakamura, H. Ito, S. Sagawa, D. Tsukanaka, in: Work-In Progress Poster Colloquium at 32th International Symposium on Combustion, 2008.
[65] Y. Tsuboi, T. Yokomori, K. Maruta, Proceedings of the Combustion Institute, 32 (2009) 3075-3081.
[66] K. Maruta, T. Kataoka, N.I. Kim, S. Minaev, R. Fursenko, Proceedings of the Combustion Institute, 30 (2005) 2429-2436.
[67] H. Nakamura, A. Fan, S. Minaev, E. Sereshchenko, R. Fursenko, Y. Tsuboi, K. Maruta, Combustion and Flame, 159 (2012) 1631-1643.
[68] A. Andersen, E.A. Carter, Isr. J. Chem., 42 (2002) 245-260.
[69] A. Andersen, E.A. Carter, J. Phys. Chem. A, 107 (2003) 9463-9478.
[70] B.F. Gray, P.G. Felton, Combustion and Flame, 23 (1974) 295-304.

[71] Z. Chen, X. Qin, Y. Ju, Z. Zhao, M. Chaos, F.L. Dryer, Proceedings of the Combustion Institute, 31 (2007) 1215-1222.
[72] J. Holman, in, McGraw-Hill Inc, 2002.
[73] Y. Wang, J. Wu, Z. Liu, Journal of Chemical & Engineering Data, 51 (2006) 164-168.
[74] CHEMKIN-Pro release 15101, March 27, 2013.http://www.reactiondesign.com/products/open/chemkin-pro.html
[75] L.F. Loucks, K.J. Laidler, Canadian Journal of Chemistry, 45 (1967) 2767-2773.

Appendix A: Estimate of thermal conductivities

Thermal conductivities are required in the numerical calculations in Chapter 4. In the temperature range of 510 K to 540 K, the conductivity of DME is calculated by [73]:

λ (T) = 19.99 + 0.1482 * (T – 317.2) (unit: mW/m·K)

and the conductivity of air is calculated by :

λ (T) = 39.3 + 0.067 * (T - 473) (unit: mW/m·K)

conductivities of gas mixture at different equivalence ratios are estimated by:

$$\lambda = \frac{\sum \lambda_k \, y_k \, W_k^{1/3}}{y_k \, W_k^{1/3}}$$

λ_k – thermal conductivity of gas *k*;

y_k – mole fraction of gas *k*;

W_k – molecular weight of gas *k*;

Therefore, the conductivities of gas mixture and corresponding heat transfer coefficients (*h*) at different equivalence ratios are as follows:

equivalence ratio	0.5	1.0	1.6	4.1	10.7
λ (mW/m·K)	43.11	43.42	43.76	44.87	46.62
h (W/m^2·K)	13	13	13	14	14

Note that *Nu* = 3.66, the diameter of reactor *d* = 0.012 m, and *Nu* = 1000*hd*/λ

Appendix B: Determination of grid size in numerical calculation

The numerical calculation is performed using the CHEMKIN-Pro software. Current calculations are conducted with the even grid size of Δx = 0.5 μm. As shown in Fig. 1, reducing the grid size by a factor of 2 from Δx = 0.5 μm to Δx = 0.25 μm gives no significant difference in results. Therefore, grid size is set to Δx = 0.5 μm in the numerical calculations in Chapter 4.

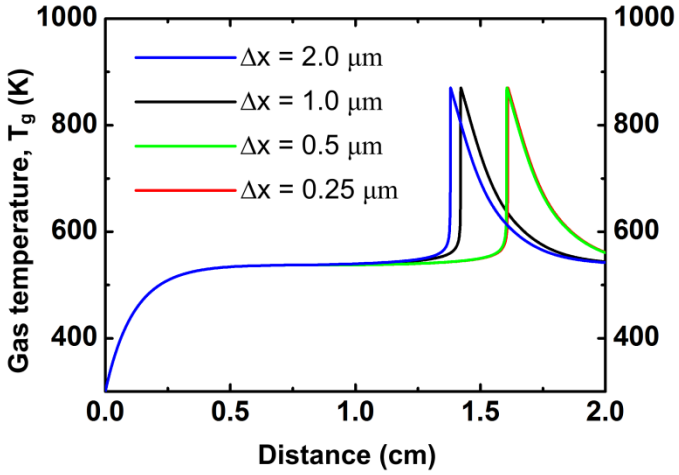

Fig. 1 Computation results of temperature using different grid sizes (T_R = 538 K and ϕ = 1.6)

Appendix C: Effect of the heat transfer coefficient

In Chapter 4, heat transfer between the reactor wall and the flowing gas mixture is considered in the numerical computations. The Nusselt number is set to Nu = 3.66 due to the fact that reactor wall temperature is uniform. Then, the results show that ignition regime strongly depends on the reaction rate constants of the elementary reaction R248. One may wonder the dependence of Nu as well, to say, whether the conclusions are solid at varied Nu?

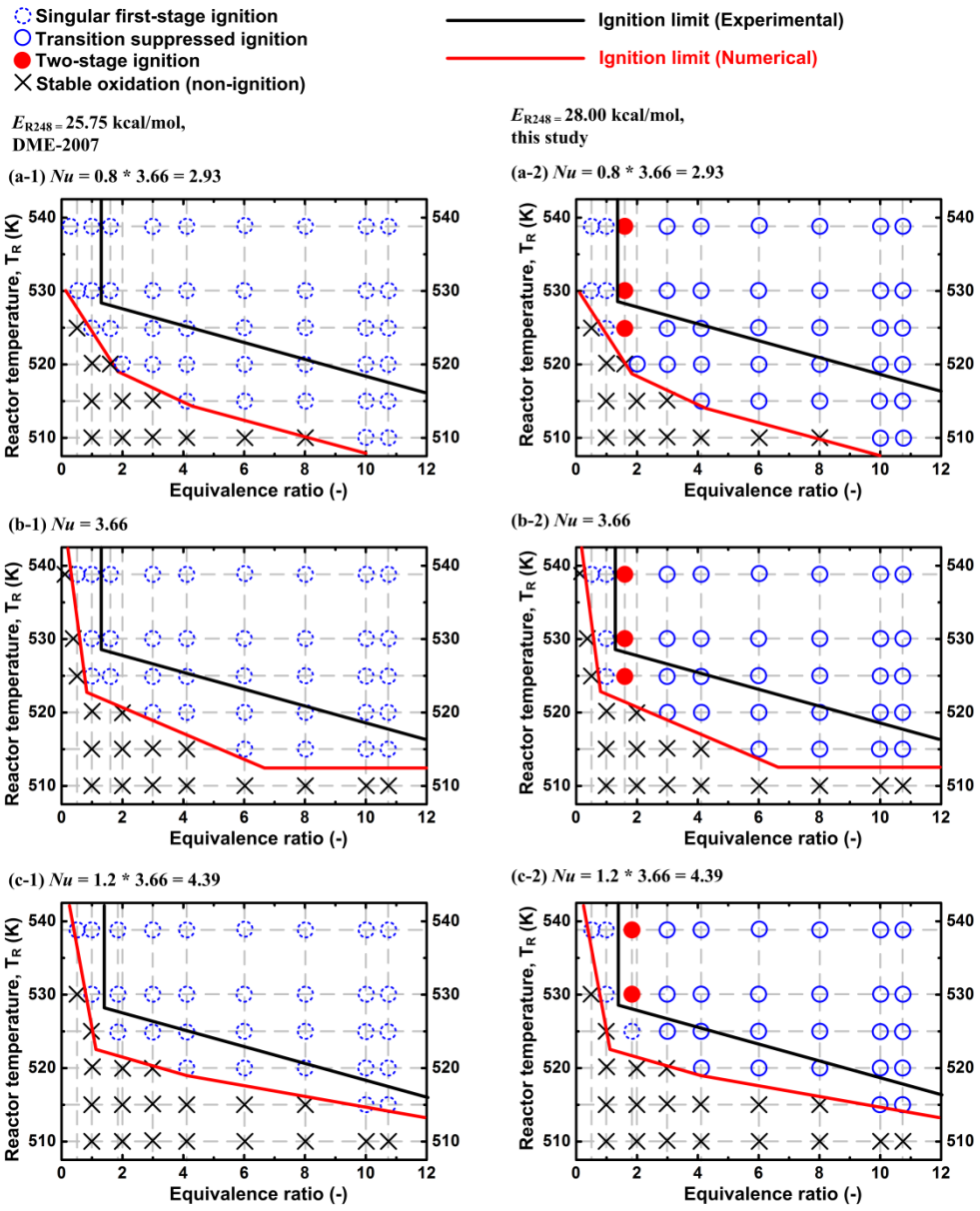

Fig. 2 Ignition limit and ignition regime at different values of Nu

Therefore, the effect of *Nu* should is checked here in the range of $2.93 < Nu < 4.36$. Note that the discussion and conclusions in Chapter 4 relies on Nu = 3.66, while Nu = 2.93 and Nu = 4.36 equals to 0.8 and 1.2 times of Nu = 3.66, respectively. The ignition regimes, at Nu = 2.93, 3.66, and 4.39, and at E_{R248} = 25.75 kcal/mol and E_{R248} = 28.00 kcal/mol are shown in Fig. 2. It is seen that the *Nu* slightly influences the ignition limit: the lower limit in temperature to achieve ignition is slightly elevated as the Nu increases from 2.93 to 4.36. However, the conclusion related to the dramatic effect of E_{R248} is solid at any *Nu* within the range of $2.93 < Nu < 4.36$. At E_{R248} = 25.75 kcal/mol, singular first-stage ignition regimes are realized at all ignition conditions; once the activation energy is modified as E_{R248} = 28.00 kcal/mol, three kinds of ignition regimes, singular first-stage ignition, two-stage ignition, and transition suppressed ignition, appear as a function of equivalence ratio.

Appendix D: Numerical computation results with the DME-2000 model

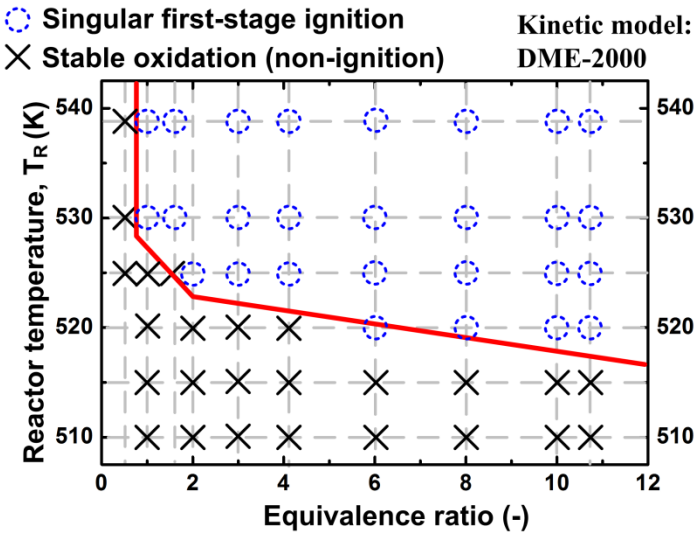

Fig. 3 Prediction of low-temperature ignition limit of DME/air mixture with DME-2000

In Chapter 4, the computations are performed with the detailed kinetic model DME-2007. Actually, the previous version DME-2000 has also been tested. The prediction using DME-2000 is shown in Fig. 3. Comparing Fig. 3 to Fig. 4.2, a good agreement in terms of the ignition limit with the experiments is observed. Moreover, comparing Fig. 3 to Fig. 4.4, DME-2000 predicts about 5 K higher limit than DME-2007. This should be caused by the update of the reaction:

$$HPMF(HOOCH_2OCHO) \rightarrow OCH_2OCHO + OH \qquad (R275)$$

Regarding the rate constants of the reaction in the two models, it has a similar activation energy, however, the pre-factor A was increased from 2.00E16 in DME-2000 to 3.00E16 in

DME-2007. As mentioned, this is a very important reaction in the chain-branching pathway to release OH radicals. The increasing of the pre-factor A leads to higher reactivity, therefore, resulting in lower ignition limit in temperature.

It shows that both the DME-2000 and the DME-2007 models predict the ignition limits with good agreement. Considering DME-2007 is the latest updated one, the discussion presented in Chapter 4 are based on DME-2007.

The activation energy of the reaction R248 in DME-2000 is E_{R248} = 25.5 kcal/mol. Similarly, with elevated E_{R248} of E_{R248} = 32.00 kcal/mol, three kinds of ignition regimes can be obtained to predict the experimental results, as shown in Fig. 4.

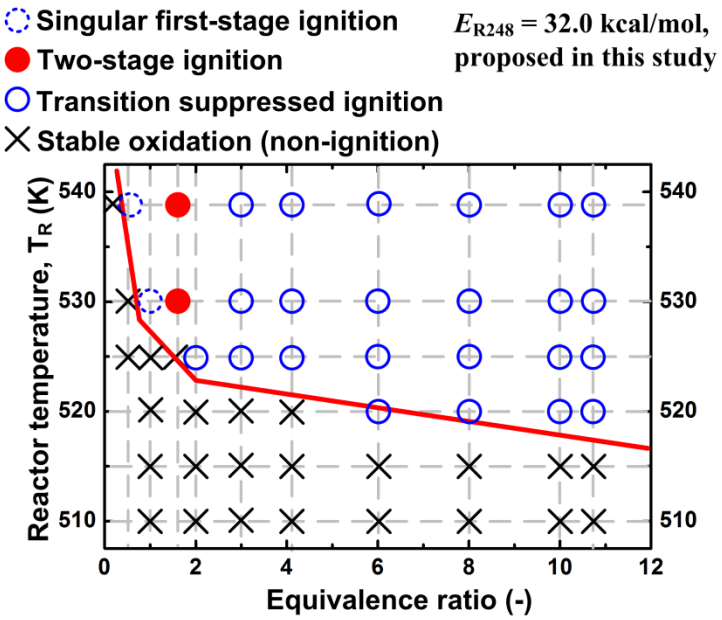

Fig. 4 Prediction of low-temperature ignition limit of DME/air mixture with the modification of E_{R248} = 32.00 kcal/mol

Appendix E: Reaction rate coefficients of the DME-2007 model

Units: cm3/mol/sec/cal; (k = A T**b exp(-E/RT))

REACTION			A	b	E
1. H+O2=O+OH			3.55E+15	-0.4	16599.0
2. O+H2=H+OH			5.08E+04	2.7	6290.0
3. H2+OH=H2O+H			2.16E+08	1.5	3430.0
4. O+H2O=OH+OH			2.97E+06	2.0	13400.0
5. H2+M=H+H+M			4.58E+19	-1.4	104380.0
H2	Enhanced by	2.500E+00			
H2O	Enhanced by	1.200E+01			
CO	Enhanced by	1.900E+00			
CO2	Enhanced by	3.800E+00			
AR	Enhanced by	0.000E+00			
HE	Enhanced by	0.000E+00			
6. H2+AR=H+H+AR			5.84E+18	-1.1	104380.0
7. H2+HE=H+H+HE			5.84E+18	-1.1	104380.0
8. O+O+M=O2+M			6.16E+15	-0.5	0.0
H2	Enhanced by	2.500E+00			
H2O	Enhanced by	1.200E+01			
AR	Enhanced by	0.000E+00			
HE	Enhanced by	0.000E+00			
CO	Enhanced by	1.900E+00			
CO2	Enhanced by	3.800E+00			
9. O+O+AR=O2+AR			1.89E+13	0.0	-1788.0
10. O+O+HE=O2+HE			1.89E+13	0.0	-1788.0
11. O+H+M=OH+M			4.71E+18	-1.0	0.0
H2	Enhanced by	2.500E+00			
H2O	Enhanced by	1.200E+01			
AR	Enhanced by	7.500E-01			
HE	Enhanced by	7.500E-01			
CO	Enhanced by	1.900E+00			
CO2	Enhanced by	3.800E+00			
12. H+OH+M=H2O+M			3.80E+22	-2.0	0.0
H2	Enhanced by	2.500E+00			
H2O	Enhanced by	1.200E+01			
AR	Enhanced by	3.800E-01			
HE	Enhanced by	3.800E-01			
CO	Enhanced by	1.900E+00			
CO2	Enhanced by	3.800E+00			
13. H+O2(+M)=HO2(+M)			1.48E+12	0.6	0.0
Low pressure limit:	0.63660E+21	-0.17200E+01 0.52480E+03			
TROE centering:	0.80000E+00	0.10000E-29 0.10000E+31			
H2	Enhanced by	2.000E+00			
H2O	Enhanced by	1.100E+01			
O2	Enhanced by	7.800E-01			
CO	Enhanced by	1.900E+00			
CO2	Enhanced by	3.800E+00			
14. HO2+H=H2+O2			1.66E+13	0.0	823.0
15. HO2+H=OH+OH			7.08E+13	0.0	295.0
16. HO2+O=O2+OH			3.25E+13	0.0	0.0
17. HO2+OH=H2O+O2			2.89E+13	0.0	-497.0
18. HO2+HO2=H2O2+O2			4.20E+14	0.0	11982.0
Declared duplicate reaction...					
19. HO2+HO2=H2O2+O2			1.30E+11	0.0	-1629.3
Declared duplicate reaction...					
20. H2O2(+M)=OH+OH(+M)			2.95E+14	0.0	48430.0
Low pressure limit:	0.12020E+18	0.00000E+00 0.45500E+05			
TROE centering:	0.50000E+00	0.10000E-29 0.10000E+31			
H2	Enhanced by	2.500E+00			
H2O	Enhanced by	1.200E+01			
CO	Enhanced by	1.900E+00			
CO2	Enhanced by	3.800E+00			

```
      AR                  Enhanced by     6.400E-01
      HE                  Enhanced by     6.400E-01
 21. H2O2+H=H2O+OH                                    2.41E+13   0.0      3970.0
 22. H2O2+H=HO2+H2                                    4.82E+13   0.0      7950.0
 23. H2O2+O=OH+HO2                                    9.55E+06   2.0      3970.0
 24. H2O2+OH=HO2+H2O                                  1.00E+12   0.0         0.0
      Declared duplicate reaction...
 25. H2O2+OH=HO2+H2O                                  5.80E+14   0.0      9557.0
      Declared duplicate reaction...
 26. CO+O(+M)=CO2(+M)                                 1.80E+10   0.0      2384.0
      Low pressure limit:  0.15500E+25 -0.27900E+01  0.41910E+04
      H2                  Enhanced by     2.500E+00
      H2O                 Enhanced by     1.200E+01
      AR                  Enhanced by     8.700E-01
      CO                  Enhanced by     1.900E+00
      CO2                 Enhanced by     3.800E+00
 27. CO+O2=CO2+O                                      2.53E+12   0.0     47700.0
 28. CO+HO2=CO2+OH                                    3.01E+13   0.0     23000.0
 29. CO+OH=CO2+H                                      2.23E+05   1.9     -1158.7
 30. HCO+M=H+CO+M                                     4.75E+11   0.7     14874.0
      H2                  Enhanced by     2.500E+00
      H2O                 Enhanced by     6.000E+00
      CO                  Enhanced by     1.900E+00
      CO2                 Enhanced by     3.800E+00
 31. HCO+O2=CO+HO2                                    7.58E+12   0.0       410.0
 32. HCO+H=CO+H2                                      7.23E+13   0.0         0.0
 33. HCO+O=CO+OH                                      3.02E+13   0.0         0.0
 34. HCO+OH=CO+H2O                                    3.02E+13   0.0         0.0
 35. HCO+O=CO2+H                                      3.00E+13   0.0         0.0
 36. HCO+HO2=CO2+OH+H                                 3.00E+13   0.0         0.0
 37. HCO+HCO=H2+CO+CO                                 3.00E+12   0.0         0.0
 38. HCO+CH3=CO+CH4                                   2.65E+13   0.0         0.0
 39. HCO+HCO=CH2O+CO                                  3.00E+13   0.0         0.0
 40. CH2O+M=HCO+H+M                                   3.30E+39  -6.3     99900.0
      H2                  Enhanced by     2.500E+00
      H2O                 Enhanced by     1.200E+01
      CO                  Enhanced by     1.900E+00
      CO2                 Enhanced by     3.800E+00
      AR                  Enhanced by     7.000E-01
 41. CH2O+M=CO+H2+M                                   3.10E+45  -8.0     97510.0
      H2                  Enhanced by     2.500E+00
      H2O                 Enhanced by     1.200E+01
      CO                  Enhanced by     1.900E+00
      CO2                 Enhanced by     3.800E+00
      AR                  Enhanced by     7.000E-01
 42. CH2O+H=HCO+H2                                    5.74E+07   1.9      2748.6
 43. CH2O+O=HCO+OH                                    1.81E+13   0.0      3080.0
 44. CH2O+OH=HCO+H2O                                  3.43E+09   1.2      -447.0
 45. CH2O+O2=HCO+HO2                                  1.23E+06   3.0     52000.0
 46. CH2O+HO2=HCO+H2O2                                4.11E+04   2.5     10210.0
 47. CH2O+CH3=HCO+CH4                                 3.64E-06   5.4       998.0
 48. CH3+O=CH2O+H                                     8.43E+13   0.0         0.0
 49. CH3+O2=CH3O+O                                    1.99E+18  -1.6     29230.0
 50. CH3+O2=CH2O+OH                                   3.74E+11   0.0     14640.0
 51. CH3+HO2=CH3O+OH                                  2.41E+10   0.8     -2325.0
 52. CH3+CH3(+M)=C2H6(+M)                             2.28E+15  -0.7       174.9
      Low pressure limit:  0.80540E+32 -0.37500E+01  0.98160E+03
      TROE centering:      0.00000E+00  0.57000E+03  0.00000E+00  0.10000E+31
      H2O                 Enhanced by     5.000E+00
      CO                  Enhanced by     2.000E+00
      CO2                 Enhanced by     3.000E+00
 53. CH3+H(+M)=CH4(+M)                                1.27E+16  -0.6       383.0
      Low pressure limit:  0.24770E+34 -0.47600E+01  0.24400E+04
      TROE centering:      0.78300E+00  0.74000E+02  0.29410E+04  0.69640E+04
      H2                  Enhanced by     2.000E+00
      H2O                 Enhanced by     6.000E+00
      CH4                 Enhanced by     2.000E+00
      CO                  Enhanced by     1.500E+00
      CO2                 Enhanced by     2.000E+00
```

C2H6 Enhanced by 3.000E+00
AR Enhanced by 7.000E-01

54. CH4+H=CH3+H2 5.47E+07 2.0 11210.0
55. CH4+O=CH3+OH 3.15E+12 0.5 10290.0
56. CH4+OH=CH3+H2O 5.72E+06 2.0 2639.0
57. CH3+HO2=CH4+O2 3.16E+12 0.0 0.0
58. CH4+HO2=CH3+H2O2 1.81E+11 0.0 18580.0
59. CH2OH+M=CH2O+H+M 1.00E+14 0.0 25100.0
60. CH2OH+H=CH2O+H2 6.00E+12 0.0 0.0
61. CH2OH+H=CH3+OH 9.64E+13 0.0 0.0
62. CH2OH+O=CH2O+OH 4.20E+13 0.0 0.0
63. CH2OH+OH=CH2O+H2O 2.40E+13 0.0 0.0
64. CH2OH+O2=CH2O+HO2 2.41E+14 0.0 5017.0
Declared duplicate reaction...
65. CH2OH+O2=CH2O+HO2 1.51E+15 -1.0 0.0
Declared duplicate reaction...
66. CH2OH+HO2=CH2O+H2O2 1.20E+13 0.0 0.0
67. CH2OH+HCO=CH3OH+CO 1.00E+13 0.0 0.0
68. CH2OH+HCO=CH2O+CH2O 1.50E+13 0.0 0.0
69. 2CH2OH=CH3OH+CH2O 3.00E+12 0.0 0.0
70. CH2OH+CH3O=CH3OH+CH2O 2.40E+13 0.0 0.0
71. CH3O+M=CH2O+H+M 8.30E+17 -1.2 15500.0
72. CH3O+H=CH3+OH 3.20E+13 0.0 0.0
73. CH3O+O=CH2O+OH 6.00E+12 0.0 0.0
74. CH3O+OH=CH2O+H2O 1.80E+13 0.0 0.0
75. CH3O+O2=CH2O+HO2 9.03E+13 0.0 11980.0
Declared duplicate reaction...
76. CH3O+O2=CH2O+HO2 2.20E+10 0.0 1748.0
Declared duplicate reaction...
77. CH3O+HO2=CH2O+H2O2 3.00E+11 0.0 0.0
78. CH3O+CO=CH3+CO2 1.60E+13 0.0 11800.0
79. CH3O+HCO=CH3OH+CO 9.00E+13 0.0 0.0
80. 2CH3O=CH3OH+CH2O 6.00E+13 0.0 0.0
81. OH+CH3(+M)=CH3OH(+M) 2.79E+18 -1.4 1330.0
Low pressure limit: 0.40000E+37 -0.59200E+01 0.31400E+04
TROE centering: 0.41200E+00 0.19500E+03 0.59000E+04 0.63940E+04
H2 Enhanced by 2.000E+00
H2O Enhanced by 6.000E+00
CH4 Enhanced by 2.000E+00
CO Enhanced by 1.500E+00
CO2 Enhanced by 2.000E+00
C2H6 Enhanced by 3.000E+00
82. H+CH2OH(+M)=CH3OH(+M) 1.06E+12 0.5 86.0
Low pressure limit: 0.43600E+32 -0.46500E+01 0.50800E+04
TROE centering: 0.60000E+00 0.10000E+03 0.90000E+05 0.10000E+05
H2 Enhanced by 2.000E+00
H2O Enhanced by 6.000E+00
CH4 Enhanced by 2.000E+00
CO Enhanced by 1.500E+00
CO2 Enhanced by 2.000E+00
C2H6 Enhanced by 3.000E+00
83. H+CH3O(+M)=CH3OH(+M) 2.43E+12 0.5 50.0
Low pressure limit: 0.46600E+42 -0.74400E+01 0.14080E+05
TROE centering: 0.70000E+00 0.10000E+03 0.90000E+05 0.10000E+05
H2 Enhanced by 2.000E+00
H2O Enhanced by 6.000E+00
CH4 Enhanced by 2.000E+00
CO Enhanced by 1.500E+00
CO2 Enhanced by 2.000E+00
C2H6 Enhanced by 3.000E+00
84. CH3OH+H=CH2OH+H2 3.20E+13 0.0 6095.0
85. CH3OH+H=CH3O+H2 8.00E+12 0.0 6095.0
86. CH3OH+O=CH2OH+OH 3.88E+05 2.5 3080.0
87. CH3OH+OH=CH3O+H2O 1.00E+06 2.1 496.7
88. CH3OH+OH=CH2OH+H2O 7.10E+06 1.8 -596.0
89. CH3OH+O2=CH2OH+HO2 2.05E+13 0.0 44900.0
90. CH3OH+HCO=CH2OH+CH2O 9.64E+03 2.9 13110.0
91. CH3OH+HO2=CH2OH+H2O2 3.98E+13 0.0 19400.0
92. CH3OH+CH3=CH2OH+CH4 3.19E+01 3.2 7172.0

```
 93. CH3O+CH3OH=CH3OH+CH2OH                          3.00E+11   0.0     4060.0
 94. CH3+CH3=H+C2H5                                  4.99E+12   0.1    10600.0
 95. CH4+CH2=CH3+CH3                                 2.46E+06   2.0     8270.0
 96. CH4+CH2(S)=CH3+CH3                              1.60E+13   0.0     -570.0
 97. CH3+OH=CH2+H2O                                  5.60E+07   1.6     5420.0
 98. CH3+OH=CH2(S)+H2O                               2.50E+13   0.0        0.0
 99. CH3+CH2=C2H4+H                                  4.00E+13   0.0        0.0
100. CH3+CH2(S)=C2H4+H                               1.20E+13   0.0     -570.0
101. CH3O+H=CH2(S)+H2O                               1.60E+13   0.0        0.0
102. CH2(S)+H2O(+M)=CH3OH(+M)                        4.82E+17  -1.2     1145.0
      Low pressure limit:  0.18800E+39 -0.63600E+01  0.50400E+04
      TROE centering:      0.60270E+00  0.20800E+03  0.39220E+04  0.10180E+05
      H2                Enhanced by    2.000E+00
      H2O               Enhanced by    6.000E+00
      CH4               Enhanced by    2.000E+00
      CO                Enhanced by    1.500E+00
      CO2               Enhanced by    2.000E+00
      C2H6              Enhanced by    3.000E+00
103. C2H6+H=C2H5+H2                                  1.15E+08   1.9     7530.0
104. C2H6+O=C2H5+OH                                  8.98E+07   1.9     5690.0
105. C2H6+OH=C2H5+H2O                                3.54E+06   2.1      870.0
106. C2H6+O2=C2H5+HO2                                4.00E+13   0.0    50900.0
107. C2H6+HO2=C2H5+H2O2                              2.94E+11   0.0    14940.0
108. C2H6+CH3=C2H5+CH4                               6.14E+06   1.7    10450.0
109. C2H5+H(+M)=C2H6(+M)                             5.21E+17  -1.0     1580.0
      Low pressure limit:  0.19900E+42 -0.70800E+01  0.66850E+04
      TROE centering:      0.84220E+00  0.12500E+03  0.22190E+04  0.68820E+04
      H2                Enhanced by    2.000E+00
      H2O               Enhanced by    6.000E+00
      CH4               Enhanced by    2.000E+00
      CO                Enhanced by    1.500E+00
      CO2               Enhanced by    2.000E+00
      C2H6              Enhanced by    3.000E+00
      AR                Enhanced by    7.000E-01
110. C2H5+H=C2H4+H2                                  2.00E+12   0.0        0.0
111. C2H5+O=CH3+CH2O                                 1.32E+14   0.0        0.0
112. C2H5+O2=C2H4+HO2                                2.00E+10   0.0        0.0
113. C2H5+C2H5=C2H4+C2H6                             1.40E+12   0.0        0.0
114. C2H5+HCO=C2H6+CO                                1.20E+14   0.0        0.0
115. C2H5+O=CH3HCO+H                                 8.02E+13   0.0        0.0
116. C2H4(+M)=H2+C2H2(+M)                            8.00E+12   0.4    88770.0
      Low pressure limit:  0.70000E+51 -0.93100E+01  0.99860E+05
      TROE centering:      0.73450E+00  0.18000E+03  0.10350E+04  0.54170E+04
      H2                Enhanced by    2.000E+00
      H2O               Enhanced by    6.000E+00
      CH4               Enhanced by    2.000E+00
      CO                Enhanced by    1.500E+00
      CO2               Enhanced by    2.000E+00
      C2H6              Enhanced by    3.000E+00
      AR                Enhanced by    7.000E-01
117. C2H4+H(+M)=C2H5(+M)                             1.08E+12   0.5     1820.0
      Low pressure limit:  0.12000E+43 -0.76200E+01  0.69700E+04
      TROE centering:      0.97530E+00  0.21000E+03  0.98400E+03  0.43740E+04
      H2                Enhanced by    2.000E+00
      H2O               Enhanced by    6.000E+00
      CH4               Enhanced by    2.000E+00
      CO                Enhanced by    1.500E+00
      CO2               Enhanced by    2.000E+00
      C2H6              Enhanced by    3.000E+00
      AR                Enhanced by    7.000E-01
118. C2H3+H(+M)=C2H4(+M)                             6.08E+12   0.3      280.0
      Low pressure limit:  0.14000E+31 -0.38600E+01  0.33200E+04
      TROE centering:      0.78200E+00  0.20750E+03  0.26630E+04  0.60950E+04
      H2                Enhanced by    2.000E+00
      H2O               Enhanced by    6.000E+00
      CH4               Enhanced by    2.000E+00
      CO                Enhanced by    1.500E+00
      CO2               Enhanced by    2.000E+00
      C2H6              Enhanced by    3.000E+00
```

```
      AR                  Enhanced by      7.000E-01
119. C2H4+H=C2H3+H2                                   1.32E+06    2.5     12240.0
120. C2H4+OH=C2H3+H2O                                 1.80E+06    2.0      2500.0
121. C2H4+CH3=C2H3+CH4                                2.27E+05    2.0      9200.0
122. C2H4+O=CH3+HCO                                   1.92E+07    1.8       220.0
123. C2H3+OH=C2H2+H2O                                 5.00E+12    0.0         0.0
124. C2H4+O=OH+C2H3                                   1.51E+07    1.9      3740.0
125. C2H4+O2=C2H3+HO2                                 4.22E+13    0.0     57600.0
126. C2H3+H=C2H2+H2                                   9.64E+13    0.0         0.0
127. C2H3+O=CH2CO+H                                   6.00E+13    0.0         0.0
128. C2H3+H2O2=C2H4+HO2                               1.21E+10    0.0      -596.0
129. C2H3+CH3=C2H2+CH4                                3.90E+11    0.0         0.0
130. C2H3+C2H3=C2H4+C2H2                              9.60E+11    0.0         0.0
131. C2H3+O2=HCO+CH2O                                 4.58E+16   -1.4      1015.0
132. C2H3+O2=HO2+C2H2                                 1.34E+06    1.6      -384.0
133. C2H3+O2=O+CH2HCO                                 1.00E+11    0.3        11.0
134. C2H2+H(+M)=C2H3(+M)                              5.60E+12    0.0      2400.0
      Low pressure limit:  0.38000E+41 -0.72700E+01  0.72200E+04
      TROE centering:      0.75070E+00  0.98500E+02  0.13020E+04  0.41670E+04
      H2                  Enhanced by      2.000E+00
      H2O                 Enhanced by      6.000E+00
      CH4                 Enhanced by      2.000E+00
      CO                  Enhanced by      1.500E+00
      CO2                 Enhanced by      2.000E+00
      C2H6                Enhanced by      3.000E+00
      AR                  Enhanced by      7.000E-01
135. C2H2+O=HCCO+H                                    1.63E+07    2.0      1900.0
136. C2H2+O=C2H+OH                                    4.60E+19   -1.4     28950.0
137. C2H2+O=CH2+CO                                    4.08E+06    2.0      1900.0
138. C2H2+OH=CH2CO+H                                  2.18E-04    4.5     -1000.0
139. C2H2+OH=HCCOH+H                                  5.04E+05    2.3     13500.0
140. C2H2+OH=C2H+H2O                                  3.37E+07    2.0     14000.0
141. C2H2+OH=CH3+CO                                   4.83E-04    4.0     -2000.0
142. C2H2+HO2=CH2CO+OH                                6.03E+09    0.0      7944.0
143. HCCO+H=CH2(S)+CO                                 1.00E+14    0.0         0.0
144. HCCO+O=H+CO+CO                                   1.00E+14    0.0         0.0
145. HCCO+O2=OH+2CO                                   1.60E+12    0.0       854.0
146. HCCO+OH=HCO+H+CO                                 1.00E+13    0.0         0.0
147. HCCO+CH2=C2H3+CO                                 3.00E+13    0.0         0.0
148. HCCO+HCCO=C2H2+CO+CO                             1.00E+13    0.0         0.0
149. CH3+HCCO=C2H4+CO                                 5.00E+13    0.0         0.0
150. C2H+H(+M)=C2H2(+M)                               1.00E+17   -1.0         0.0
      Low pressure limit:  0.37500E+34 -0.48000E+01  0.19000E+04
      TROE centering:      0.64640E+00  0.13200E+03  0.13150E+04  0.55660E+04
      H2                  Enhanced by      2.000E+00
      H2O                 Enhanced by      6.000E+00
      CH4                 Enhanced by      2.000E+00
      CO                  Enhanced by      1.500E+00
      CO2                 Enhanced by      2.000E+00
      C2H6                Enhanced by      3.000E+00
      AR                  Enhanced by      7.000E-01
151. C2H+OH=H+HCCO                                    2.00E+13    0.0         0.0
152. C2H+O2=HCO+CO                                    5.00E+13    0.0      1500.0
153. C2H+H2=H+C2H2                                    4.90E+05    2.5       560.0
154. CH2+H(+M)=CH3(+M)                                2.50E+16   -0.8         0.0
      Low pressure limit:  0.32000E+28 -0.31400E+01  0.12300E+04
      TROE centering:      0.68000E+00  0.78000E+02  0.19950E+04  0.55900E+04
      H2                  Enhanced by      2.000E+00
      H2O                 Enhanced by      6.000E+00
      CH4                 Enhanced by      2.000E+00
      CO                  Enhanced by      1.500E+00
      CO2                 Enhanced by      2.000E+00
      C2H6                Enhanced by      3.000E+00
      AR                  Enhanced by      7.000E-01
155. CH2+O=HCO+H                                      8.00E+13    0.0         0.0
156. CH2+OH=CH2O+H                                    2.00E+13    0.0         0.0
157. CH2+H2=H+CH3                                     5.00E+05    2.0      7230.0
158. CH2+O2=HCO+OH                                    1.32E+13    0.0      1500.0
159. CH2+HO2=CH2O+OH                                  2.00E+13    0.0         0.0
```

160. CH2+CO(+M)=CH2CO(+M) 8.10E+11 0.5 4510.0
Low pressure limit: 0.26900E+34 -0.51100E+01 0.70950E+04
TROE centering: 0.59070E+00 0.27500E+03 0.12260E+04 0.51850E+04
H2 Enhanced by 2.000E+00
H2O Enhanced by 6.000E+00
CH4 Enhanced by 2.000E+00
CO Enhanced by 1.500E+00
CO2 Enhanced by 2.000E+00
C2H6 Enhanced by 3.000E+00
AR Enhanced by 7.000E-01
161. CH2+CH2=C2H2+H2 3.20E+13 0.0 0.0
162. CH2(S)+M=CH2+M 9.00E+12 0.0 600.0
H2O Enhanced by 0.000E+00
CO Enhanced by 0.000E+00
CO2 Enhanced by 0.000E+00
AR Enhanced by 0.000E+00
163. CH2(S)+H2O=CH2+H2O 3.00E+13 0.0 0.0
164. CH2(S)+CO=CH2+CO 9.00E+12 0.0 0.0
165. CH2(S)+CO2=CH2+CO2 7.00E+12 0.0 0.0
166. CH2(S)+AR=CH2+AR 9.00E+12 0.0 600.0
167. CH2(S)+O=CO+H2 1.50E+13 0.0 0.0
168. CH2(S)+O=HCO+H 1.50E+13 0.0 0.0
169. CH2(S)+OH=CH2O+H 3.00E+13 0.0 0.0
170. CH2(S)+H2=CH3+H 7.00E+13 0.0 0.0
171. CH2(S)+O2=H+OH+CO 2.80E+13 0.0 0.0
172. CH2(S)+O2=CO+H2O 1.20E+13 0.0 0.0
173. CH2(S)+CO2=CH2O+CO 1.40E+13 0.0 0.0
174. CH3HCO=CH3+HCO 7.00E+15 0.0 81674.0
175. CH3CO(+M)=CH3+CO(+M) 3.00E+12 0.0 16722.0
Low pressure limit: 0.12000E+16 0.00000E+00 0.12518E+05
176. CH3HCO+OH=CH3CO+H2O 3.37E+12 0.0 -620.0
177. CH3HCO+OH=CH2HCO+H2O 3.37E+11 0.0 -620.0
178. CH3HCO+O=CH3CO+OH 1.77E+18 -1.9 2975.0
179. CH3HCO+O=CH2HCO+OH 3.72E+13 -0.2 3556.0
180. CH3HCO+H=CH3CO+H2 4.66E+13 -0.3 2988.0
181. CH3HCO+H=CH2HCO+H2 1.85E+12 0.4 5359.0
182. CH3HCO+CH3=CH3CO+CH4 3.90E-07 5.8 2200.0
183. CH3HCO+CH3=CH2HCO+CH4 2.45E+01 3.1 5727.0
184. CH3HCO+HO2=CH3CO+H2O2 3.60E+19 -2.2 14030.0
185. CH3HCO+HO2=CH2HCO+H2O2 2.32E+11 0.4 14864.0
186. CH3HCO+O2=CH3CO+HO2 1.00E+14 0.0 42200.0
187. CH2CO+O=CO2+CH2 1.75E+12 0.0 1350.0
188. CH2CO+H=CH3+CO 2.71E+04 2.8 714.0
189. CH2CO+H=HCCO+H2 2.00E+14 0.0 8000.0
190. CH2CO+O=HCCO+OH 1.00E+13 0.0 8000.0
191. CH2CO+OH=HCCO+H2O 1.00E+13 0.0 2000.0
192. CH2CO+OH=CH2OH+CO 3.73E+12 0.0 -1013.0
193. CH2HCO+H=CH3+HCO 5.00E+13 0.0 0.0
194. CH2HCO+H=CH2CO+H2 2.00E+13 0.0 0.0
195. CH2HCO+O=CH2O+HCO 1.00E+14 0.0 0.0
196. CH2HCO+OH=CH2CO+H2O 3.00E+13 0.0 0.0
197. CH2HCO+O2=CH2O+CO+OH 3.00E+10 0.0 0.0
198. CH2HCO+CH3=C2H5+CO+H 4.90E+14 -0.5 0.0
199. CH2HCO+HO2=CH2O+HCO+OH 7.00E+12 0.0 0.0
200. CH2HCO+HO2=CH3HCO+O2 3.00E+12 0.0 0.0
201. CH2HCO=CH3+CO 1.17E+43 -9.8 43756.0
202. CH2HCO=CH2CO+H 1.81E+43 -9.6 45868.0
203. C2H5OH=CH3+CH2OH 1.26E+51 -10.6 100869.0
204. C2H5OH=C2H4+H2O 8.80E+25 -3.7 70799.0
205. C2H5OH+OH=C2H4OH+H2O 1.81E+11 0.4 716.5
206. C2H5OH+OH=CH3CHOH+H2O 3.09E+10 0.5 -379.8
207. C2H5OH+OH=CH3CH2O+H2O 1.05E+10 0.8 716.9
208. C2H5OH+H=C2H4OH+H2 1.90E+07 1.8 5098.0
209. C2H5OH+H=CH3CHOH+H2 2.58E+07 1.6 2827.0
210. C2H5OH+H=CH3CH2O+H2 1.50E+07 1.6 3038.0
211. C2H5OH+O=C2H4OH+OH 9.41E+07 1.7 5459.0
212. C2H5OH+O=CH3CHOH+OH 1.88E+07 1.9 1824.0
213. C2H5OH+O=CH3CH2O+OH 1.58E+07 2.0 4448.0
214. C2H5OH+CH3=C2H4OH+CH4 2.19E+02 3.2 9622.0

215. C2H5OH+CH3=CH3CHOH+CH4	7.28E+02	3.0	7948.0
216. C2H5OH+CH3=CH3CH2O+CH4	1.45E+02	3.0	7649.0
217. C2H5OH+HO2=CH3CHOH+H2O2	8.20E+03	2.5	10750.0
218. C2H5OH+HO2=C2H4OH+H2O2	2.43E+04	2.5	15750.0
219. C2H5OH+HO2=CH3CH2O+H2O2	3.80E+12	0.0	24000.0
220. CH3CH2O+M=CH3HCO+H+M	5.60E+34	-5.9	25274.0
221. CH3CH2O+M=CH3+CH2O+M	5.35E+37	-7.0	23800.0
222. CH3CH2O+O2=CH3HCO+HO2	4.00E+10	0.0	1100.0
223. CH3CH2O+CO=C2H5+CO2	4.68E+02	3.2	5380.0
224. CH3CH2O+H=CH3+CH2OH	3.00E+13	0.0	0.0
225. CH3CH2O+H=C2H4+H2O	3.00E+13	0.0	0.0
226. CH3CH2O+OH=CH3HCO+H2O	1.00E+13	0.0	0.0
227. CH3CHOH+O2=CH3HCO+HO2	4.82E+13	0.0	5017.0
Declared duplicate reaction...			
228. CH3CHOH+O2=CH3HCO+HO2	8.43E+14	-1.2	0.0
Declared duplicate reaction...			
229. CH3CHOH+O=CH3HCO+OH	1.00E+14	0.0	0.0
230. CH3CHOH+H=C2H4+H2O	3.00E+13	0.0	0.0
231. CH3CHOH+H=CH3+CH2OH	3.00E+13	0.0	0.0
232. CH3CHOH+HO2=CH3HCO+OH+OH	4.00E+13	0.0	0.0
233. CH3CHOH+OH=CH3HCO+H2O	5.00E+12	0.0	0.0
234. CH3CHOH+M=CH3HCO+H+M	1.00E+14	0.0	25000.0
235. C2H4OH+O2=HOC2H4O2	1.00E+12	0.0	-1100.0
236. HOC2H4O2=CH2O+CH2O+OH	1.80E+11	0.0	24500.0
237. C2H4+OH=C2H4OH	2.41E+11	0.0	-2385.0
238. C2H5+HO2=CH3CH2O+OH	4.00E+13	0.0	0.0
239. CH3OCH3=CH3+CH3O	1.70E+42	-8.0	91806.6
240. CH3OCH3+OH=CH3OCH2+H2O	6.71E+06	2.0	-629.9
241. CH3OCH3+H=CH3OCH2+H2	2.97E+07	2.0	4033.6
242. CH3OCH3+CH3=CH3OCH2+CH4	2.68E+01	3.8	9631.3
243. CH3OCH3+O=CH3OCH2+OH	1.86E-03	5.3	-109.0
244. CH3OCH3+HO2=CH3OCH2+H2O2	2.00E+13	0.0	16500.0
245. CH3OCH3+O2=CH3OCH2+HO2	4.10E+13	0.0	44910.0
246. CH3OCH3+CH3O=CH3OCH2+CH3OH	6.02E+11	0.0	4074.0
247. CH3OCH3+CH3OCH2O2=CH3OCH2+CH3OCH2O2H	5.00E+12	0.0	17690.0
248. CH3OCH2=CH2O+CH3	1.20E+13	0.0	25750.0
249. CH3OCH2+CH3O=CH3OCH3+CH2O	2.41E+13	0.0	0.0
250. CH3OCH2+CH2O=CH3OCH3+HCO	5.49E+03	2.8	5862.0
251. CH3OCH2+HO2=CH3OCH2O+OH	9.00E+12	0.0	0.0
252. CH3OCH2O=CH3OCHO+H	1.74E+16	-0.7	11720.0
253. CH3OCHO=CH3+OCHO	1.39E+18	-1.0	79140.0
254. CH3OCHO+O2=CH3OCO+HO2	1.00E+13	0.0	49700.0
255. CH3OCHO+OH=CH3OCO+H2O	2.34E+07	1.6	-35.0
256. CH3OCHO+HO2=CH3OCO+H2O2	1.22E+12	0.0	17000.0
257. CH3OCHO+O=CH3OCO+OH	2.35E+05	2.5	2230.0
258. CH3OCHO+H=CH3OCO+H2	4.55E+06	2.0	5000.0
259. CH3OCHO+CH3=CH3OCO+CH4	7.55E-01	3.5	5481.0
260. CH3OCHO+CH3O=CH3OCO+CH3OH	5.48E+11	0.0	5000.0
261. CH3OCO=CH3O+CO	7.45E+12	-1.8	17150.0
262. CH3OCO=CH3+CO2	1.51E+12	-1.8	13820.0
263. OCHO+M=H+CO2+M	2.44E+15	-0.5	26500.0
264. CH3OCH2+O2=CH3OCH2O2	2.00E+12	0.0	0.0
265. CH3OCH2O2+CH2O=CH3OCH2O2H+HCO	1.00E+12	0.0	11670.0
266. CH3OCH2O2+CH3OCH2O2=O2+CH3OCH2O+CH3OCH2O	1.60E+23	-4.5	0.0
267. CH3OCH2O2+CH3OCH2O2=O2+CH3OCHO+CH3OCH2OH	6.84E+22	-4.5	0.0
268. CH3OCH2O2H=CH3OCH2O+OH	2.11E+22	-2.1	43830.0
269. CH3OCH2O=CH3O+CH2O	9.72E+15	-1.1	20640.0
270. CH3OCH2O+O2=CH3OCHO+HO2	5.00E+10	0.0	500.0
271. CH3OCH2O2=CH2OCH2O2H	6.00E+10	0.0	21500.0
272. CH2OCH2O2H=OH+CH2O+CH2O	1.50E+13	0.0	20500.0
273. CH2OCH2O2H+O2=O2CH2OCH2O2H	7.00E+11	0.0	0.0
274. O2CH2OCH2O2H=HO2CH2OCHO+OH	4.00E+10	0.0	18500.0
275. HO2CH2OCHO=OCH2OCHO+OH	3.00E+16	0.0	40000.0
276. OCH2OCHO=HOCH2OCO	1.00E+11	0.0	14000.0
277. HOCH2OCO=HOCH2O+CO	2.18E+16	-2.7	17200.0
278. HOCH2OCO=CH2OH+CO2	5.31E+15	-2.6	20810.0
279. HOCH2O=HCOOH+H	1.00E+14	0.0	14900.0
280. CH2O+OH=HOCH2O	4.50E+15	-1.1	0.0
281. HCOOH+M=CO+H2O+M	2.30E+13	0.0	50000.0

282. HCOOH+M=CO2+H2+M	1.50E+16	0.0	57000.0
283. HCOOH=HCO+OH	4.59E+18	-0.5	108300.0
284. HCOOH+OH=H2O+CO2+H	2.62E+06	2.1	916.0
285. HCOOH+OH=H2O+CO+OH	1.85E+07	1.5	-962.0
286. HCOOH+H=H2+CO2+H	4.24E+06	2.1	4868.0
287. HCOOH+H=H2+CO+OH	6.03E+13	-0.3	2988.0
288. HCOOH+CH3=CH4+CO+OH	3.90E-07	5.8	2200.0
289. HCOOH+HO2=H2O2+CO+OH	1.00E+12	0.0	11920.0
290. HCOOH+O=CO+OH+OH	1.77E+18	-1.9	2975.0

Achievements

Journal publications:

1. Gao, J., Nakamura, Y., Jiang, L., and Zhao, D., "Low-Temperature Ignition of DME/air Mixture at Atmospheric Pressure: on the Transition from Cool Flame to Hot Flame", ***Proc. Combust. Inst.***, under review.

2. Gao, J., and Nakamura, Y., "Two-stage Ignition of DME/air Mixture at Low-temperature (<500K) under Atmospheric Pressure", ***Fuel***, Vol.106 (2013), pp.241-248.

Conference publications:

3. Gao, J., Nakamura, Y., Jiang, L., and Zhao, D., "Study on NTC Behavior and Cool Flame Ignition of DME/air Mixture", ***Proc. 3rd East Asia Mechanical and Aerospace Engineering Workshop***, Sapporo, Japan (2013.6), p.53.

4. Gao, J., Nakamura, Y., Jiang, L., and Zhao, D., "Study on the Repetitive Low-temperature Ignition Mechanism of DME/air Mixture in A Flow Reactor", ***Proc. 24th International Colloquium on Dynamics of Explosion and Reactive Systems (24th ICDERS)***, Taipei, Taiwan (2013.8), No.0127 (on USB)

5. Gao, J., Nakamura, Y., Jiang, L., and Zhao, D., "Characteristics of Low-temperature (<550K) Ignition and Subsequent Flame Propagation of DME/air Mixture", ***Proc. 9th Asia-Pacific Conference on Combustion (9th ASPACC)***, Gyeongju, Korea (2013.5), p.230 (on CD-ROM).

6. Gao, J., and Nakamura, Y., "Oscillatory Cool flames and Transient Two-stage Ignition of DME/air Mixture Below 500 K under Atmospheric Pressure", ***Work-In Progress Poster Colloquium at 34th International Symposium on Combustion***, Warsaw, Poland (2012.7),

W5P071 (on USB).

7. Gao, J., Nakamura, Y., and Zhao, D., "Low Temperature Ignition of DME-air Mixture in a Straight Heated Tube Reactor", ***Proc. 7th Asian DME Conference***, Niigata, Japan (2011.11), pp.362-377.